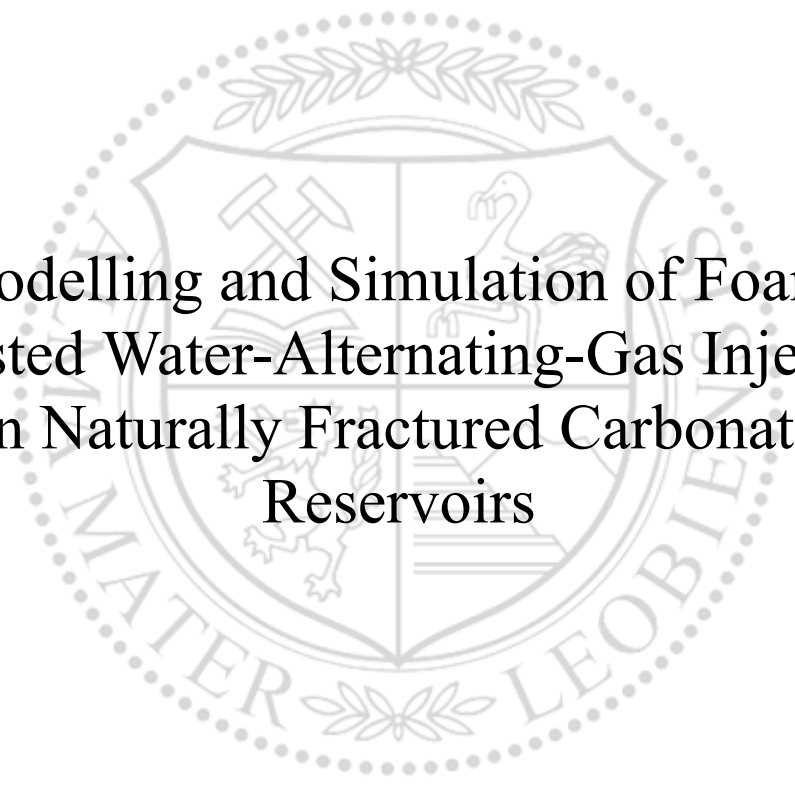




Chair of Reservoir Engineering

Master's Thesis



Modelling and Simulation of Foam-
Assisted Water-Alternating-Gas Injection
in Naturally Fractured Carbonate
Reservoirs

Ronald Gugl, BSc

September 2020



EIDESSTATTLICHE ERKLÄRUNG

Ich erkläre an Eides statt, dass ich diese Arbeit selbständig verfasst, andere als die angegebenen Quellen und Hilfsmittel nicht benutzt, und mich auch sonst keiner unerlaubten Hilfsmittel bedient habe.

Ich erkläre, dass ich die Richtlinien des Senats der Montanuniversität Leoben zu "Gute wissenschaftliche Praxis" gelesen, verstanden und befolgt habe.

Weiters erkläre ich, dass die elektronische und gedruckte Version der eingereichten wissenschaftlichen Abschlussarbeit formal und inhaltlich identisch sind.

Datum 29.09.2020

Unterschrift Verfasser/in
Ronald, Gugl



MONTANUNIVERSITÄT LEOBEN

www.unileoben.ac.at

BSc
Ronald Gugl
Maisgasse 4
3100 St. Pölten

An den Studiendekan der Montanuniversität Leoben

**Zustimmungserklärung zur digitalen Veröffentlichung
von wissenschaftlichen Abschlussarbeiten**

Mir ist bekannt, dass die Arbeit mit dem Titel "Modelling and Simulation of Foam-Assisted WAG Injection in Naturally Fractured Carbonate Reservoirs" durch technische Hilfsmittel einer Plagiatsprüfung unterzogen wird und dass die Arbeit in digitaler Form unbefristet an der Montanuniversität Leoben gespeichert werden darf.

Darüber hinaus erkläre ich mich damit einverstanden, dass die Universitätsbibliothek der Montanuniversität Leoben die oben genannte Arbeit im World Wide Web frei zugänglich zur Verfügung stellt. Für gesperrte Abschlussarbeiten erfolgt dies nach Ablauf der Sperre.

Hinweis: wenn Sie der elektronischen Veröffentlichung nicht zustimmen, wird die Arbeit nur in gedruckter Form (ggf. nach Ablauf einer allfälligen Sperre) in der Universitätsbibliothek (Dissertationen auch in der Österreichischen Nationalbibliothek) veröffentlicht.

Der Veröffentlichung meiner Arbeit im World Wide Web stimme ich hiermit zu:

Ja

Nein

Datum 29.09.2020

Unterschrift Verfasser/in

Ronald Gugl

Master Thesis 2020

Supervisor: Univ.-Prof. MSc PhD Riyaz Kharrat

Modelling of Foam- Assisted Water- Alternating-Gas Injection in Naturally Fractured Reservoirs

To my parents, and my sister.

Acknowledgements

I want to thank my supervisor Prof. Kharrat for his great aid, time commitment for helping me resolve any issues that came up, and encouragement to finish my research.

I also want to thank Ph.D. Shariat for his endless help in resolving the problems I faced working with CMG and a big thanks to CMG for the provision of a licence that allowed me to simulate a model as huge as the sector model.

And a special thanks to my colleague and dear friend Dipl.-Ing. Markus Frauwallner for his support and time helping me throughout the past year that I was working on this thesis.

Abstract

In this research, carbonate core flooding experimental results of three different EOR methods were replicated numerically using CMG to study the enhancement of oil recovery in the gas invaded zone of carbonate fractured reservoirs. Experimental results for carbon dioxide injection, Water-alternating-gas injection [WAG], and foam-assisted water-alternating-gas injection [FAWAG] that were conducted in Iranian low-temperature fractured carbonate cores under both secondary and tertiary recovery conditions were used for this purpose. From these experiments, the relative permeability curves of the cores and the fitting foam parameters were derived using CMG. These findings were then used in a pilot model, that consists of a quarter five-spot pattern, and in a sector model where a double five-spot setup was used as the primary method of oil extraction. Additionally, all these models were first simulated, having been saturated by live-oil and connate water and secondly with a present gas invaded zone of 40% consisting out of methane. The foam-assisted recovery process was found to be a very useful aid in the recovery of gas invaded fractured reservoirs increasing the recovery factor in the pilot model by an astonishing twenty percent and in the sector model by more than two percent. By tuning the ratio of injected water and gas the recovery can be raised to as far as 7% additional recovery after 1 PVI for a tertiary stage.

Zusammenfassung

In dieser wissenschaftlichen Arbeit wurden Resultate von Bohrkernflutungen mittels verschiedener Methoden der tertiären Ölgewinnung herangezogen und numerisch mit dem von CMG zur Verfügung gestellten Lagerstättensimulator untersucht und reproduziert. Dazu wurden experimentelle Resultate von Kohlenstoffdioxidinjektion, alternierende Injektion von Wasser und Gas und Schaum-unterstützte alternierende Injektion von Wasser und Gas, welche in niedertemperierten und geklüfteten iranischen Karbonatbohrkernen unter sekundären und tertiären Rückgewinnungsbedingungen durchgeführt wurden, herangezogen. Von diesen Experimenten wurden die relativen Permeabilitätskurven und die passend Schaumparameter mit Hilfe von CMG abgeleitet. Diese Ergebnisse wurden dann in einer Vorstudie, die ein Viertel eines Fünf-Punkt Sondenschemas darstellt und in einem Sektormodell, wo ein doppeltes Fünf-Punkt Schema die primäre Methode der Erdölextraktion angewendet wird, implementiert. Zusätzlich wurden diese Simulationen zum einen mit Lebendöl mit immobilem Salzwasser gesättigt, und zum anderen mit einer in die Klüfte eingedrungenen Gassättigung von 40% durchgeführt. Die schaubasierte Rückgewinnungsmethode leistete in allen Fällen eine beachtliche Hilfe und konnte vor allem in geklüfteten Lagerstätten, worin Gas eingedrungen war, im Modell der Vorstudie die Rückgewinnung um mehr als zwanzig Prozent und im Sektormodell um mehr als zwei Prozent erhöhen. Durch Verbessern des Verhältnisses zwischen dem injizierten Wasser und dem Gas kann die Rückgewinnung sogar um 7% nach Injektion eines Porenvolumens erhöht werden.

Table of Contents

Acknowledgements	iii
Abstract	v
Zusammenfassung	vi
Table of Contents	vii
List of Figures	x
List of Tables.....	xiii
Abbreviations	xv
Chapter 1	17
1.1 Background and Context.....	18
1.2 Scope and Objectives	18
1.3 Achievements.....	19
1.4 Technical Issues	19
1.5 Overview of Dissertation	19
Chapter 2.....	20
2.1 Production Mechanisms in Fractured Reservoirs	21
2.1.1 Primary Recovery	21
2.1.2 Gas Cap Expansion	21
2.1.3 Solution Gas Drive.....	21
2.1.4 Secondary Recovery	22
2.1.5 Tertiary Recovery	22
2.2 Reservoir Zonation.....	23
2.3 Fundamental Reservoir Rock Properties.....	24
2.3.1 Relative Permeability and Hysteresis	24
2.3.2 Relative Permeability Reduction through Hysteresis	27
2.3.3 Relative Permeability Correlations	28
2.4 Miscibility	28
2.4.1 First-Contact Miscible Displacement (FCM).....	28
2.4.2 Multiple-Contact Miscible Displacement [MCM].....	29
2.4.3 Vaporising Gas Drive [VGD]	29
2.4.4 Condensing Gas Drive [CGD]	31
2.4.5 Condensing/Vaporising-Gas Drive (Enriched-Gas)	32
2.4.6 CO ₂ Miscible Displacement Process	33
2.4.7 Minimum Miscibility Pressure (MMP).....	34
2.5 Physical and Chemical Properties of CO ₂	34
2.5.1 Advantages and Disadvantages of CO ₂ Usage.....	35
Chapter 3.....	37

3.1	Enhanced Oil Recovery Methods [EOR].....	37
3.2	Gas Injection and CO2 Flooding.....	37
3.3	Water-Alternating-Gas Injection [WAG].....	38
3.4	Chemical EOR.....	40
3.5	Foam Flooding.....	40
3.6	Foam Characteristics.....	41
3.6.1	Foam Stability.....	43
3.6.2	Mobility Reduction.....	44
3.6.3	Foam Formation, Decay, and Collapse.....	45
3.6.4	Foam States.....	47
3.6.5	Foam Flooding Mechanism.....	48
3.7	Petrophysics of Naturally Fractured Carbonate Rocks.....	49
3.7.1	Fractures in Carbonate Rocks.....	49
3.7.2	Porosity in Fractured Reservoirs.....	50
3.7.3	Permeability in Fractured Reservoirs.....	51
Chapter 4.....		53
4.1.1	Mathematical Basis for Simulation Runs.....	54
4.1.2	Reservoir Model.....	56
4.1.3	Grid Orientation Effects.....	57
4.1.4	Foam Modelling.....	58
4.1.5	Fracture Modelling.....	59
Chapter 5.....		61
5.1	Experimental Background and Reservoir Description.....	61
5.2	Experimental Procedure and Workflow.....	63
5.3	PVT data matching.....	64
5.3.1	De-Lumping.....	64
5.3.2	Regression.....	65
5.3.3	Minimum Miscibility Pressure (MMP).....	68
5.4	Core Flooding Model Setup.....	69
5.4.1	CO2 Core Flooding.....	69
5.4.2	WAG Core Flooding.....	71
5.4.3	FAWAG Core Flooding.....	74
5.4.4	Optimum Water to Oil Ratio in FAWAG Processes.....	76
5.5	Gas Invaded Core [Tertiary Recovery].....	78
5.6	Pilot Model Setup.....	79
5.7	Sector Model [Gas Invaded Zone].....	80
Chapter 6.....		85
6.1	Pilot Model [Secondary Recovery].....	85
6.2	Pilot Model [Tertiary Recovery].....	87

6.3	Homogeneous Cross-Section	89
6.4	Sensitivity Analysis	92
6.5	Sector Model [Tertiary Recovery]	95
Chapter 7	99
7.1	Discussion of the Gas Mobility Reduction Mechanisms	99
7.1.1	Core Model	99
7.1.2	Pilot Model.....	100
7.1.3	Cross-Sectional Model.....	101
7.1.4	Sensitivity Analysis	101
7.1.5	Sector Model	102
Chapter 8	103
8.1	Summary	103
8.2	Evaluation	104
8.3	Future Work	104
References	105

List of Figures

Figure 2-1: Zonation of a conventional reservoir. (a) initial conditions; (b) during production	23
Figure 2-2: Zonation of a fractured reservoir	23
Figure 2-3: Typical two-phase flow behaviour (Ahmed, 2010).	25
Figure 2-4: Gas-oil relative permeability curves (Ahmed, 2010).	26
Figure 2-5: Hysteresis effects in relative permeability (Ahmed, 2010).	27
Figure 2-6: Ternary diagram for mixtures of C ₁ , C ₄ , and C ₁₀ . Compositions A and B are miscible by first contact (Pedersen, et al., 2015).	29
Figure 2-7: The principle of vaporising gas drive illustrated in a ternary diagram for a mixture of C ₁ , C ₄ , and C ₁₀ (Pedersen, et al., 2015).	30
Figure 2-8: Miscibility obtained through a vaporising drive. Passing through the reservoir, the gas takes up components from the oil phase and develops miscibility at the gas-oil front (Pedersen, et al., 2015).	31
Figure 2-9: The principle of a condensing drive illustrated in a ternary diagram for a mixture of C ₁ , C ₄ , and C ₁₀ (Pedersen, et al., 2015).	31
Figure 2-10: Miscibility obtained through a condensing drive. Miscibility develops near the injection well (Pedersen, et al., 2015).	32
Figure 2-11: Comparison of two-phase envelopes for methane/hydrocarbon and CO ₂ /hydrocarbon systems (Green & Willhite, 2018).	33
Figure 2-12: CO ₂ Phase Diagram (Witowski, et al., 2014) [modified]	35
Figure 3-1: During WAG, gas can move upward owing to its low density, while injected water can move downwards (Jarrell, et al., 2002).	39
Figure 3-2: drawing by Joe Lindley, U.S. Department of Energy, Bartlesville, OK.	39
Figure 3-3: Schematic of a foam system (Sheng, 2013).	41
Figure 3-4: Bubble size frequency distributions (David & Marsden, 1969).	42
Figure 3-5: Surface tension and adsorption of a surfactant versus concentration (Lake, 1989).	43
Figure 3-6: The mechanism of film stability (Lake, 1989).	44
Figure 3-7: Effective permeability-viscosity ratio versus foam quality for consolidated permeable media and 0.1% aerosol foam (Lake, 1989).	44
Figure 3-8: Schematic of snap-off mechanism (A) gas penetrates to a constriction and a new bubble is formed (B) (Ransohoff & Radke, 1988).	45
Figure 3-9: Schematic of lamella division mechanism, lamella at the branch point (A) and divided gas bubbles formation (B) (Ransohoff & Radke, 1988).	46
Figure 3-10: Schematic of leave-behind mechanism showing gas invasion (A) and forming lens (B) (Ransohoff & Radke, 1988).	46
Figure 3-11: Illustration of conventional gas-liquid two-phase flow in porous media (Sheng, 2013).	47
Figure 3-12: Development of fracture porosity in carbonate rocks that have low insoluble residue, (a)-(c), and high insoluble residue, (d) and (e) (Tiab & Donaldson, 2016).	51
Figure 3-13: (a) Carbonate rock showing porosity: A, vugs; B, joint channels; C, bedding plane channels; D, solution channel adapted by (Tiab & Donaldson, 2016) from (Pirson, 1958).	52
Figure 4-1: Optimisation of well spacing based on reservoir simulation (Satter & Iqbal, 2016).	54
Figure 4-2 Demonstration of grid orientation effects on the flow of fluids between injector and producer (Satter & Iqbal, 2016).	57
Figure 4-3: Dual Porosity (Single Permeability) Model.	59
Figure 4-4: Dual porosity representation of a fractured reservoir (Lemonnier & Bourbiaux, 2010).	60
Figure 4-5: Dual Porosity - Dual Permeability Model.	60
Figure 5-1: Schematic of the core flooding laboratory setup (Gandomkar & Kharrat, 2012).	62

Figure 5-2: Foam Simulation Study Workflow	63
Figure 5-3: Relative Oil Volume (CCE) vs. Pressure	65
Figure 5-4: Gas-Oil Ratio and Relative Oil Volume (DL) vs. Pressure	66
Figure 5-5: Gas Z Factor (DL) vs. Pressure.....	66
Figure 5-6: Oil SG and Gas SG (DL) vs. Pressure	67
Figure 5-7: Oil Viscosity (DL) vs. Pressure	67
Figure 5-8 Phase Envelope of the matched Reservoir Oil	68
Figure 5-9: Core Simulation Model.....	69
Figure 5-10: CO ₂ Recovery Factor – History Match	70
Figure 5-11: Gas relative permeability curve after history match	71
Figure 5-12: WAG Recovery Factor – History Match	72
Figure 5-13: WAG Pressure – History Match	73
Figure 5-14: Water relative permeability curve after the history match.	73
Figure 5-15: Adsorption density vs. surfactant concentration	74
Figure 5-16: FAWAG Recovery Factor – History Match	75
Figure 5-17: FAWAG Pressure – History Match	75
Figure 5-18: FAWAG Gas Production – History Match	76
Figure 5-19: Comparison of the recovery factor of different water-gas-ratios for FAWAG injection	77
Figure 5-20: Comparison of the core pressure for different water-gas ratios for FAWAG injections.....	77
Figure 5-21: Comparison of the recovery factor for WAG and FAWAG as a tertiary recovery process.	78
Figure 5-22: Comparison of the core pressure for WAG and FAWAG as a tertiary recovery process.	79
Figure 5-23: Quarter five-spot pilot simulation model (porosity profile).....	80
Figure 5-24: The sector model and its dual-five-spot well-placement.	81
Figure 5-25: Well-placement for the creation of the gas invaded zone; left: injectors (layer 1), right: producers (layer 7). [Grid Top in metres]	81
Figure 5-26: Gas saturation after the creation of a gas invaded zone in layer 1 (a), 2 (b) and 3 (c).	82
Figure 5-27: Oil saturation after the creation of the gas invaded zone in layer 1 (left) and layer 7 (right).	83
Figure 5-28: Oil saturation after 1 PV of WAG displacement in layer 1 (left) and layer 7 (right).	83
Figure 5-29: Oil saturation after 1 PV of FAWAG displacement in layer 1 (left) and layer 7 (right).	83
Figure 6-1: Comparison of the recovery factor of WAG, FAWAG and CO ₂ injection in the pilot model.	86
Figure 6-2: Comparison of the reservoir pressure for WAG, FAWAG and CO ₂ injection in the pilot model.	86
Figure 6-3: Comparison of the cumulative gas production in WAG and FAWAG processes in the pilot model.	87
Figure 6-4: Comparison of the recovery factor of WAG, FAWAG, and CO ₂ injection in the pilot model with a gas invaded zone of 40%.	88
Figure 6-5: Comparison of the reservoir pressure for WAG, FAWAG, and CO ₂ injection in the pilot model with a gas invaded zone of 40%.	88
Figure 6-6: Comparison of the cumulative gas production in WAG and FAWAG processes in the pilot model with a gas invaded zone of 40%.	89
Figure 6-7: Homogeneous Cross-Section Model.....	89
Figure 6-8: Comparison of gas-phase movement for FAWAG (left) and WAG (right) displacement processes after injection of 0.05 PV of CO ₂ (gas saturation).....	91

Figure 6-9: Comparison of gas-phase movement for FAWAG (left) and WAG (right) displacement processes after the injection of 0.02 PV of CO ₂ in a model with a 40% gas invaded zone (CO ₂ mole fraction).	91
Figure 6-10: Sensitivity Analysis - Block Height	93
Figure 6-11: Sensitivity Analysis - Fracture Permeability.....	93
Figure 6-12: Sensitivity Analysis - Fracture Spacing	94
Figure 6-13: Sensitivity Analysis – Recovery factor comparison after 0.4 PVI (red: decrease / blue: increase).....	94
Figure 6-14: Recovery Factor - Sector Model	95
Figure 6-15: Cumulative Gas Production - Sector Model	96
Figure 6-16: Average Pressure - Sector Model.....	96
Figure 6-17: Cumulative Water Production - Sector Model.....	97
Figure 6-18: Gas-Oil-Ratio - Sector Model	97
Figure 6-19: Water Cut - Sector Model	98
Figure 6-20: Comparison RF of FAWAG - CO ₂ with 0.1 PV and 0.2 PV slugs, and associated gas with 0.1 PV slugs.....	98
Figure 7-1: Core Model - Oil Recovery Factor Comparison WAG vs. FAWAG.	100

List of Tables

Table 1: Core properties, experimental parameters, water, and oil properties.....	62
Table 2: Oil and gas composition before and after de-lumping.....	64

Abbreviations

EOR	Enhanced Oil Recovery
GOR	Gas-Oil Ratio
GOC	Gas-Oil Contact
WOC	Water-Oil Contact
IFT	Interfacial Tension
ROS	Residual Oil Saturation
HCPV	Hydrocarbon Pore Volume
WAG	Water-Alternating-Gas
FAWAG	Foam-Assisted Water-Alternating-Gas
MCM	Multiple Contact Miscibility
VGD	Vaporising Gas Drive
CGD	Condensing Gas Drive
FCM	First Contact Miscibility
MMP	Minimum Miscibility Pressure
PVT	Pressure-Volume-Temperature
CCE	Constant Composition Expansion
DL	Differential Liberation
EOS	Equation of State
FZI	Flow Zone Indicator
CMG	Computer Modelling Group Ltd.

Chapter 1

Introduction

Two thirds of all recoverable oil reserves and a third of all recoverable gas reserves are found in carbonate rocks. Most of these reservoirs are found on the Arabian plate region (roughly the Arabian Peninsula, the Fertile Crescent, Southeast Turkey, and Southwest Iran. They are the focus of many studies, as most fields are approaching their final stage of primary production (Beydoun, 1998). Most of these fields are highly fractured and therefore require a different development approach compared to conventional reservoirs. Especially the creation of gas invaded zones during production poses a major problem. Hence, the implementation of a proper enhanced oil recovery [EOR] process requires extensive laboratory work and simulation studies to be effective.

In this work, the enhanced oil recovery method of foam-assisted water-alternating-gas injection [FAWAG] was compared to the regular water-alternating-gas injection [WAG] in naturally fractured reservoir models. In addition, the same EOR methods were studied in the presence of a gas invaded zone to clarify the foams viability in a later development stage. The first usage of WAG injection dates back many decades as a means of reducing gas and water mobility in order to increase sweep efficiency and improve oil recovery as pure gas injection suffers from major problems with poor sweep efficiency due to viscous fingering, gravity override, and heterogeneity despite its favourable characteristics for oil displacement. Furthermore, the fractured matrix in carbonate reservoirs may act as a “highway” for injection gas, bypassing much of the remaining oil in the matrix. In CO₂ injection, the mobility is usually high in comparison to other fluids. Hence, sweep efficiency is low and early gas breakthrough occurs (Syahputra, et al., 2000). WAG injection is, therefore, considered an effective tool in the control of gas production and inexpensive in cost.

A possible advantage of adding surfactants to the injected water is to decrease the mobility of the gas even further and reduce the needed injection water to reach the same effect. Another favourable characteristic of foam is its high apparent viscosity that is greater than the viscosity of its components. A high viscosity leads to an improved oil recovery because increased viscosity improves mobility ratio (Gandomkar & Kharrat, 2012). Furthermore, a high trapped gas saturation leads to a decrease in the gas phase mobility, which is also favourable for WAG injection. Despite these favourable effects, the addition of surfactants to the recovery process can impose huge costs on the production expenses. Despite these reasons for concern, the implementation of foam-assisted water-alternating-gas injection promises to be an effective upgrade to WAG to improve overall sweep efficiency.

1.1 Background and Context

As primary recovery comes to halt for many fractured carbonate reservoirs, oil companies are in dire need for new cost-effective recovery processes to enhance oil recovery. Foam-assisted WAG is one of such promising methods. The main idea is to decrease gas mobility of the injected gas to have a sharper displacement front and to contact more of the reservoir by avoiding gravity override of the injected gas and underdrive by the injected water. Research has been done on FAWAG reporting of increased oil recovery compared to WAG. In this work, research done on carbonate cores was taken into consideration to create simulation models that replicate the experimental results obtained in the laboratory. The obtained data and foam parameters were then used to further investigate the effects the foam has on the gas mobility and displacement efficiency in a field scale sector model. Especially the movement of the gas movement in fractured reservoirs is of great interest, as research on foam injection in fractured reservoirs is little and production related alteration of reservoir by the formation of gas invaded zones only rarely studied. This research, therefore, tries to elaborate on the fundamental principles and benefits of foam injection in fractured reservoirs with regards to having a high gas saturation occupying the fracture space and surrounding the oil matrix blocks.

1.2 Scope and Objectives

The objective of the thesis is to study the effects of foam-assisted water-alternating-gas injection in naturally fractured carbonate reservoirs on oil recovery, and the foam's ability to decrease gas mobility. By doing so, the potential recovery of field scale operations may be inferred, and the viability of this recovery process can be evaluated.

1.3 Achievements

The mechanisms of foam displacement that lead to an increase of the oil recovery by using a foaming agent as a means of mobility control were studied diligently and compared to previous research done in core flooding experiments. A novelty in this research work is the investigation of the application of foam-assisted recovery processes in gas invaded fractured carbonate reservoirs by applying the derived foam parameters on a field scale model. This has not been done previously.

1.4 Technical Issues

Technical issues that occurred were the unresolved numerical issues that came up in the cross-sectional model to investigate gas phase movement with the hysteresis effect turned on. The simulator could not handle these numerical issues and terminated the simulation runs prematurely. Furthermore, due to the outbreak of the pandemic (COVID-19), access to facilities and devices with proper processing power was severely limited, downsizing the scope of this research and narrowing the time frame for resolving issues such as the one mentioned above.

1.5 Overview of Dissertation

The main purpose of this work was to study the effects that a foam-assisted recovery process has on the gas mobility and the sweep efficiency in naturally fractured carbonate reservoirs and to which extent it can be applied in aiding the oil recovery in gas invaded fracture zones. The analysis of gas movement and oil displacement in gas invaded reservoir zones was the main focus of this research. This thesis is based on research work done on core flooding experiments using CO₂, WAG, and FAWAG injection. PVT data of the reservoir oil was used in regression to achieve a match that suits the phase behaviour of the original oil. History matches of the core floods were then performed using the characterised fluid data to obtain the according relative permeability curves and fitting foam parameters, which were then implemented into a field scale sector model. Furthermore, a sensitivity analysis was done on important fracture parameters used in the reservoir simulator to study their effect on the ultimate oil recovery in gas invaded fractured reservoirs

Chapter 2

State of the Art

Recovery processes in fractured reservoirs vary substantially from those used in non-fractured reservoirs. The reason is related to is the high contrast of capillarity between the fractures and the matrix (Lemonnier & Bourbiaux, 2010). One of the main characteristics of a fractured reservoir is high rate wells in the early stages of development of the reservoir, due to high effective single-phase permeability of the matrix-fracture system in the porous medium. Although the same processes that are active in single-porosity systems are important in fractured reservoirs, there is a stark contrast in flow behaviour between fractures and matrix under two- or three-phase conditions (Lemonnier & Bourbiaux, 2010). These include mechanisms such as (Heinemann & Mittermeir, 2014):

- Rock compressibility and compaction
- Single phase fluid expansion
- Solution gas drive
- Gas cap expansion
- Gravity drainage
- Capillary imbibition
- Diffusion
- Viscous Displacement

For example, in gas-oil gravity drainage, capillary forces impede positive gravity displacement effects on matrix oil recovery. Furthermore, drained oil from the matrix to the fractures can partially or totally re-imbibe neighbouring blocks under the effect of capillary forces. This mechanism is governed by capillary, gravity, and viscous forces. It is affected by compositional effects, such as mass-transfer between phases and diffusion, rendering it a highly complex process with many variables (Lemonnier & Bourbiaux, 2010).

2.1 Production Mechanisms in Fractured Reservoirs

Fractured reservoirs can be produced using several recovery processes depending on their matrix block sizes and matrix/fissure permeabilities (e.g., primary recovery, gas cap expansion, solution gas drive, waterflood, miscible/immiscible gas flood, and enhanced oil recovery) (Lemonnier & Bourbiaux, 2010).

2.1.1 Primary Recovery

In the early stages of production, the total compressibility of the fluids and the fractured rock is the most crucial factor that affects recovery performance, especially when the oil is highly undersaturated (Lemonnier & Bourbiaux, 2010). High compressibility is favourable for an economical depletion of fractured reservoirs with little to no matrix porosity. The duration of the initial high-rate production phase is dependent on the pressure difference between the initial reservoir pressure and the bubble point pressure (Lemonnier & Bourbiaux, 2010).

2.1.2 Gas Cap Expansion

The expansion of gas is a predominant production mechanism in gas fractured reservoirs owing to its high fluid compressibility. In the presence of an active aquifer, the duration of the pressure depletion in the matrix is dependent on the height of the gas column above the gas-water contact (Lemonnier & Bourbiaux, 2010). The expansion of a gas cap is dominated by gravity drainage, and highly permeable matrix blocks are most affected by it.

2.1.3 Solution Gas Drive

During the depletion of a reservoir, the pressure declines. When the pressure falls below the bubble point, mostly in low-pressure regions such as the upper regions of the reservoir or close to the well-bore, gas bubbles start to form within the oil phase. Once reaching the saturation pressure in the matrix blocks, gas bubbles start to appear within the pore network of the matrix (Lemonnier & Bourbiaux, 2010). As long as these bubbles are growing while they remain immobile, an oil phase deprived of gas will be expelled from the matrix blocks and carried to the production wells (Lemonnier & Bourbiaux, 2010). A low gas-oil-ratio [GOR] can be noticed very early on. However, as soon as enough gas bubbles have formed, they start to coalesce and form their own phase and become mobile when the critical gas saturation has been reached (Lemonnier & Bourbiaux, 2010).

Generally, a solution gas drive is an ineffective recovery process for fractured reservoirs, because the gas bubbles expelled from the matrix blocks may segregate within the fractures and form a secondary gas cap. The only exceptions for this are hard-to-produce fields, such as tight,

viscous, and oil-wet reservoirs, where other recovery mechanisms, driven by capillarity and gravity forces, are not effective (Lemonnier & Bourbiaux, 2010).

2.1.4 Secondary Recovery

Injection of water is the preferred method for secondary recovery as it tends to flow through the fracture network. This establishes a high water-saturation boundary on the matrix blocks. The displacement of oil by water in the matrix is then caused by three mechanisms (Lemonnier & Bourbiaux, 2010):

- Spontaneous capillary imbibition of water-wet matrix rocks
- Viscous displacement driven by the pressure gradient generated by flow in the fracture network
- Gravity effects due to the density difference of water and oil

Spontaneous capillary imbibition has been shown to be an ineffective recovery process in oil-wet reservoirs. That is why in such reservoirs other mechanisms such as gravity forces and viscous drive due to fracture flow (Lemonnier & Bourbiaux, 2010).

Gas injection is a compositional secondary recovery process that depends highly on the composition of the oil and the gas, and the reservoir pressure and temperature. Under the right conditions, miscibility can be achieved in theory, creating favourable displacement conditions. However, to achieve such favourable displacement in a fractured reservoir, the injected gas is required not to bypass the matrix oil, but to be driven into the matrix blocks (Lemonnier & Bourbiaux, 2010). Fracture viscous flow effects are negligible in gas injection and only matter in poorly fractured porous media. Diffusion processes are more prevalent in gas injection and are the main driver for gas being pushed into the matrix blocks causing oil swelling and oil viscosity reduction (Lemonnier & Bourbiaux, 2010).

2.1.5 Tertiary Recovery

The efficiency of enhanced oil recovery methods [EOR] varies considerably from one fractured reservoir to another depending on the flow properties of the porous medium and the characteristics of the fracture network (Lemonnier & Bourbiaux, 2010). There are many methods that can be applied, ranging from chemical to miscible displacement to thermal recovery process.

2.2 Reservoir Zonation

Conventional reservoirs and fractured reservoirs are very different in nature. The distribution of the fluids is not the same for both. In a conventional reservoir, the two-phase contacts of water-oil and gas-oil are smooth, and the transition zone may be large in static conditions and thus will remain so in dynamic conditions too (Van Golf-Racht, 1982). During production, gas invaded zones, and water invaded zones may form as a result of extracting oil from the reservoir (Figure 2-1). On the contrary, the transition zone in a fractured zone is sharp and abrupt. The transition zone is, thus, horizontal in static and dynamic conditions, since the transmissivity in a fracture network is high owing to its large permeability of the fractures, and any change in level is rapidly re-equilibrated (Van Golf-Racht, 1982). These fractures are then mostly occupied by only one phase (Figure 2-2).

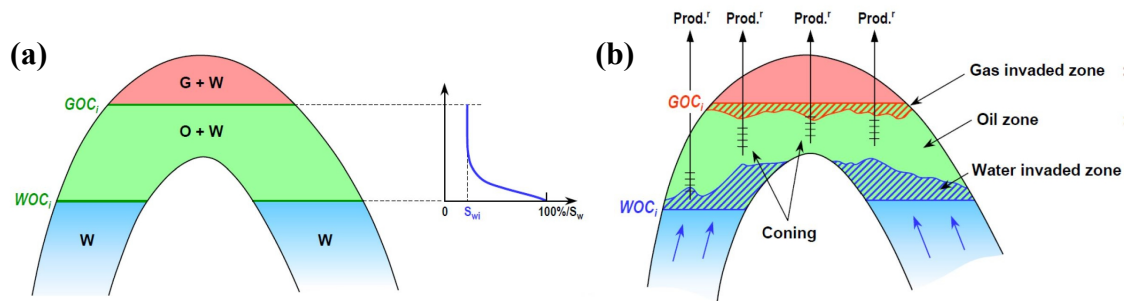


Figure 2-1: Zonation of a conventional reservoir. (a) initial conditions; (b) during production

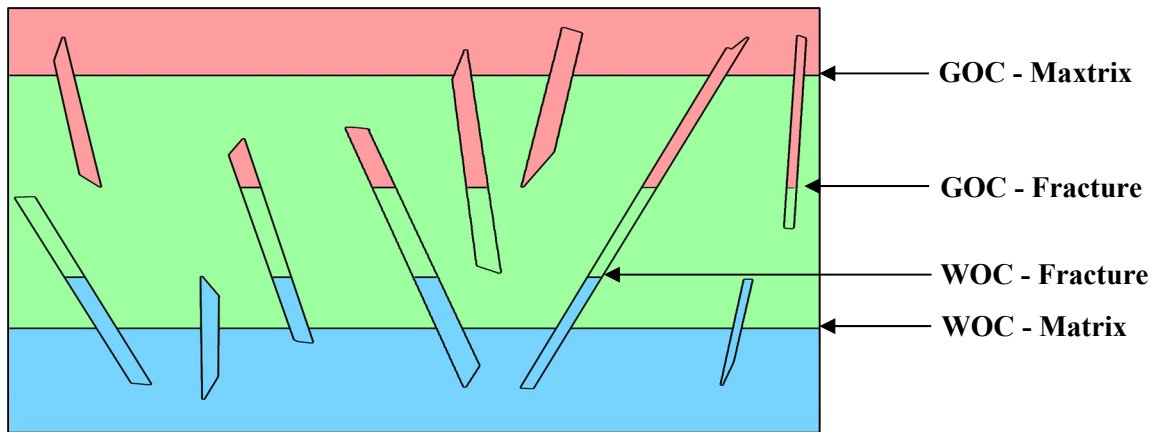


Figure 2-2: Zonation of a fractured reservoir.

According to Van Golf-Racht (1982), a fractured reservoir can be divided into four zones during depletion. Each zone can be a target for EOR depending on the amount of residual oil found in these zones:

- **Gas invaded zone:** in the gas invaded zone, the matrix blocks will be partially or entirely surrounded by gas by having the fractures filled with gas. The oil in the gas invaded zone will be flowing to a large extent through the matrix in spite of the presence of highly permeable fractures. This means that the fracture permeability is not an important factor for the drainage process (Clemens & Wit, 2001). A gas invaded zone may form as result of several mechanisms. First, due to the compressibility of the gas, the gas cap may expand displacing the oil in the fractures. Second, a secondary gas cap may form and surround the oil in the matrix. Lastly, gas injection may form a gas cap and occupy the space in the fractures.
- **Oil gassing zone:** in the gassing zone the liberation of gas from the oil is the main driving mechanism for production. In this zone the pressure tends to be one of the lowest and when reaching the bubble point pressure gas bubble start to form. Circulating liberated gas in the fractures saturated with oil, and the contact between the heavier oil in the fracture network with the lighter oil that is remaining in the matrix blocks, allows for the development of more complex transfer mechanisms (Van Golf-Racht, 1982).
- **Undersaturated oil zone:** in this zone there is only an oil-phase without any free-gas. There is a difference between the pressure between the higher pressured matrix blocks and the lower pressured fractures which leads to an expansion of the rock-fluid system, which in turn acts as a driving mechanisms that pushes the oil from the matrix into the fractures (Van Golf-Racht, 1982). In both the oil gassing zone and the undersaturated zone, which form the oil rim, flow happens predominantly through the fracture network and the fracture permeability determines the well performance (Clemens & Wit, 2001).
- **Water invaded zone:** in the water invaded is characterised by having water occupying the fractures surrounding the oil matrix blocks. Oil recovered from these matrix blocks is sensitive to capillary and gravitational forces and can be aided by injecting water into the aquifer (Van Golf-Racht, 1982).

2.3 Fundamental Reservoir Rock Properties

2.3.1 Relative Permeability and Hysteresis

The relative permeability concept is based on the presence of multiple fluids in a system. They are crucial for understanding a multi-phase system and predicting the performance of immiscible displacement. The relative permeability is a dimensionless measure coefficient of the effective permeability of a specific phase in a multi-phase system. Implementing the relative

permeability into the Darcy equation will give it the ability to describe the multi-phase flow. For phase i is defined as given in eq. (2.1):

$$k_{ri} = \frac{k_i}{k} \tag{2.1}$$

$$q_i = \frac{k_{ri}k}{\mu_i} \nabla P_i \tag{2.2}$$

, where k_i is the effective permeability and k the absolute permeability. The parameters q_i , μ_i , ∇P_i are defined as the flux, the viscosity, and the pressure drop, respectively. The relative permeability is dependent on factors such as phase saturation and pore size distribution (Tiab & Donaldson, 2016).

In a system of two phases, a wetting and a non-wetting phase, each phase flows on its own distinct path. The phases' distribution is subject to the wetting and non-wetting phase's characteristics since the wetting phase occupies largely occupies the small pore space and the non-wetting phase, on the other hand, the free pore space that materially contributes to flow (Ahmed, 2010). The relative permeability highly depends on the saturation of both phases. A low wetting phase saturation is accompanied by a high relative non-wetting phase permeability and vice-versa.

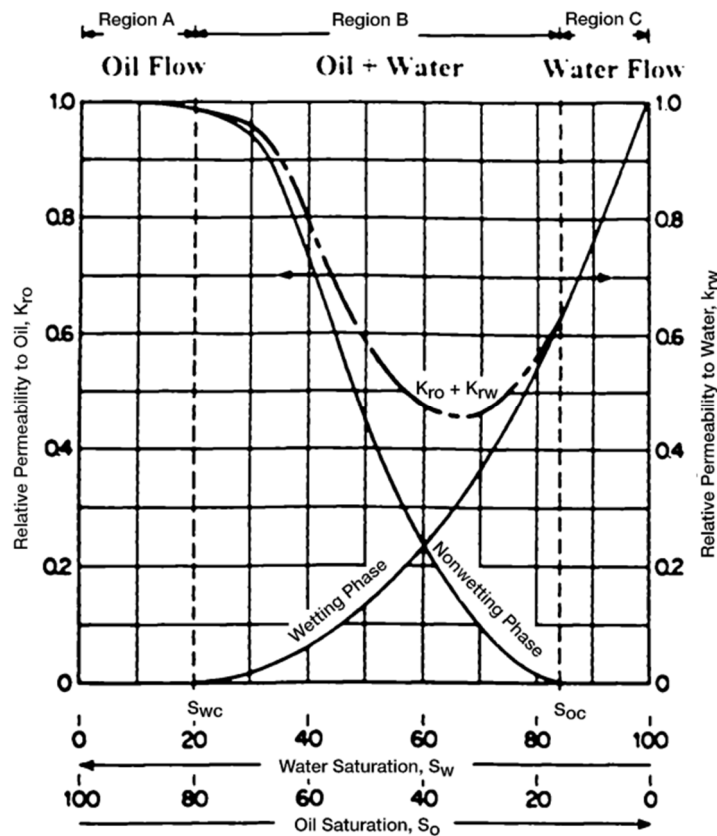


Figure 2-3: Typical two-phase flow behaviour (Ahmed, 2010).

Figure 2-3 shows a typical water-wet system where the water is considered to be the wetting phase. Here a small non-wetting phase saturation, in this case oil, shows a drastic difference in relative permeability with regards to water, where in a single-phase system it would be 1. This can be explained by the aforementioned distribution of the phases. Since the oil occupies the large open pore spaces where the main material flow is taking place, the water flow paths are restricted to the small pore spaces (Ahmed, 2010). Another important fact is that water ceases to flow as soon as the water saturation reaches a low value where the oil saturation is relatively large because water is occupying the small pore space where the capillary forces are the greatest. This point is called the connate water saturation [S_{wc}] and is of great importance to understanding a multiphase system (Ahmed, 2010). One more observation can be made when looking at the lower wetting phase saturations. A change only slightly affects the relative permeability of the non-wetting phase. This can also be attributed to the non-wetting phase's characteristic of occupying the large open pore spaces (Ahmed, 2010). All these observations can also be found in gas-liquid systems, as shown in Figure 2-4.

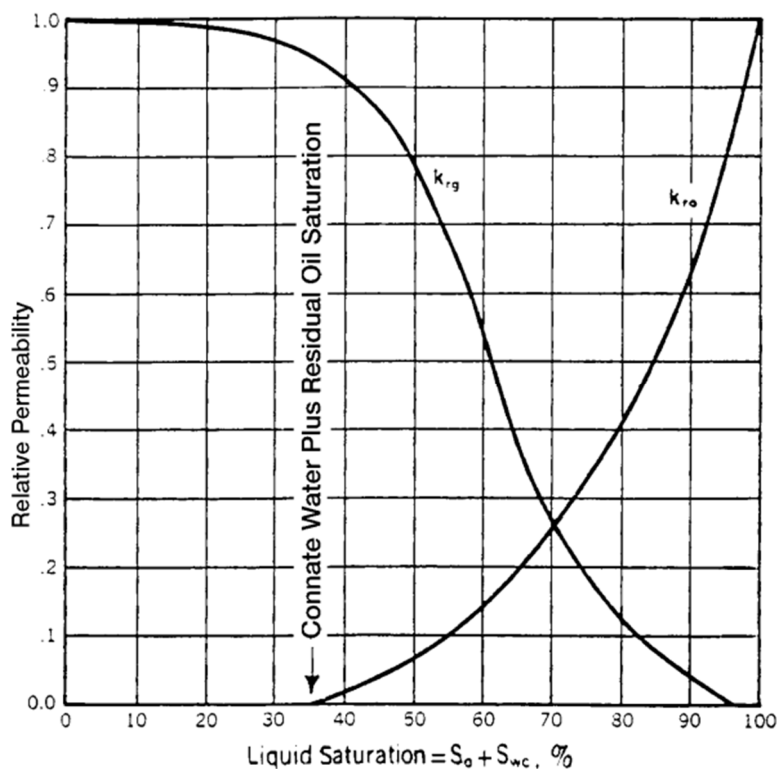


Figure 2-4: Gas-oil relative permeability curves (Ahmed, 2010).

There is another important phenomenon associated with multi-phase flow through a porous medium is the concept of residual saturations. This concept illustrates that two immiscible fluids will never be able to reduce one another to zero. At some small saturation, the flow of the displaced fluid will inevitably cease (Ahmed, 2010). This saturation is known as the residual saturation and it determines the ultimate recovery of a reservoir. Conversely, a fluid must reach a certain minimum saturation before the phase starts to flow, which is referred to as the critical saturation (Ahmed, 2010). This is noticeable in the previously shown relative permeability curves. In theory, the residual saturation and the critical saturation should be the exact equal saturation, but they are not. The main difference is that the critical saturation is measured in the direction of increasing saturation, while the residual saturation is measured in the direction of reducing saturation (Ahmed, 2010).

2.3.2 Relative Permeability Reduction through Hysteresis

The saturation history has an effect on the relative permeability. The difference in relative permeability when changing the saturation history by imbibition (increasing the saturation of the wetting phase) or drainage (increasing the saturation of the non-wetting phase) is referred to as hysteresis and is shown in Figure 2-5.

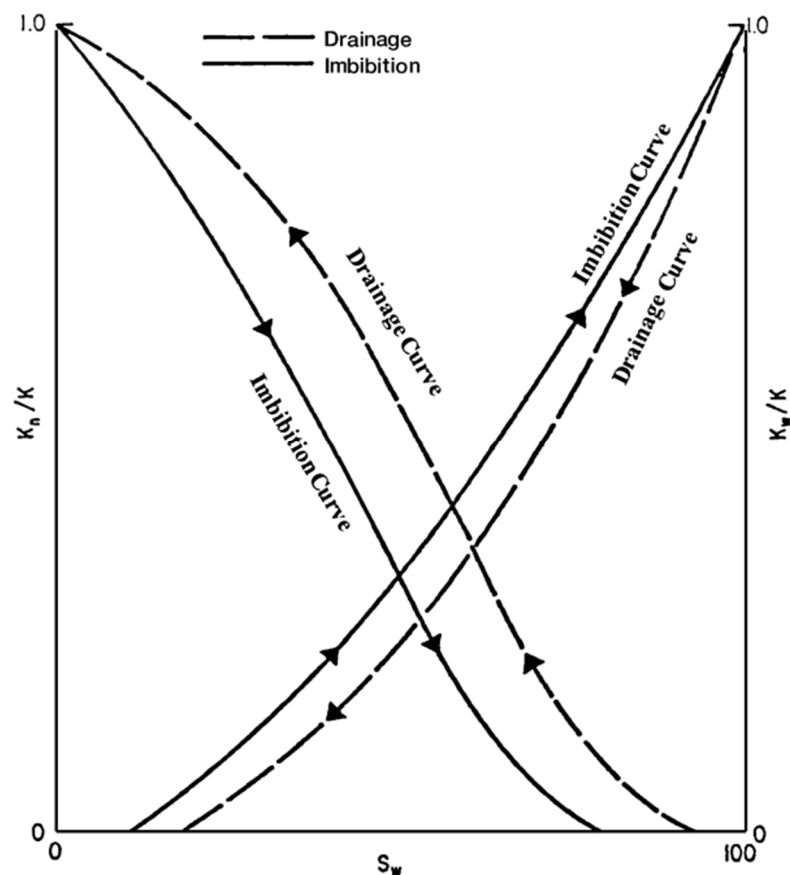


Figure 2-5: Hysteresis effects in relative permeability (Ahmed, 2010).

2.3.3 Relative Permeability Correlations

To simplify the characterisation of permeability properties of a reservoir, several models and correlations have been empirically deduced from real-life experimental data. By entering the required endpoints and exponents, one can create relative permeability models that fit the studied reservoir rock. Corey (1954) postulated such a formulation which is called the “Generalised Corey Correlation”:

$$k_{rw} = k_{rwiro} * \left(\frac{S_w - S_{wcrit}}{1 - S_{wcrit} - S_{oirw}} \right)^{Nw} \quad (2.3)$$

$$k_{row} = k_{roco} * \left(\frac{S_o - S_{orw}}{1 - S_{wc} - S_{orw}} \right)^{Now} \quad (2.4)$$

$$k_{rog} = k_{rogcg} * \left(\frac{S_l - S_{org} - S_{wc}}{1 - S_{gcrit} - S_{oirg} - S_{wc}} \right)^{Nog} \quad (2.5)$$

$$k_{rg} = k_{rgcl} * \left(\frac{S_g - S_{gcrit}}{1 - S_{gcrit} - S_{oirg} - S_{wc}} \right)^{Ng} \quad (2.6)$$

2.4 Miscibility

Miscibility assumes a special role in gas injection as miscibility increases displacement efficiency and ultimate recovery. When a state of miscibility between the oil phase and the injected gas is reached, mobilisation of the trapped oil by initiating a mass-transfer between those two phases.

An increase in the oil phase will result due to this mass transfer which leads to higher mobility of the oil phase. Furthermore, the oil phase’s viscosity is hereby lowered (Green & Willhite, 2018). There are mainly two types of miscible displacement. The first one is classified as first-contact miscible [FCM] and multiple-contact miscible [MCM]. They are distinct in their way of developing miscibility.

2.4.1 First-Contact Miscible Displacement (FCM)

Gas injection is very much based on considerations about three-component mixtures and the illustration by ternary diagrams. Figure 2-6 shows such a three-component mixture consisting of C_1 , C_4 , and C_{10} . The points A and B represent an oil mixture and a heavy gas mixture, respectively. The dashed lines are tie-lines connecting the two equilibrium phases of the gas and liquid compositions. The tangent to the two-phase envelope passing through the critical

point (plait point) is termed the critical tie-line. Miscibility is determined by the position of the initial oil and gas compositions relative to the critical tie-line (Green & Willhite, 2018).

If the straight line of the dilution path between the two mixtures A and B does not intersect the two-phase area of the crude oil. In this case, the requirement is met, and the displacement of all mixtures between A and B will consist of a single hydrocarbon phase. A displacement that occurs entirely within one hydrocarbon phase is “first-contact miscible” (Lake, 1989).

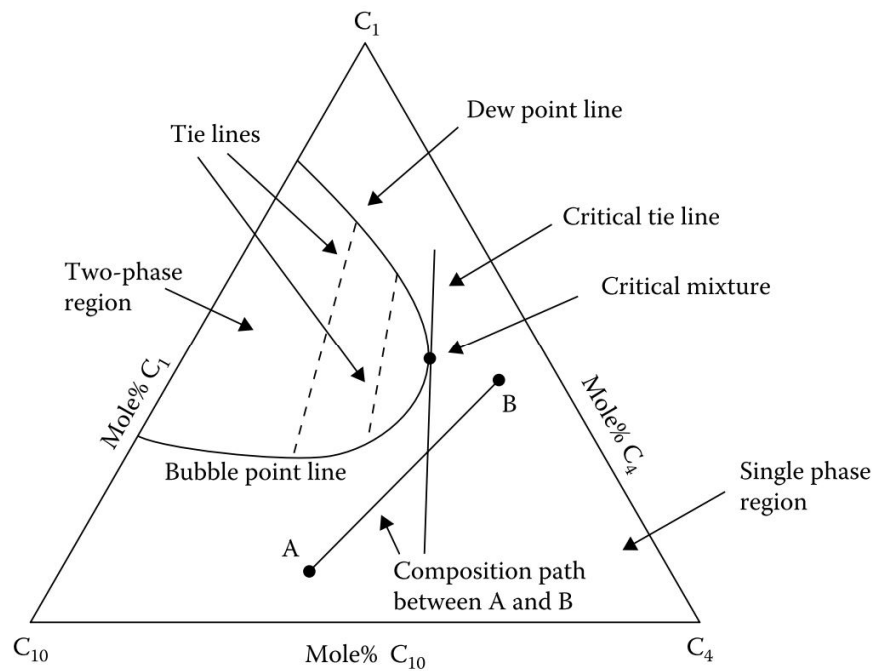


Figure 2-6: Ternary diagram for mixtures of C_1 , C_4 , and C_{10} . Compositions A and B are miscible by first contact (Pedersen, et al., 2015).

2.4.2 Multiple-Contact Miscible Displacement [MCM]

A displacement is called “multiple-contact miscible” when an injected gas, which is not miscible with oil at first contact, achieves miscibility during a dynamic fluid-mixing process that involves multiple contacts and mass transfer between the crude oil and the gas. These in-situ mass transfers of intermediate molecular weight components between the gas and oil phases lead to the formation of mixtures that are miscible with either the injected gas or the crude oil. Multiple-contact miscible displacements can be categorised as “vaporising-gas (lean gas)”, “condensing”, “condensing/vaporising-gas (enriched-gas)” displacements and CO_2 displacements (Green & Willhite, 2018).

2.4.3 Vaporising Gas Drive [VGD]

A vaporising gas is characterised by the fact that the composition of the injection gas is located on the two-phase side of the critical tie-line and the composition of the original oil on the single-

phase side. In Figure 2-7, we can see that the critical tie-line intersects the two-phase area. Herein miscibility is achieved through a vaporising process. By injecting enough gas into the original oil, two phases are formed (Pedersen, et al., 2015). The newly formed gas composition may contact the original reservoir oil and a new gas phase, which contains more heavy components and is more alike to the composition at the critical point, will form as a result (Pedersen, et al., 2015).

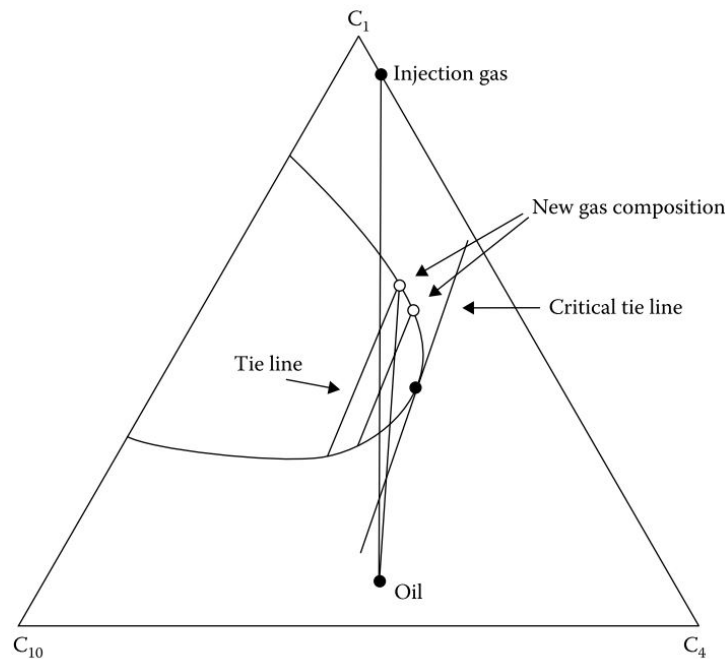


Figure 2-7: The principle of vaporising gas drive illustrated in a ternary diagram for a mixture of C_1 , C_4 , and C_{10} (Pedersen, et al., 2015).

After multiple contacts, the gas composition may become equal to that of the critical point, which is miscible with the original oil. Therefore, only one phase will form, regardless of the proportion at which the critical mixture and the oil are mixed. The term “vaporising” is used because the gas is gradually enriched with intermediate-molecular-weight components. In Figure 2-8, the vaporising process is illustrated. Here the injection gas contacts the oil directly at the injection well and gradually takes up intermediate-molecular-weight components. Because of the higher mobility of the gas, the gas is then pushed away from the injection well, while constantly gathering more components from the oil, until full miscibility is reached after multiple contacts (Pedersen, et al., 2015).

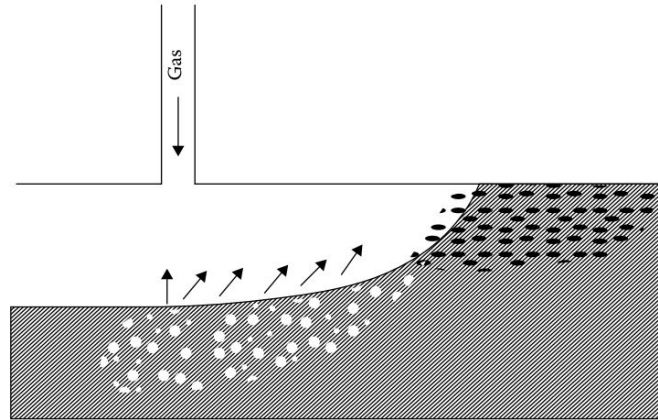


Figure 2-8: Miscibility obtained through a vaporising drive. Passing through the reservoir, the gas takes up components from the oil phase and develops miscibility at the gas-oil front (Pedersen, et al., 2015).

2.4.4 Condensing Gas Drive [CGD]

In the case of the condensing gas drive process (Figure 2-9), the composition of the injected gas is found on the single-phase side, whereas the composition of the original oil happens to be on the two-phase side of the critical tie-line. The line connecting both fluids intersects the two-phase area.

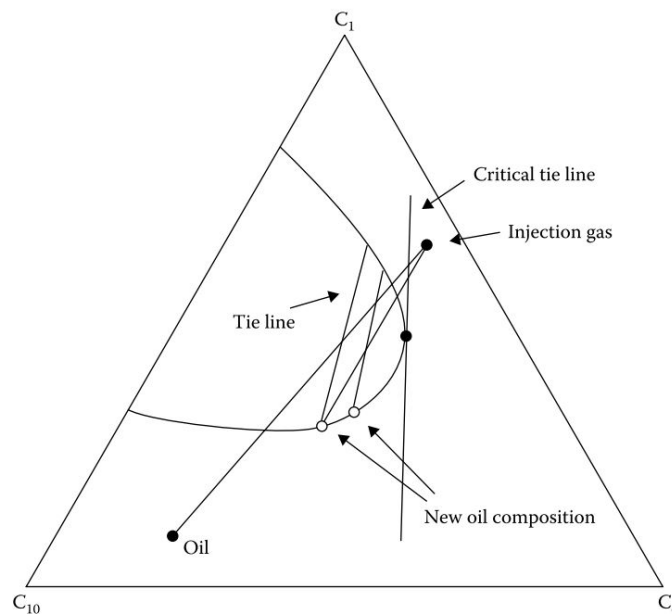


Figure 2-9: The principle of a condensing drive illustrated in a ternary diagram for a mixture of C_1 , C_4 , and C_{10} (Pedersen, et al., 2015).

When the oil gets in contact with enough the injection gas, two phases are formed, and the oil will take up intermediate-molecular-weight components from the gas phase, increasing its similarity to the composition at the critical point (Pedersen, et al., 2015). The old gas is then

pushed away by new injection gas. When the oil that has already taken up some of the gas' components is contacted again by fresh gas, more heavy gaseous components will condense into the oil phase. At some point, the oil phase will reach a composition that is identical to the one at the critical point and, thus, miscibility will be achieved (Pedersen, et al., 2015). **Fehler! Verweisquelle konnte nicht gefunden werden.** Figure 2-10 illustrates the condensing gas drive process.

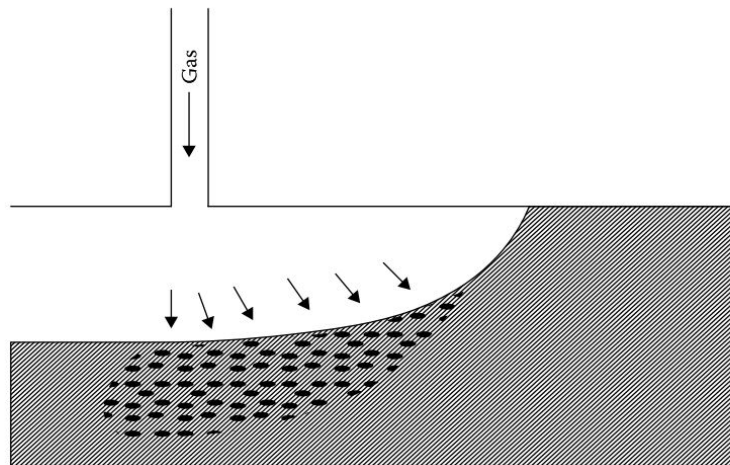


Figure 2-10: Miscibility obtained through a condensing drive. Miscibility develops near the injection well (Pedersen, et al., 2015).

2.4.5 Condensing/Vaporising-Gas Drive (Enriched-Gas)

A combination of both condensing and vaporising gas drive is also a possibility. The description of such a process is difficult because there are limitations to a pseudo-ternary diagram as it is only able to describe three components. In contrast, oil and gas are usually composed of many more components. To improve the description of this mechanism, it is assumed that the oil and gas system is composed of four groups of hydrocarbons (Green & Willhite, 2018):

1. Lean components (C_1 , N_2 , and CO_2)
2. Light intermediate components (C_2 to C_4)
3. Intermediate components (C_4 to C_{10})
4. High-molecular-weight components (components that cannot be vaporised from the oil)

The oil becomes lighter when enriched gas, containing components from groups 1 and 2, contacts the oil reservoir, and light intermediates condense into the oil (Green & Willhite, 2018). The lighter gas moves ahead of the oil while fresh gas is being injected simultaneously. This could be a condensing gas drive when continued, but there is a countereffect. Middle intermediate components in the oil are stripped from the oil phase into the gas phase because

these components were not initially present in the gas. This means that the oil at the upstream location tends to become saturated with light intermediates but depleted of middle intermediates (Green & Willhite, 2018). If this were all that occurred, no miscibility between the injected gas and the reservoir oil could be achieved, and the process would be inefficient. However, after some period of injection, a gas that is rich both in light and middle intermediates can be observed at the downstream. This is due to the middle intermediates being stripped away from the oil, enriching the downstream gas. Although this condensing/vaporising process may never reach full miscibility, the displacement process is still very efficient (Green & Willhite, 2018).

2.4.6 CO₂ Miscible Displacement Process

CO₂ miscible displacement can be described by a pseudo-ternary diagram that is essentially the same for the high-pressure vaporising process. The primary difference is that at same pressure and temperature conditions, the two-phase area is substantially smaller for a CO₂ system than for CH₄ system (Figure 2-11). Furthermore, the limiting tie-line for the carbon dioxide system tends to have a slope that is more parallel to the CO₂/C₇₊ side of the ternary diagram than a CH₄ system. This means that miscibility between carbon dioxide and the reservoir oil can be achieved at much lower pressures than between methane and the reservoir oil (Green & Willhite, 2018). Achieving miscibility at much lower pressures is the most beneficial characteristic of CO₂.

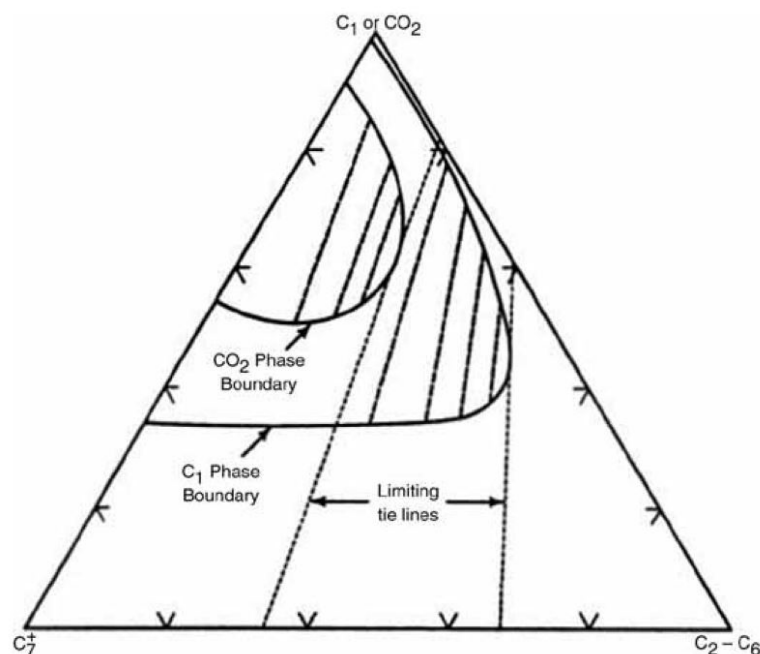


Figure 2-11: Comparison of two-phase envelopes for methane/hydrocarbon and CO₂/hydrocarbon systems (Green & Willhite, 2018).

Adding CH₄ to the system will change the phase behaviour, namely increasing the pressure at which miscibility occurs. This is also achieved by adding non-condensable gases, such as N₂ or O₂. Liquefied petroleum gas components, such as C₂ or C₃, or H₂S, are helpful to offset the effect that methane has on the miscibility pressure (Green & Willhite, 2018). Another characteristic of the CO₂ phase behaviour is that often two liquid phases or two liquid phases and a vapour phase are formed at lower temperatures (below 50°C) (Green & Willhite, 2018). Under such conditions, the process is difficult to depict on a pseudo-ternary diagram.

2.4.7 Minimum Miscibility Pressure (MMP)

The reservoir must be operated at or above MMP to develop miscibility. Any pressure below will lead to immiscible displacement. Oil recovery has been observed when increasing the displacement pressure, however, recovery above MMP is usually small (Ahmed, 2016). The extraction of hydrocarbons from crude oil is strongly influenced by the density of the CO₂, and it can be improved by increasing the density of the CO₂ that is usually accompanied by increasing pressure, which in turn accounts for the development of miscibility. The presence of N₂, O₂, or CH₄ is known to increase the minimum miscibility pressure of carbon dioxide (Ahmed, 2016).

2.5 Physical and Chemical Properties of CO₂

CO₂ has long been a valuable gas used in EOR projects. Understanding its physical and chemical properties are crucial when injecting it into a reservoir or core to maximise oil recovery. It is a colourless gas with a density of 1.977 kg/m³. At reservoir conditions, CO₂ mostly assumes a supercritical state where it behaves like a gas while exhibiting a liquid-like density. This state is reached when the temperature is above 31.04 °C or 304.19 °K, and the pressure above 7.39 MPa or 73 bar. Under this state, CO₂ may be called “scCO₂” or “sCO₂”.

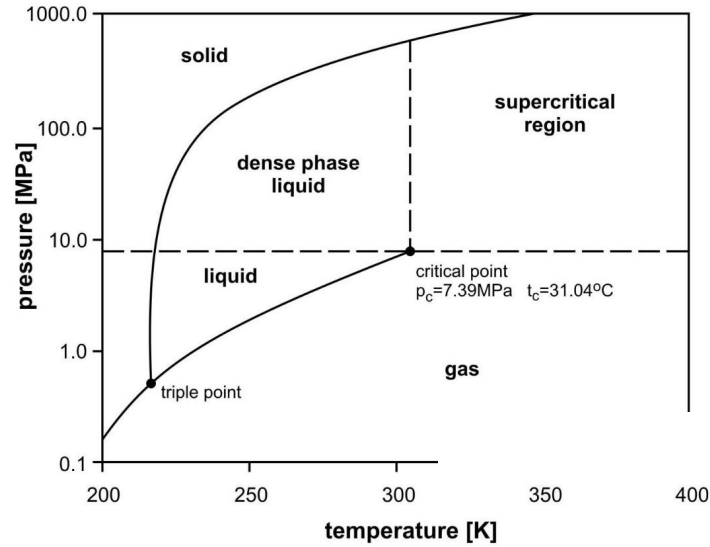


Figure 2-12: CO₂ Phase Diagram (Witowski, et al., 2014) [modified]

CO₂ also has the ability to dissolve into water and exists in chemical equilibrium with carbonic acid, which is classified as a weak acid. In such a form, the carbonic acid can interact with the reservoir rock and may alter the rock structure and its flow properties.



Carbon dioxide is characterised by its vapour-like viscosity and its oil-like density (Sheng, 2013). The injection of CO₂ is a process called “multiple-contact-miscible process”. This means that the carbon dioxide is not miscible with the reservoir oil at first contact and, instead, relies on the modification of the injected phase, or oil phase through multiple contacts between the phases and mass transfer of components between them (Green & Willhite, 2018). The high and intermediate hydrocarbons are extracted into the CO₂ phase through the multiple contacts between the carbon dioxide and the oil phase. This is aided by the fact that CO₂ has a very low minimum miscibility pressure. The goal is to contact as much of the reservoir as possible to mobilise the oil that is trapped by capillary forces. Under proper conditions, miscible conditions exist at the displacing front interface and ideally exhibits a piston-like displacement (Sheng, 2013).

2.5.1 Advantages and Disadvantages of CO₂ Usage

CO₂ is a gas with a relatively low minimum miscibility pressure compared to other gases. Miscibility is achieved at pressures of only 100 to 300 bars (Skjæveland & Kleppe, 1992). This means that CO₂ can theoretically displace all the oil on a microscopic level that it gets in contact

with. However, its high mobility makes it more difficult for the carbon dioxide to contact the whole reservoir and makes it inefficient on a macroscopic level. CO₂ possesses a higher density compared to other gases, and with pressure, it can even reach densities similar to oil. Such a high density is especially viable in horizontal displacement processes because a large density difference between the fluids is favourable in a gravity-stable process and minimises the chance of segregation (Skjæveland & Kleppe, 1992). CO₂ is soluble in water and can, therefore, more easily reach oil that is shielded by water.

Furthermore, CO₂ causes oil swelling. Oil swelling is the process when CO₂ enters the oil phase and decreases the oil viscosity, leading to a more favourable mobility ratio (Skjæveland & Kleppe, 1992). Given enough time, oil swelling can lead to the mobilisation of trapped immobile oil by breaking through the water barrier (Grogan & Pinszewski, 1984).

The disadvantages of CO₂ are plenty. As mentioned before, the density difference leads to an unfavourable mobility ratio. This can cause carbon dioxide to flow through high permeable zones and may even lead to fingering. Furthermore, CO₂ has acidic properties that can corrode piping equipment. Lastly, CO₂ is quite expensive to separate from the oil and expensive to capture, making it a costly investment.

Chapter 3

Enhanced Oil Recovery

3.1 Enhanced Oil Recovery Methods [EOR]

The economic viability of a well is dependent on the ultimate oil recovery of the reservoir. Conventional recovery methods, which include primary and secondary recovery, are only able to support an ultimate recovery rate of up to 45% in the best cases (Tzimas, et al., 2005). This means that an increase of a few percent would significantly improve the economic outlook of a well and the oil field.

There are many kinds of EOR methods. The three major types applied are chemical flooding, miscible displacement, and thermal recovery. Chemical flooding includes alkaline flooding, polymer flooding, and foam flooding. Miscible displacement is mostly the injection of carbon dioxide or light hydrocarbons. Thermal recovery uses the heat of steam or in-situ combustion to decrease the viscosity of the oil for an increase in oil production. The optimal application of the types of EOR methods mentioned above is highly dependent on the characterisation of the reservoir and its properties, such as the pressure, temperature, depth, permeability, porosity, saturation, etc. and fluid properties.

Water flooding is not included in the definition of enhanced oil recovery methods, as it is considered a pressure maintenance process. Often it is not clear as many pressure maintenance processes have displacement character (Lake, 1989). Furthermore, neither carbon dioxide nor methane does satisfy the definition, yet both are EOR processes (Lake, 1989).

3.2 Gas Injection and CO₂ Flooding

Injection of different gases has been used commercially as viable improved and enhanced oil recovery strategies to recover oil from hydrocarbon reservoirs for more than 40 years. The

injection of CO₂ is a gas injection strategy where carbon dioxide is injected into a reservoir at a high pressure to typically increase the oil recovery of already waterflooded reservoirs that reached residual oil saturation.

Although its longstanding success and its capability of displacing nearly all of the oil located in the porous media through which it flows, flooding a reservoir with carbon dioxide does not guarantee recovery of more than 10%-20% of the original oil in place. Not surprisingly, the injection of CO₂ at immiscible conditions yields even less recovery, 5%-10% (Enick, et al., 2012). Unfortunately, ideal conditions are rarely reached. Carbon dioxide has a critical temperature of 31.04°C and is mostly injected at temperatures above its critical temperature, meaning that the viscosity is between 0.06 and 0.10 cp, and this leads to unfavourable mobility ratio conditions (Green & Willhite, 2018). The low density of super critical CO₂ relative to the oil's density leads to gravity override, reducing oil recovery in the lower portions of the reservoir (Enick, et al., 2012). Combined with reservoir heterogeneities and gravity override, fingering of the CO₂ phase occurs in the high permeability layers and, thus, lowers displacement efficiency and leads to an earlier breakthrough (Green & Willhite, 2018). To overcome this problem, the approach of alternating water and gas injection or the use of mobility reducing agents have been proposed.

3.3 Water-Alternating-Gas Injection [WAG]

As a means to improve oil recovery, while reducing the cost of pure gas injection, the alternate injection of water and gas has been developed. When using this method, several slugs of water are injected alternately. WAG can may significantly improve sweep efficiency. Since water is less mobile owing to its greater viscosity than CO₂ it can therefore improve the average mobility ratio of the flood. It can also cover more of the deeper sections of a reservoir due to underriding (Sheng, 2013). It has been found to be an excellent method for mobility control and cost lowering as it injects less gas in favour of cheaper water and has ever since been the first choice in improving overall sweep efficiency (Sheng, 2013). A common problem that may arise during displacement is that gas may tongue upward (gravity overriding) in the formation during the gas injection cycle, whereas water tongues downward during the water injection cycle (Sheng, 2013). This effect is illustrated in Figure 3-1.

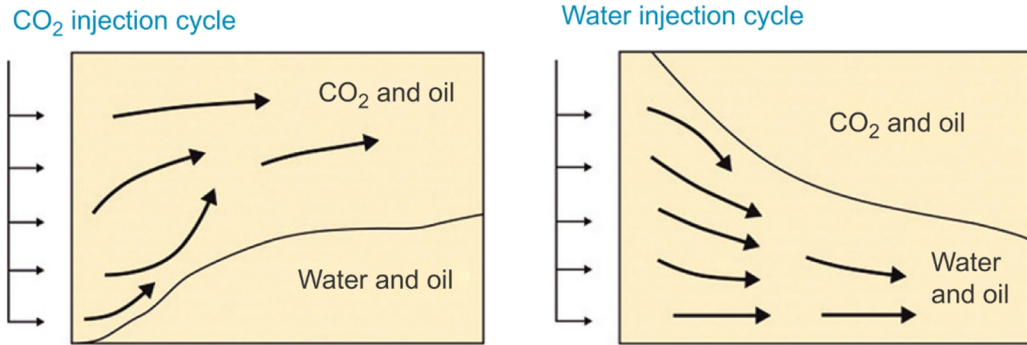


Figure 3-1: During WAG, gas can move upward owing to its low density, while injected water can move downwards (Jarrell, et al., 2002).

For this to happen, there must be a sufficient vertical permeability and density difference between the gas and the reservoir fluids. Water and gas usually form a channel in the high-permeability layers while dominating over gravity tonguing. The channelling becomes more significant with increasing heterogeneities, increasing permeability differences, decreasing density differences, and increasing fluid velocities (Sheng, 2013). The design of the WAG process is of utmost importance as the injection of too much water or too much gas may impair the vertical sweep efficiency. Therefore, the volumes should be adjusted accordingly. Reservoirs that own a low-permeability layer at their top perform better than those which have a high-permeability layer (Sheng, 2013). Figure 3-2 shows a typical water-alternating-gas process where CO₂ is injected in several slugs is illustrated in.

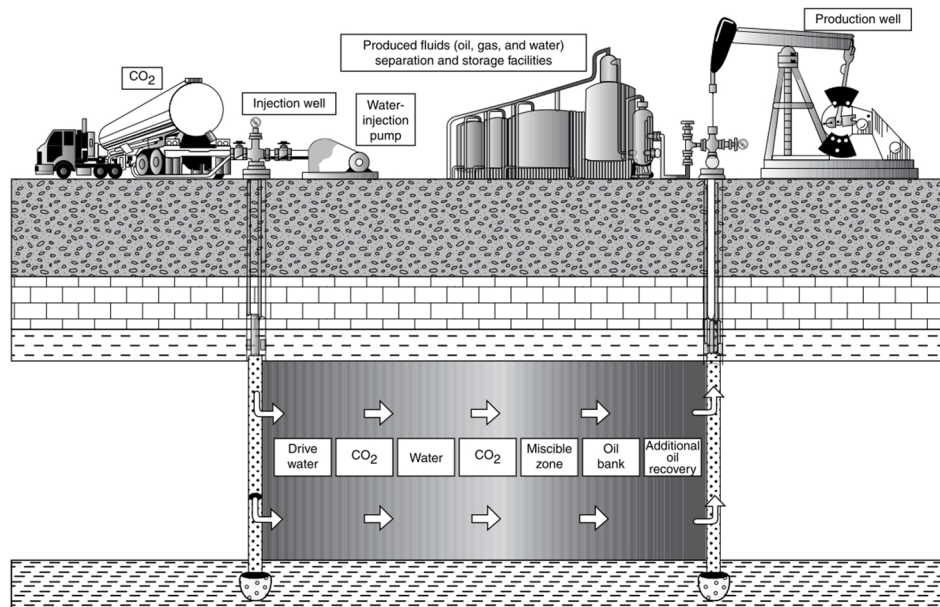


Fig. 1.5—CO₂ miscible process (after US DOE).

Figure 3-2: drawing by Joe Lindley, U.S. Department of Energy, Bartlesville, OK.

3.4 Chemical EOR

Chemical flooding is one of the three major types of EOR techniques, which includes foam, alkali, polymer and surfactant injection, and several combinations of them. The goal of the process is the increase of the oil recovery by a reduction of the displacing agent's mobility (control of mobility) or by lowering the interfacial surface tension between the oil phase and the water phase (Lake, 1987).

Mobility control processes inject a high viscosity agent such as polymers into the reservoir to achieve an increase in viscosity of the displacing agent (usually water). Foam flooding, on the other hand, attains lower mobility by applying surfactants to form stable gas-liquid foams.

Lowering the interfacial surface tension is the other principal of chemical EOR for enhancing recovery. Methods based on this principle rely on injecting or forming in-situ surface agents that target the interface between water and oil and lower its tension. A reduction of the IFT leads to improved recovery and a lower residual oil saturation [ROS] (Lake, 1989).

3.5 Foam Flooding

Foam flooding is a chemical enhanced oil recovery method that uses surfactants to reduce gas-phase mobility through the formation of stable gas-liquid foams. They find many uses in mobility control and well treatment. The most important of them might be the application of foam as a mobility control agent in miscible floods (Lake, 1989).

Foams are dispersions of relatively large gas bubbles in rather small volumes of liquid (Raza, 1970). Foam is produced when a liquid containing a small concentration of surfactants (foaming agent) comes into contact with a gas, provided that there is enough kinetic energy to initiate the generation. Common for such dispersions is their instability and their tendency to break quickly. The addition of surfactants as foaming agents to the liquid greatly enhances the stability of the foams (Lake, 1989). Foams are used in EOR processes mainly because of their high resistance to flow when displaced through a porous medium. The resistance of the individual phases that make up the foam is markedly lower than the foam itself. Therefore, foams are a suitable candidate for improving displacement efficiency (Green & Willhite, 2018). (Raza, 1970) proposed three different applications for foam to be used as an EOR agent:

1. For blocking or restricting the flow of unwanted fluids (inhibiting the formation of gas or water cones in production wells).
2. For blocking or restricting the flow of injected fluids in high permeability streaks or fracture networks.

3. For improving the mobility ratio by achieving a reduction of the mobility of the injected phase (mostly gas).

3.6 Foam Characteristics

Figure 3-3 is a schematic of a foam system. In Figure 3-3, one can see that a gas phase is separated from a thin liquid film by an interface. Each one of these thin liquid films is sided by two interfaces. A thin liquid film connected to a junction is called a lamella. A junction connected to three lamellae is referred to as a Plateau border (Sheng, 2013).

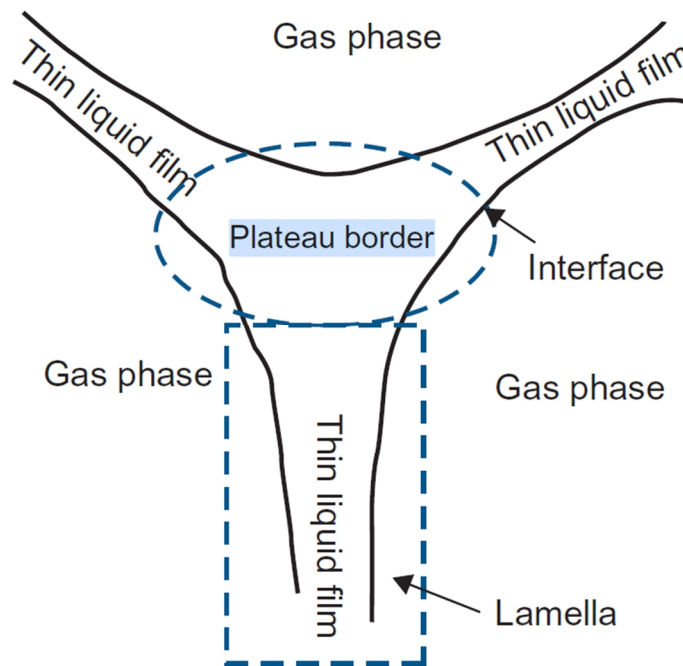


Figure 3-3: Schematic of a foam system (Sheng, 2013).

Three different kinds of constellations may appear (Nikolov, et al., 1986):

- Foam films (gas – water – gas)
- Emulsion films (oil – water – oil)
- Pseudoemulsion films (oil – water – gas)

Other foam constellations include (Sheng, 2013):

- Wet foam (kugelschaum): spherical bubbles separated by thick layers of liquid
- Dry foam (polyederschaum): polyhedral bubbles separated by thin, plane films

Foams are a mixture of water, gas, and foaming agents (surfactants). Foam appears by agitating a liquid that contains a small amount of foaming agent and is in direct contact with a gas. Foaming agents are necessary. Otherwise, the foams are short-lived and unstable.

Foams are described by three different qualities (Lake, 1989):

1. **Foam quality:** The volume of gas in the foam is expressed as a percentage of the total foam volume. The quality depends highly on temperature and pressure as the gas volume is highly variable. Furthermore, gas may be dissolved in the liquid phase and come out of the solution. Foam quality higher than 90% is referred to as dry foam (Lake, 1989).
2. **Foam texture (average bubble size):** Texture size may range from 0.01 – 01. μm up to that of a macroemulsion. The texture determines the flow characteristics of the foam through a permeable medium. Figure 3-4 shows the distribution of bubble sizes:

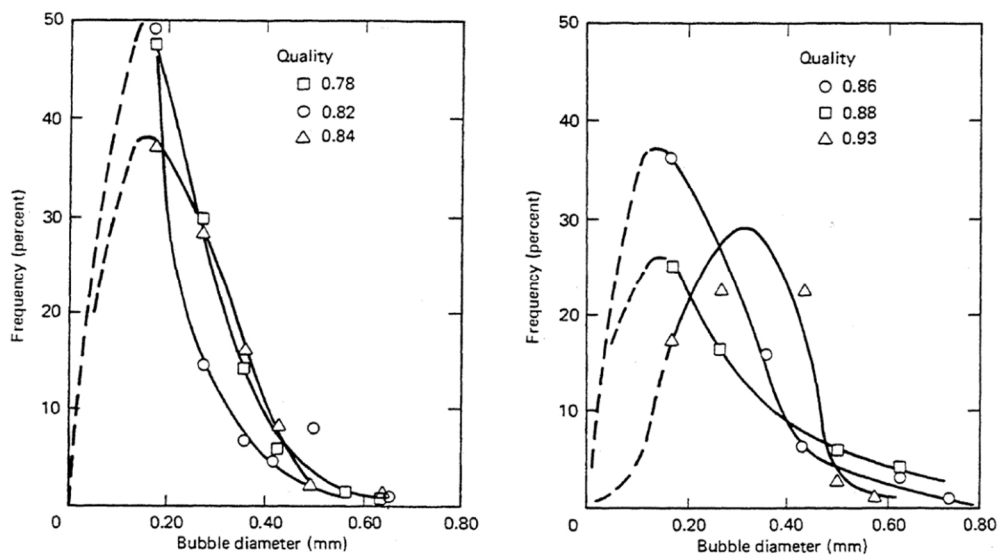


Figure 3-4: Bubble size frequency distributions (David & Marsden, 1969).

An average bubble size smaller than the average pore diameter leads to a dispersed flow of the foam bubbles through the pore channels. Bigger bubble sizes will cause the foam to flow as a progression of films that separate individual gas bubbles. Bigger bubble sizes are often attributed to high quality foams and more easily realised (Lake, 1989).

3. **Range of bubble sizes:** Foams with a large distribution range are prone to instability (Lake, 1989).

Foam measures are therefore undoubtedly analogue to permeable media properties. The foam quality is similar to porosity, and texture resembles the mean pore size, and the bubble size and pore size distributions are alike. Comparing similar qualities is a valid method explaining foam flow in porous media (Lake, 1989).

3.6.1 Foam Stability

Essentially, foams are not thermodynamically stable. They are bound to collapse eventually. The term stability is used in a kinetic sense (Sheng, 2013). The stability of foams is influenced by many factors, including the bulk solution and interfacial properties. When looking at the liquid film separating the two gas bubbles, one can see that the polar heads of the surfactants are facing the interior of the film and that the nonpolar tails are oriented towards the gas phase, except in rare cases (Lake, 1989). The surface tension between the gas and the liquid is a function of the surface adsorption and it is defined as the difference between surface and bulk concentration. As an example, a typical surface tension and adsorption profile for a surfactant is shown in Figure 3-5.

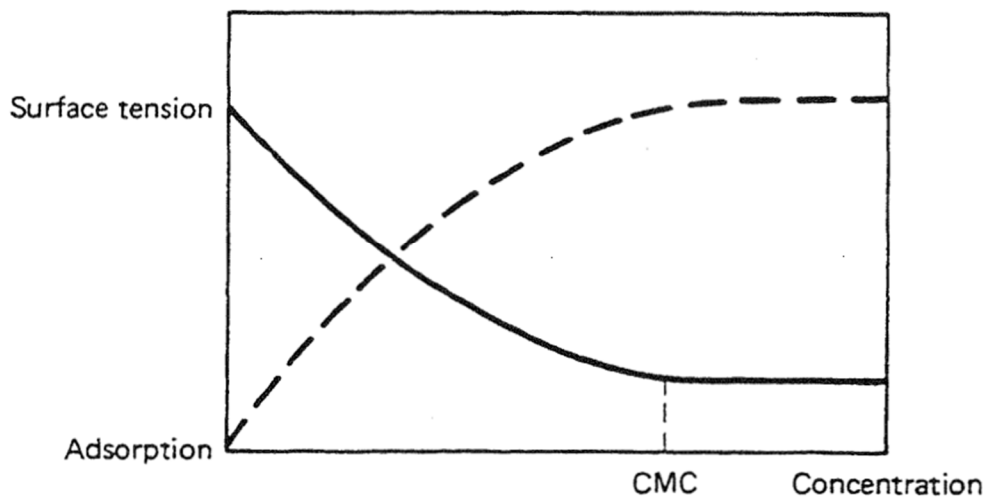


Figure 3-5: Surface tension and adsorption of a surfactant versus concentration (Lake, 1989).

Should an external force thin out the film, the surface area would increase and therefore cause the surface surfactant concentration to decrease. The, thereby, surface tension, which, on the other hand, promotes a surface tension boundary along the film. That allows the film to easily regain its original state, since the capillary pressure is inversely proportional to the interfacial curvature and the pressure in the thinner portion is lower. This effect is called Gibbs-Marangoni effect and can be seen in Figure 3-6 (Lake, 1989).

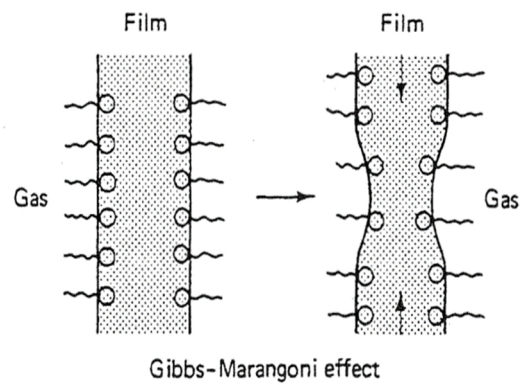


Figure 3-6: The mechanism of film stability (Lake, 1989).

Usually, gas-liquid surface tensions are rarely lower than 20 mN/m and are, therefore, rather favourable for foam stability. In general, the film is always in a state of equilibrium when no external forces are exerted on it (Lake, 1989).

3.6.2 Mobility Reduction

Foams are known to drastically reduce the mobility of the gas phase when flowing through porous media. Figure 3-7 shows the steady-state mobility of foams of differing qualities at three different permeabilities (Lake, 1989).

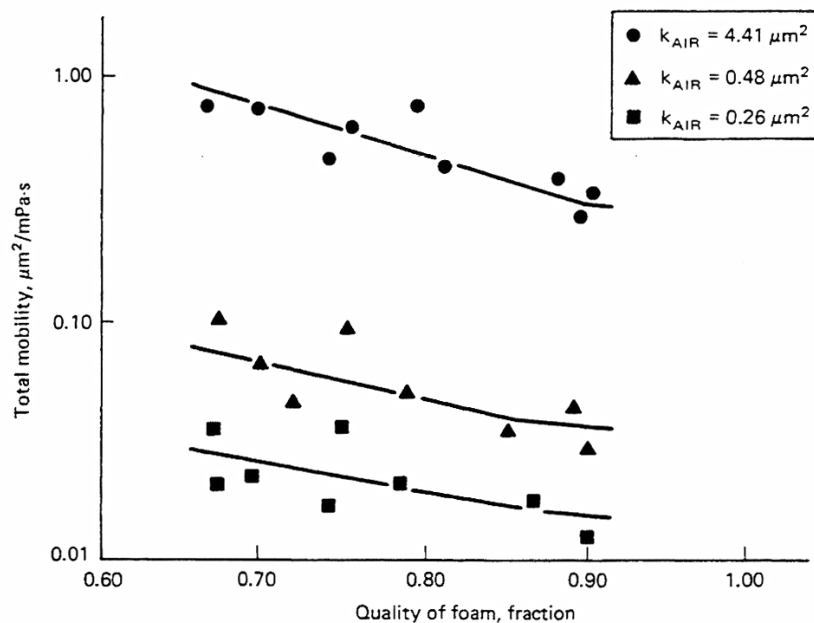


Figure 3-7: Effective permeability-viscosity ratio versus foam quality for consolidated permeable media and 0.1% aerosol foam (Lake, 1989).

Here the observed mobilities are less than the single phase mobility of water and substantially less than the single phase mobility of the gas, proving that the foam's mobility is lower than

that of either constituent (Lake, 1989). An increase in foam quality is followed by a decrease in foam mobility until the films between the gas bubbles break. The collapse of the foam bubbles leads to an increase in gas mobility. The effect of the foam quality is rather similar for lower permeabilities but increasingly stronger for higher values.

It is assumed that mobility decrease is caused by two particular mechanisms (Lake, 1989):

1. Formation of or the increase in trapped residual gas phase saturation.
2. Blockage of pore throats due to gas films.

3.6.3 Foam Formation, Decay, and Collapse

There are essentially three different mechanisms that allow the foam to form (Sheng, 2013):

1. **Snap-off:** This mechanism occurs when a bubble penetrates a pore throat and a new bubble is formed. The gas is thereby put into a discontinuous form, which alters the flow properties of the gas phase. The newly formed gas bubbles may get stuck in the porous medium and impede the gas pathways, hence reducing the gas permeability (Sheng, 2013). This incident may repeatedly occur at the same pore throat. That means that a single site may affect a relatively large portion of the flow field. This mechanism is shown in Figure 3-8 and is the main driving mechanism for foam generation (Ransohoff & Radke, 1988).

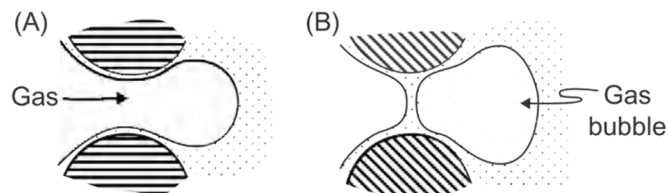


Figure 3-8: Schematic of snap-off mechanism (A) gas penetrates to a constriction and a new bubble is formed (B) (Ransohoff & Radke, 1988).

2. **Lamella division:** This mechanism occurs when a lamella approaches a branchpoint dividing the lamella into two or more lamellae. This mechanism resembles a snap-off in many ways as separate bubbles are formed that can flow or block pathways. Numerous occurrences are also possible. Both mechanisms are mainly in effect at high velocities (Sheng, 2013). Figure 3-9 depicts a lamella division.

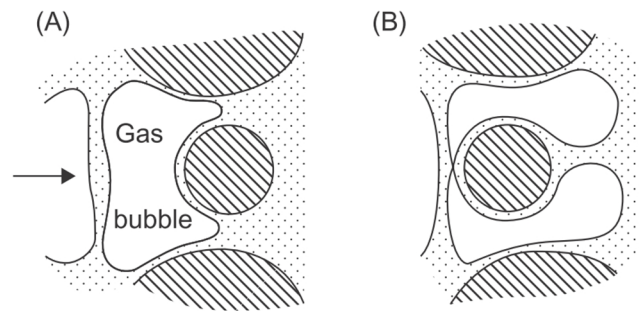


Figure 3-9: Schematic of lamella division mechanism, lamella at the branch point (A) and divided gas bubbles formation (B) (Ransohoff & Radke, 1988).

3. **Leave-behind:** This mechanism starts as soon as two gas menisci invade adjacent liquid-filled pore bodies from different directions (shown in Figure 3-10). As the two menisci are converging downstream, a lens is left behind. A large quantity of lamellae may form a barrier to the gas pathways. This type of blockage and the formation of dead-end pathways ultimately reduce the relative permeability to gas. The leave-behind mechanism is especially prevalent in low velocity domains and typically generates weak foams (Sheng, 2013).

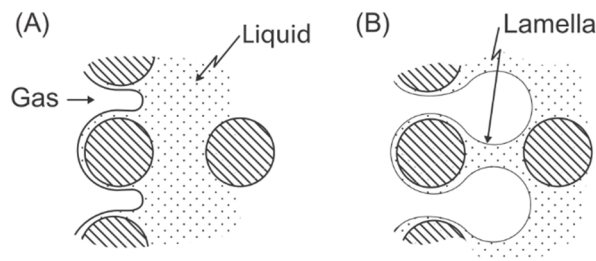


Figure 3-10: Schematic of leave-behind mechanism showing gas invasion (A) and forming lens (B) (Ransohoff & Radke, 1988).

Leave-behind generates stationary aqueous lenses when the aqueous phase saturation is high. It is not a repetitive process. That is the reason for its low impact on mobility reduction (Ransohoff & Radke, 1988).

The destruction of foam (coalescence and decay) is believed to be the result of two different mechanisms (Chambers & Radke, 1991). The first one being capillary suction and the second one being gas diffusion:

1. **Capillary suction** is the primary coalescence mechanism for the extinction of lamellae. Gas diffusion happens from the concave to the convex side of the film and dissolves in the liquid because of the pressure difference between the concave side of a foam film

and the convex side. The pressure on the concave side is usually substantially higher (Sheng, 2013).

2. **Gas diffusion** may be induced by a pressure difference between bubbles. Gas bubbles appear in very different sizes in the foam. As previously discussed, the capillary forces are inversely proportional to interface curvature. Hence, smaller bubbles will have a higher pressure than larger bubbles. Such a pressure difference leads to a chemical potential difference. This chemical potential causes the gas to diffuse through the liquid film from the small to the large bubbles. Eventually, the small bubbles disappear and cause big bubbles to collapse because the increasing volume will thin out the film until the bubble cannot sustain itself anymore (Lake, 1989).

These two are the driving mechanisms for foam decay and are highly dependent on the surfactant type, temperature, and pH value. It was reported that the half-life of the foam heights to range from 1 to 45 minutes and that anionic surfactants possess greater stability than non-ionic surfactants (Patton, et al., 1985). Furthermore, water hardness has a great effect on the stability of sulfonate foams. Generally, foams were unstable at high temperatures and may only be stabilised by the addition of cosurfactants (Lake, 1989).

3.6.4 Foam States

Foam appears in three different states in the porous medium, all of which possess very different characteristics and qualities. Figure 3-11 illustrates all three states that can probably occur.

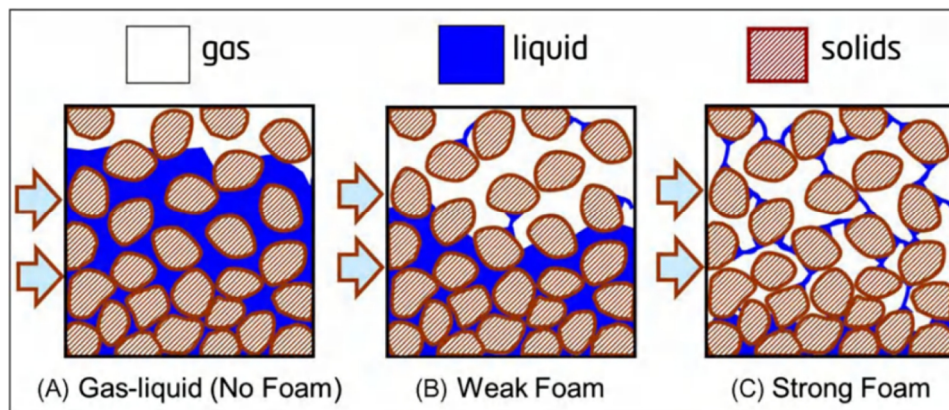


Figure 3-11: Illustration of conventional gas-liquid two-phase flow in porous media (Sheng, 2013).

- A. **The first state (A)** is characterised by either the non-existence of initial foam or the destabilisation and destruction of pre-existing foams. Such a state can be commonly found in a strongly oil-wet formation, a medium with a high oil saturation, or in a high capillary pressure environment. Foam flow resembles in this case a mere conventional gas-liquid two-phase flow without the presence of foam films. This state results in high water saturation filling smaller pores (Sheng, 2013).

- B. **The second state (B)** is called a weak foam. The presence of a moderate amount of foams exhibits a small increase in apparent foam viscosity, usually by less than a few orders of magnitude and thus, increasing the pressure gradient or reducing the water saturation (Sheng, 2013).
- C. **The third state (C)** is referred to as a strong foam. In a strong foam state, a large number of very finely textured foam films can be found in the medium. This leads to a dramatic increase in the foam's apparent viscosity (up to several orders of magnitude). This in turn is followed by a significant increase in pressure gradient or reduction in water saturation (Sheng, 2013). Strong foam has been shown to exhibit two distinct flow behaviours. It can either follow a near-Newtonian flow behaviour or a slightly shear-thickening behaviour in the high-quality regime and a highly shear-thinning behaviour in the low-quality regime (Sheng, 2013).

3.6.5 Foam Flooding Mechanism

As previously noted, foam addresses the problem of high gas mobility by achieving an increase in the gas's apparent viscosity situated in the foam. This in turn improves the sweep efficiency, which is crucial to enhance the ultimate oil recovery. When surfactants are in contact with both gas and liquid phase while being exposed to the addition of low kinetic energy (low velocity), liquid films form. These liquid foams partially block the pore throats in the porous medium. Consequently, the relative gas permeability is reduced. When high-velocity gas flows through the liquid, liquid films and gas clusters break. In this case, the pore throats are blocked by the broken separate gas bubbles, ultimately reducing the gas phase permeability. Both instances improve sweep efficiency (Sheng, 2013). Foams can be used to improve poor sweep efficiency that is caused by reservoir heterogeneity because foams tend to be stronger in high-permeability layers than in low-permeability layers. This can be explained as the non-wetting gas preferably occupies high-permeability channels. This feature aids the diversion of the injected flow to the low-permeability channels. Foam flow requires a high-pressure gradient to overcome the capillary pressure and hence lower the residual oil saturation (Sheng, 2013).

3.7 Petrophysics of Naturally Fractured Carbonate Rocks

Carbonate reservoirs can be found in the Arabian plate region, which accounts for a tremendous 66.4% and 33.9% of the world's recoverable oil and gas reserves, respectively (Beydoun, 1998). In Beydoun's (1998) paper, the Arabian plate includes the Arabian Peninsula, the Persian-Arabian Gulf, and the Fertile Crescent, where the latter spans from southeast Turkey to southwest Iran lying south and southwest of the Taurus and Zagros suture zones. The cores extracted in the experimental data on which this thesis is based on were all extracted from the Zagros fold. Carbonate rocks are largely composed of calcium carbonate (CaCO_3) in the mineral form calcite. They form in shallow marine environments and are usually of biogenic origin. Calcite is a chemically reactive component. This leads to primary intergranular porosity to be infilled by cement very quickly by either diagenesis, the introduction of acid compounds, and the injection of water containing carbon dioxide (Tiab & Donaldson, 2016), creating secondary pores (Selley, 2005). This means that carbonate reservoirs are generally dual or triple porosity systems and have been found to range in wettability from neutral to strongly oil-wet (Tiab & Donaldson, 2016).

3.7.1 Fractures in Carbonate Rocks

Fractures commonly occur in carbonate rocks. They have a significant impact (either positive or negative) on the permeability and the fluid flow in carbonate reservoirs. This depends on whether the fractures are open or sealed as a result of mineralisation. However, in most fracture modelling studies, fractures are mostly considered open and thus have a positive effect on fluid flow (Tiab & Donaldson, 2016).

Nelson identified in his research (1987) four types of naturally fractured reservoirs, based on the extent to which fractures alter the porosity and permeability of the reservoir matrix. Consideration of these reservoir types is crucial for the correct interpretation of pressure transient tests and the selection of an adequate reservoir management programme.

- **Type I:** In this reservoir type, the fractures provide the essential permeability and storage capacity and generally show a sharp production decline and therefore lead to early water and gas coning (Tiab & Donaldson, 2016).
- **Type II:** In type two reservoirs, the fractures provide only the essential permeability, whereas the matrix provides the essential storage capacity. Such reservoirs respond very well to infill drilling or the selection of improved recovery processes (Tiab & Donaldson, 2016).
- **Type III:** In type three reservoirs, the fractures augment the already good matrix permeability, enhancing the overall reservoir permeability. High flow rates can be

reached. During pressure maintenance, in such a reservoir, unusual behaviour exhibited by water or gas injection may be observed because of the unique permeability trends of this reservoir type (Tiab & Donaldson, 2016).

- **Type IV:** Fractures found in type four reservoirs are filled with minerals greatly reducing permeability and porosity. Reservoirs containing such fractures are characterised by significant reservoir anisotropy. The fluid flow and partition formations into relatively small blocks are impeded (Tiab & Donaldson, 2016). They are often uneconomic and not viable to develop or produce from.

3.7.2 Porosity in Fractured Reservoirs

Depending on the type of reservoir and the degree of solution channelling (as shown in Figure 3-12), the fracture porosity ranges from as low as 0.01% to as high as 9.64%. The width may range from 0.01 to more than 6 mm (Tiab & Donaldson, 2016). Also, the spacing may vary from a few inches to many feet. Accurate estimation of the fracture porosity is, therefore, important for an efficient development and an economic exploitation of the given naturally fractured reservoir. If the oil is trapped in both the reservoir matrix and the fractures, the total oil in place is then calculated as follows (Tiab & Donaldson, 2016):

$$N_{ot} = N_{om} + N_{of} \quad (3.1)$$

where N_{om} and N_{of} are the oil volumes trapped in the matrix and fractures, respectively. The fracture porosity can then be expressed as the ratio of the fracture pore volume (V_{Pf}) over the total bulk volume (V_{bt}) (Tiab & Donaldson, 2016):

$$\phi_f = \frac{V_{Pf}}{V_{bt}} \quad (3.2)$$

Thus, the total porosity is (Tiab & Donaldson, 2016):

$$\phi_t = \phi_m + \phi_f = \frac{V_{Pm}}{V_{bt}} + \frac{V_{Pf}}{V_{bt}} = \frac{V_{Pf}}{V_{bt}} + \frac{V_{Pm}}{(1 - \phi_f)V_{bt}} \quad (3.3)$$

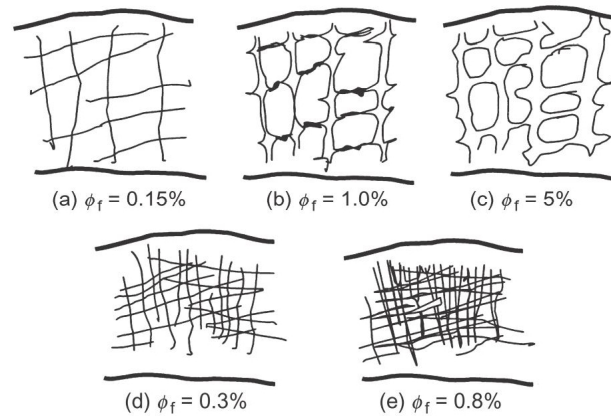


Figure 3-12: Development of fracture porosity in carbonate rocks that have low insoluble residue, (a)-(c), and high insoluble residue, (d) and (e) (Tiab & Donaldson, 2016).

Although the absolute porosity provided by natural fractures in the reservoir is miniscule (<3% on average), the available pore volume is much better connected and, thus, the effective porosity is usually much higher (Tiab & Donaldson, 2016).

3.7.3 Permeability in Fractured Reservoirs

Because the effective porosity is greatly enhanced, the effective permeability is also increased as a consequence. Therefore, the fractures have a great impact on the petroleum recovery and the overall connectivity in the reservoir and should always be considered when exploiting a particular reservoir (Tiab & Donaldson, 2016).

The basic approach to estimate the fracture permeability and its influence on fluid flow in a naturally fractured reservoir is the equation for volumetric flow rate between two smooth plates combined with Darcy's law (Tiab & Donaldson, 2016). Many other correlations and equations are based on this approach. By assuming that fluid flow through porous media is analogous, McGuire and Sikora (1960) showed that the width of artificial fractures has a greater impact on communication among fractures than their length (Tiab & Donaldson, 2016). Furthermore, it can be said that the permeability of a natural fracture network is greatest where the reservoir bed contains fractures that are wide and closely spaced, and oriented parallel to the fluid pressure gradient (Stearns & Friedman, 1972).

Fracture permeability cannot be derived from well logs. Therefore, a combination of core-derived parameters and processed log data is used to build a statistical relationship between the permeability of the matrix-fracture system and other parameters (including the connate water saturation or porosity). Such a relationship does not need core data to deduce the permeability distribution but can only be used in rather homogeneous systems. Carbonate formations, on the other hand, are mostly heterogeneous systems where textural and structural dissimilarities are

common. In such cases, only a few wells are cored to lower expenses and are used to derive a correlation (Tiab & Donaldson, 2016).

Fracture porosity is a common trait of sedimentary rocks that is formed by structural failure of the reservoir rock under loads caused by folding and faulting. Solution or vuggy porosity is a result of leaching of carbonate rocks by circulating acidic waters. Although these solution channels found in naturally fractured reservoirs contain less than three percent of the total oil in place, they are crucial for the oil recovery management of the field as the matrix porosity is usually of lower permeability (Tiab & Donaldson, 2016). Figure 3-13 shows porosity of fracturing and fissuring origin, and from solution along joints and bedding planes, respectively. Carbonate reservoirs differ strongly in their reservoir performance to that of sandstone reservoirs. In sandstone reservoirs the vertical permeability [k_v] is generally much less than the horizontal permeability [k_h]. In carbonate reservoirs, on the other hand, the vertical permeability frequently is well above the horizontal permeability. This can be accredited to the dissolution of hot and acidic compaction-derived fluids moving upwards, creating channels and vugs and, thus, enlarging existing fractures (Tiab & Donaldson, 2016).

Many a carbonate reservoir exhibits fractures with some degree of filling with precipitation of the circulating leaching solution. Therefore, the range of fracture porosity may vary from a few percent to 100%. Furthermore, the connate water saturation can vary between zero and 100% depending on the wettability characteristics of the reservoir rock (Tiab & Donaldson, 2016).

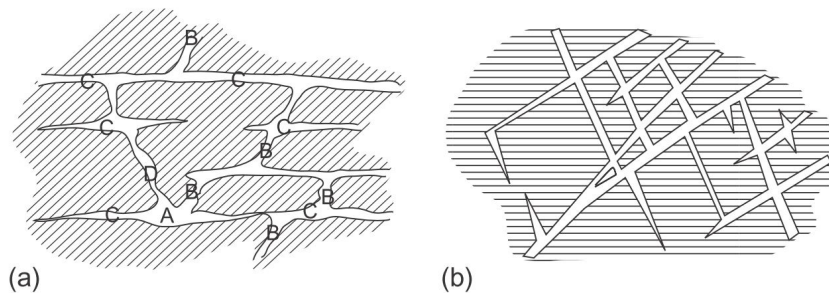


Figure 3-13: (a) Carbonate rock showing porosity: A, vugs; B, joint channels; C, bedding plane channels; D, solution channel adapted by (Tiab & Donaldson, 2016) from (Pirson, 1958).

Chapter 4

Reservoir Simulation

A reservoir simulator is a programme that is used to simulate the flow of fluids (water, oil, gas, etc.) through a porous medium. The 3D model that is created tries to replicate the real reservoir that is being studied as closely as possible. Such a model is constructed based on geological and physical parameters that describe the properties of a reservoir. On top of that, a development process is needed for forecasting future oil/gas production, decision making, and reservoir management. A typical reservoir simulation study seeks to forecast one or more of the following (Satter & Iqbal, 2016):

- Oil and gas in place estimates
- Recovery efficiency of a reservoir under various development scenarios
- Economic analysis and rate of return from the venture over the life of the reservoir
- Economic viability of marginal reservoirs
- Suitability of a particular well at a given location to attain maximum productivity
- Optimisation of waterflood based on the pattern, location, and rate of injection wells
- Optimisation of EOR operations
- Deliverability of a gas reservoir
- Optimisation of the water-oil ratio and gas-oil ratio
- Study of water coning in a well followed by corrective action
- Spacing between wells to optimise production and maximise economic value
- Design and location of well patterns

Matching the results of the simulation with the production history of the reservoir up until the time of study is crucial for obtaining a reliable forecast. Furthermore a simulation accounts for fluid phase changes such as vaporisation or condensation that occur with reservoir pressure changes and affect reservoir performance (Satter & Iqbal, 2016). Such studies indicate the

optimum well number that needs to be drilled at their specific locations. An example of that was provided by Satter & Iqbal (2016), where they showed how a reservoir simulation study generated various scenarios with different well spacing Figure 4-1. The conclusion was that closely spaced wells increase the production but require more up-front capital investment. Such a simulation run, and economic analysis are highly dependent on the characteristics of the studied reservoir. Reservoir heterogeneity and low transmissibility usually demand drilling of more wells to be economically viable. There are many uses to be found for reservoir simulation and each serves a specific purpose and aids in designing an appropriate and optimal reservoir management strategy (Satter & Iqbal, 2016).

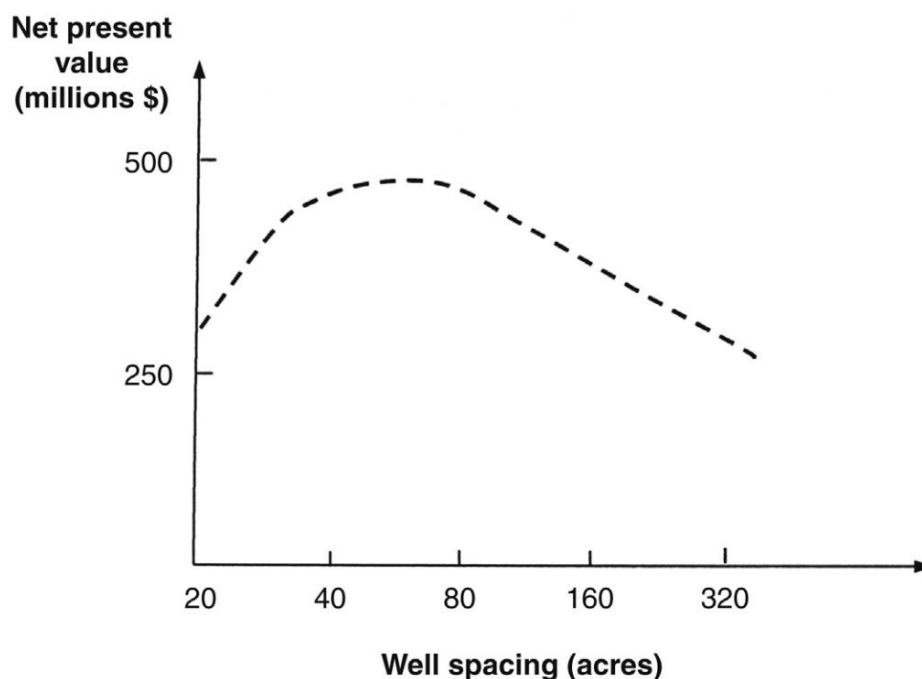


Figure 4-1: Optimisation of well spacing based on reservoir simulation (Satter & Iqbal, 2016).

4.1.1 Mathematical Basis for Simulation Runs

The forecasting capabilities of reservoir simulations are based on several models and conservation laws. These are needed to set up numerical simulations.

- **Mass Balance:** This law allows the usage of saturation as an independent variable, because the formulations are considered volumetric (Alvarado & Manrique, 2010). There are three types of simulators (black-oil, compositional and thermal).
- **Momentum Balance:** This law is represented by Darcy's law. It includes relative permeability curves and capillary pressure curves (Alvarado & Manrique, 2010).

- **Energy Conservation:** This conservation law is crucial for the simulation of thermal processes such as energy transfer in steam injection or huff and puff (Alvarado & Manrique, 2010).
- **Pressure-Volume-Temperature [PVT]:** Phase behaviour, phase changes, and thermodynamic conditions are all described by the PVT properties of the fluids and rock. Fluid pressure changes from cell to cell during the simulation as a function of space (Satter & Iqbal, 2016).

There are basically two ways of numerical solutions to be calculated. The first approach is explicit. Here, the value of, for example, the pressure is based on the values obtained at the current time step. Any coefficient that appears in a discretised equation is also evaluated at the current time step. The second approach is implicit. In an implicit solution, the pressure, for example, is assumed for the next time step, and any coefficient appearing in the equations is also calculated at the assumed pressure. The pressure is then calculated by iterating the values of the assumed cell pressure until a convergence between the assumed and calculated values of the pressure are achieved (Satter & Iqbal, 2016). All equations in a reservoir simulation are formulated in two according to the sought objectives and available computing power. These are:

- **IMPES:** The abbreviation stands for “Implicit Pressure and Explicit Saturation” and is a popular methodology as it requires little computing power. As the name suggests, the grid block pressure is calculated implicitly, followed by the explicit calculation of fluid saturations for the grid block. This method is highly efficient at computing and provides accurate results in a variety of circumstances when used appropriately. It is suitable for models where fluid phase saturations do not change significantly within a short timeframe in the reservoir. Full field models are most suitable for this method due to their large block sizes (Satter & Iqbal, 2016).
- **Fully Implicit:** In this approach, the coefficients that are used in both pressure and saturation equations are implicitly calculated at the current time step. It is calculated iteratively until convergence is reached for both pressure and saturation. The coefficients are updated with each iteration. This method is most suitable for models where a rapid change in fluid saturation is anticipated. The vicinity of a well would be a good candidate (Satter & Iqbal, 2016).

4.1.2 Reservoir Model

A reservoir model is a typical representation of a reservoir based on grid cells of various shapes and sizes in 1D, 2D, 3D, or radial geometry. Each grid block contains information on the local description of the reservoir, fluid saturations, permeability, porosity, to name a few (Satter & Iqbal, 2016). More than one region may be assigned to a reservoir model so that different reservoir characteristics can be accounted for in the simulation runs. The development of a reservoir model starts with the creation of a static model. This model is built from geological and geophysical data that include the reservoir structure and rock characteristics. Then the dynamic data is implemented into this static representation of the reservoir. It includes changes in fluid saturations and properties, pressure, components, reservoir heterogeneities, well locations, and perforations, well completions, and operating constraints (Satter & Iqbal, 2016). By that, the static model is turned into a dynamic model that can then be used for creating a forecast and for reservoir management purposes.

A dynamic model can be classified as the following:

- **Black-oil model:** A black-oil simulator basically distinguishes between three phases: oil, water, and gas. The oil and gas are lumped hydrocarbon components, and the solubility of vapour in the liquid phase is assumed to be a function of pressure and temperature only (Satter & Iqbal, 2016). Mass-transfer between the oil and the gas is possible and it is controlled by pressure-volume-temperature [PVT] properties (Alvarado & Manrique, 2010). Water is regarded as a separate phase. It is the most widely used reservoir simulation model in the industry due to its simplicity and its reliability for providing acceptable results for most petroleum reservoirs. Good candidates for a black-oil model are the primary production of less volatile oil and the secondary production of oil by waterflooding or immiscible gas injection (Satter & Iqbal, 2016).
- **Compositional model:** A compositional simulator is much more complex and accounts for components that are present in the oil and the gas phases. Although it is very resource heavy, it is necessary for problems where the vaporisation and condensation of hydrocarbon components play a vital role in the performance of a reservoir. Usually, the PVT properties of lightweight hydrocarbon components, such as CH₄ to C₆, are treated individually. In contrast, intermediate to heavy components are lumped together into a C₇₊ fraction to reduce the overall complexity of the model (Satter & Iqbal, 2016). Furthermore, recovery processes that rely on mass-transfer mechanisms, such as CO₂, N₂, or enriched gas injections, require some form of compositional material balance (Alvarado & Manrique, 2010). The model considers

the compositional changes in the liquid and vapour phases under dynamic reservoir conditions. For example, in a gas condensate reservoir, a reduction in reservoir pressure leads to the condensation of heavier hydrocarbon components from the gas phase into the oil phase. Accordingly, the injection of methane in an oil reservoir as an enhanced oil recovery method results in the vaporisation of light hydrocarbons from the liquid phase into the gas phase (Satter & Iqbal, 2016). Both mechanisms cause significant changes in the composition of both oil and gas.

- **Thermal model:** To account for thermal effects, a thermal simulator is used. It is used for simulating thermal enhanced oil recovery processes that involve fluid and heat transport. Steam injection or huff and puff are the most common EOR process for enhancing the recovery in heavy-oil reservoirs (Satter & Iqbal, 2016).

4.1.3 Grid Orientation Effects

In simulation models, the geometry poses a limitation for finite difference approximations. This means that the orientation of grid cells concerning injectors and producers affects the results of the simulation to a pivotal degree. When an injector and a producer are located parallel to the grid line in a reservoir model, the breakthrough at the producers occurs relatively early (Satter & Iqbal, 2016). When the injector and producer are located diagonally, the breakthrough occurs at a later simulation stage. Furthermore, greater sweep efficiency and recovery are predicted for the latter case (Satter & Iqbal, 2016).

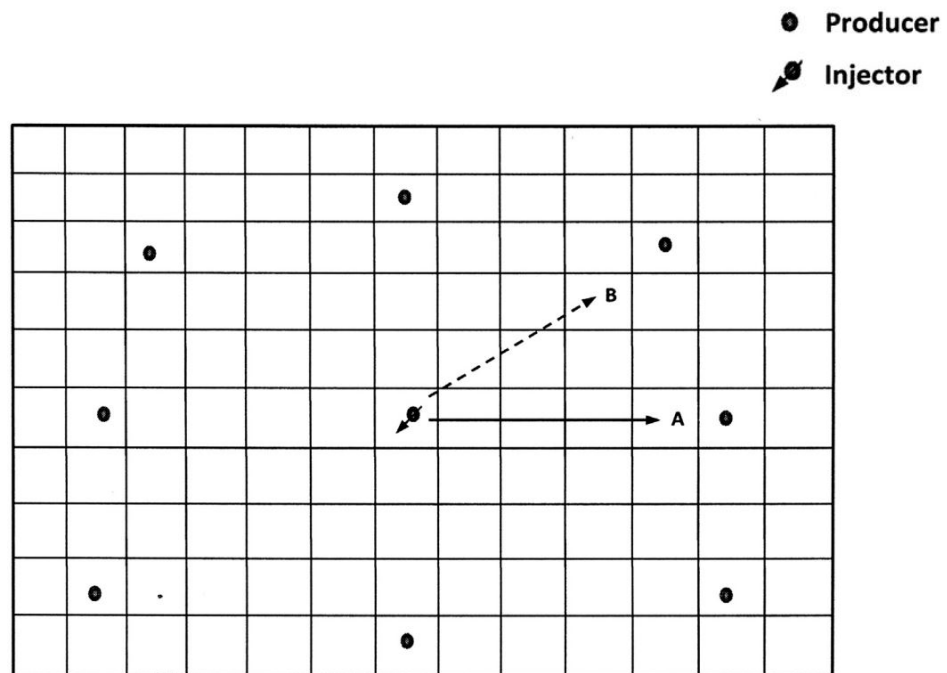


Figure 4-2 Demonstration of grid orientation effects on the flow of fluids between injector and producer (Satter & Iqbal, 2016).

4.1.4 Foam Modelling

Compositional reservoir simulators allow the modelling of foam injection. They function basically the same in most commercial simulators such as GEM or Eclipse 300. The empirical model used in this study was provided in CMG Suite's compositional reservoir simulator "GEM". This model interpolates the gas relative permeability curves in the presence or absence of foam. This is done by using a rescaling factor that reduces the gas relative permeability in the presence of foam. The rescaling factor influences the foam's behaviour and is dependent on water and surfactant concentrations, capillary pressure, oil saturation, and other factors such as brine salinity and permeability dependence (AlMaqbali, et al., 2015). This rescaling factor is represented by the dimensionless mobility reduction factor "FM" given by the equation:

$$FM = \frac{1}{1 + FMMOB * F1 * F2 * F3 * F4 * F5 * F6 * F7 * FDRY} \quad (4.1)$$

$$F1 = \left(\frac{\text{Mole Fraction (Surfactant)}}{FMSURF} \right)^{EPSURF} \quad (4.2)$$

$$F2 = \left(\frac{FMOIL - S_o}{FMOIL - FLOIL} \right)^{EPOIL} \quad (4.3)$$

$$F3 = \left(\frac{FMCAP}{\text{Capillary Number}} \right)^{EPCAP} \quad (4.4)$$

$$F4 = \left(\frac{\text{Capillary Number} - FMGCP}{FMGCP} \right)^{EPGCP} \quad (4.5)$$

$$F5 = \left(\frac{FMOMF - X_{comp_name}}{FMOMF} \right)^{EPOMF} \quad (4.6)$$

$$F6 = \left(\frac{X_{salt} - FLSALT}{FMSALT - FLSALT} \right)^{EPSALT} \quad (4.7)$$

$$F7 = \frac{1}{FMPERM1} * \ln \left(\frac{PERMAV}{FMPERM2} + 1 \right) \quad (4.8)$$

$$FDRY = 0.5 + \frac{\arctan(SFBET(S_w - SF))}{\pi} \quad (4.9)$$

FM is an inverse mobility reduction factor which varies between 1 (= no foam) and ~0 (= strongest foam). Its dependency factor FMMOB represents the foam mobility reduction factor when no other parameters are influencing the foam mobility (Computer Modelling Group LTD., 2019). This parameter is determined experimentally, and it represents the foam strength (AlMaqbali, et al., 2015). It ranges between 5 and 100. The FMMOB factor is multiplied by several other factors to make it dependent on other effects.

- F1: surfactant concentration
- F2: oil saturation
- F3: shear-thinning
- F4: limited capillary pressure
- F5: oil components
- F6: salt concentration
- F7: permeability dependence
- FDRY: foam dry-out

If any of these factors equals zero during calculations, FM will imminently equal to 1 which acts as the absence of foam. The foam dry-out factor “FDRY” is dependent on surfactant concentration, oil saturation, capillary number, and the brine salinity. The main application of the foam dry-out factor is to rescale the relative permeability of the foam back to the gas relative permeability (at no foam conditions) over the saturation range 0 to SF, where SF varies between 1 (= no foam) and 0 (= no dry-out). SFBET is the reference dry-out slope used to control the abruptness of the dry-out function (AlMaqbali, et al., 2015). More details can be found in the CMG GEM Manual (2019).

4.1.5 Fracture Modelling

The implementation of fractures in a reservoir model is done by enabling the options “dual porosity” or “dual-porosity – dual-permeability”. A naturally fractured reservoir is normally characterised as either of these. A distinct characteristic of a dual porosity system is that flow to the wellbore only happens through the fracture network. As it can be seen in Figure 4-3, there are two continua where the matrix blocks are connected to fractures but not to other matrix blocks. Fractures, on the other hand are interconnected.

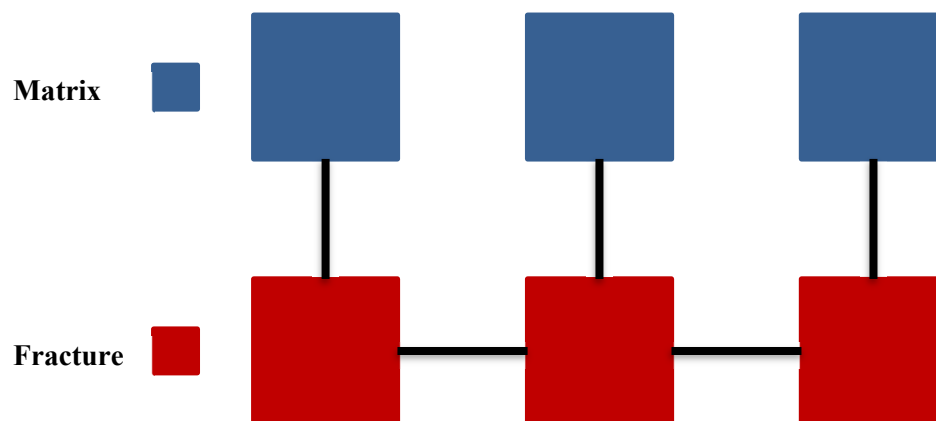


Figure 4-3: Dual Porosity (Single Permeability) Model.

Figure 4-4 shows the numerical model of a dual porosity system. The fractured system consists of two identical superimposed grids (a matrix grid and a fracture grid).

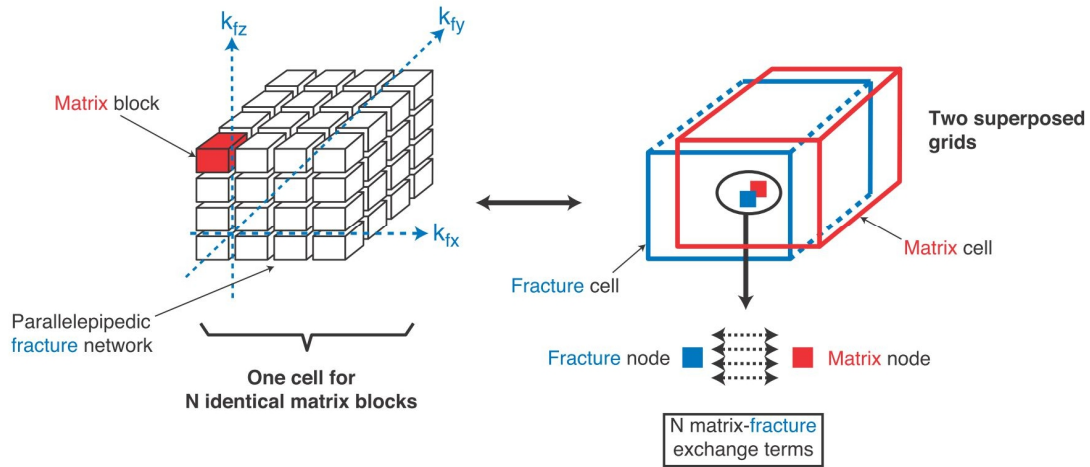


Figure 4-4: Dual porosity representation of a fractured reservoir (Lemonnier & Bourbiaux, 2010).

The same types of properties can be assigned to the fracture system. It is often the case that the permeability of the matrix is significantly lower than that of the fractures and/or is not continuous (the matrix blocks are broken into discontinuous chunks) (Heinemann & Mittermeir, 2014). The matrix just serves as a volume source or sink for the continuous fracture system.

In contrast, in a dual-porosity – dual-permeability system, flow from the fracture and the matrix is considered (Satter & Iqbal, 2016). In this case, both systems are continuous, as shown in Figure 4-5.

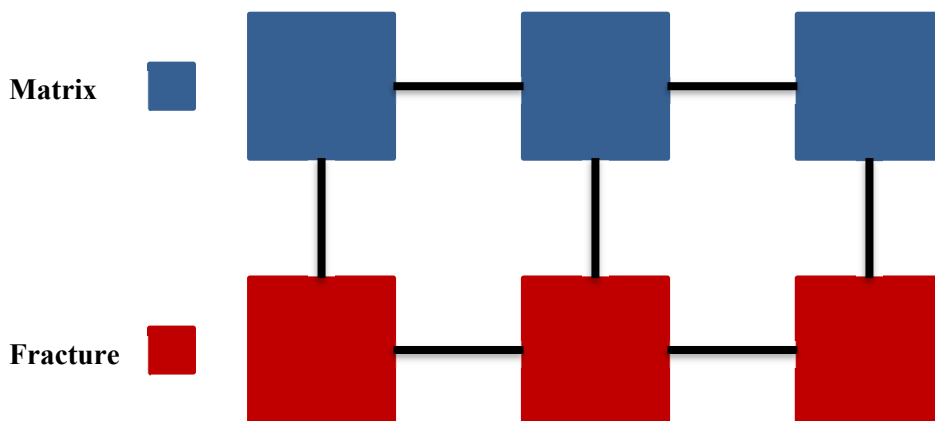


Figure 4-5: Dual Porosity - Dual Permeability Model

Chapter 5

Experimental Setup and Procedure

5.1 Experimental Background and Reservoir Description

This work is based on the works of Gandomkar & Kharrat (2012), Gandomkar et al. (2012), Nematzadeh, et al. (2012) and Motealleh, et al. (2012), wherein they studied the effects of carbon dioxide gas injection, WAG and FAWAG injection into naturally fractured carbonate cores as a secondary and tertiary recovery method. The cores are of a diameter of 1.5 in and are characterised by their low permeability. The experiments were conducted using live-oil, brine with 5000 ppm of salts (4000 ppm NaCl, 500 ppm CaCl₂ and MgCl₂), and sodium lauryl sulphate as the anionic surfactant and foaming agent. All these cores were initially saturated with the same live oil and brine at reservoir conditions (115°F or 46.11°C). However, the pressure changed from experiment to experiment and ranged between 1600 psi and 2300 psi, which correspond to roughly 110.3 bar and 158.6 bar, respectively. For the experiments, the cores were flooded with about two pore volumes of each method. All properties, values, and parameters for the experiments can be found in Table 1.

The reservoir, where those cores were obtained from, is located in the northern part of the Zagros fold in western Iran and was discovered in 1919. The oil is contained in grey/brown dolomite and carbonate-dolomite rocks, and the reservoir fluid was characterised as light oil of 43°API. The formation is littered with oil field fissures and fractures. Both permeability and permeability are in a range of between 0.10% and 15% and 0.01 mD to 8 mD, respectively.

All the experiments were conducted similarly. The cores were mounted onto the core flooding apparatus like the one shown in the schematic in Figure 5-1. They started at irreducible water saturation and were then flooded with either CO₂, WAG, or FAWAG at certain rates. The main conclusion was that foam-assisted WAG injection was by far the most efficient oil recovery method as it can delay gas breakthrough and reduce the mobility of the gas.

1st Part		Core Properties			
Core used for	Length [cm]	Pore Volume [cm ³]	Porosity [%]	Permeability [mD]	S _{wc} [%]
CO ₂	10.79	14.52	11.8	0.6	27.8
WAG	15.94	24.9	13.7	0.87	27.3
FAWAG	15.88	24.8	14.22	0.86	28.0
2nd Part		Experimental Parameters			
Core used for	WAG Ratio / Cycles	Gas Rate [cm ³ /min]	Water Rate [cm ³ /min]	Pressure [psi]	
CO ₂	/	0.045	/	2300	
WAG	2:1 / 20	0.26	0.26	1600	
FAWAG	1:1 / 10	0.185	0.24	1700	
3rd Part		Water Properties			
Water	Density [kg/m ³]	Compressibility [1/bar]	Reference pressure [psi]	Viscosity [cP]	
Laboratory	989.747	4.35e-06	14.7	0.5822	
Sector	1094	2.3519e-06	2450	0.854	
4th Part		Oil Properties			
GOR [m ³ /m ³]	Temperature [°C]	Initial Pressure [psi]	Bubble Point [psi]	Density [°API]	Viscosity [cP]
128.24	46.11 (115°F)	2450	1960	43	0.82

Table 1: Core properties, experimental parameters, water, and oil properties

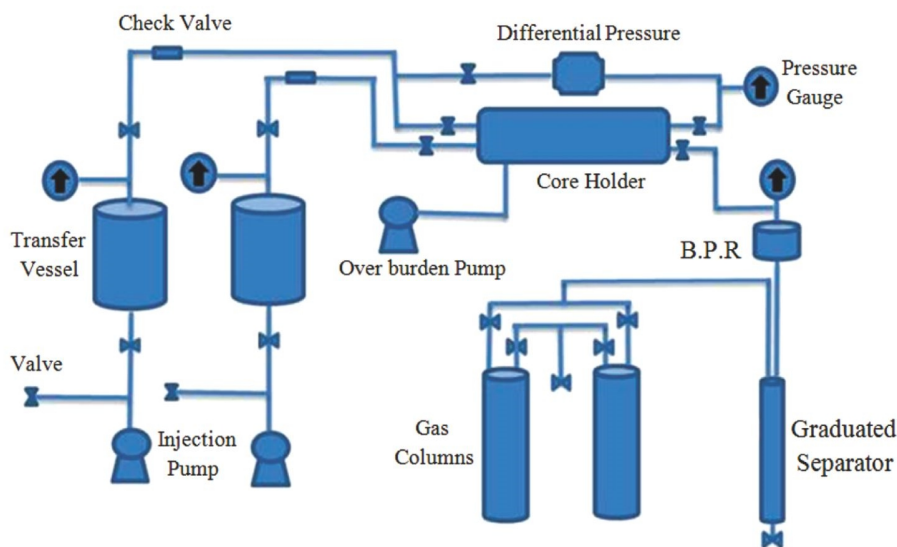


Figure 5-1: Schematic of the core flooding laboratory setup (Gandomkar & Kharrat, 2012).

5.2 Experimental Procedure and Workflow

The simulations done in this work underlie a straightforward workflow on how to go from a small-scale model (core scale) to a large-scale model (sector or field-scale) while still obtaining reasonable data in the large-scale model. This workflow is charted in Figure 5-2. In the very beginning, a compositional model had to be created by matching the experimental data of the oil that was used in the experimental core floods. This PVT data was then used in the setup of the core. Core parameters that were deduced from the experiments are then defined in the model. First, the main objective was to find a suitable gas relative permeability curve for the CO₂ injection history match. This gas relative permeability curve was then used in the WAG injection model to get a fitting water-oil relative permeability curve and adequate hysteresis parameters. These relative permeability curves were then used in the FAWAG injection model. Here, only the foam parameters were changed to achieve a good match. This match was then further used in the large-scale pilot and sector models.

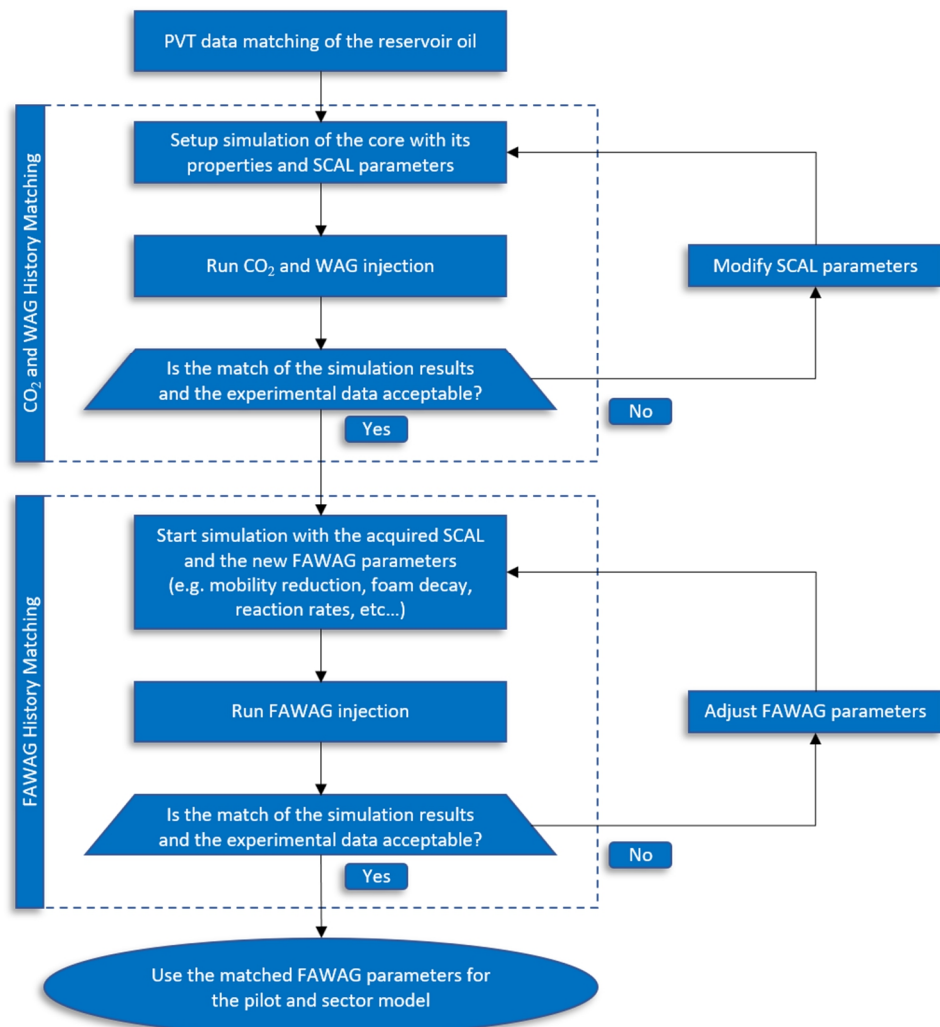


Figure 5-2: Foam Simulation Study Workflow

5.3 PVT data matching

PVT simulation is done to create a compositional model that accurately represents the oil present in the reservoir. Usually, the fraction of heavy components is difficult to be well represented, and that is why a characterisation of this fraction should be done to obtain a good match. The oil composition used in the experiments can be found in Table 2. PVT experiments such as constant composition expansion [CCE], differential liberation [DL], and separator tests, were available for the oil. They were used to create a representative fluid model.

Composition:	Oil [mol%]		Gas [mol%]
Component	before de-lumping	after de-lumping	
H2S	0.005	0.94	3.71
CO2	9.621	0.6	3.45
N2	0	0	0.23
C1	26.459	37.38	81.48
C2	2.628	8.34	5.37
C3	10.83	5.48	2.22
IC4	0.467	1.94	0.34
NC4	0.695	4.89	0.65
IC5	0.627	1.44	0.23
NC5	2.475	1.12	0.22
C6+	46.937		2.1
C6		6.01	
C7		4.3756231	
C8-C12		11.643469	
C13-C19		7.9641352	
C20-C30+		7.8767731	
M.W. of C6+	199 [kg/kg.mol]	S.G. of C6+	0.8181

Table 2: Oil and gas composition before and after de-lumping

5.3.1 De-Lumping

Usually, all components lighter than C_7 are defined. Compositional reservoir simulation studies often require high computing power. Therefore, the plus fraction, which in our case is C_{6+} , is heavily lumped to reduce the pseudo-components in the model and reduce computation time (Pedersen, et al., 2015). In our case, to achieve the best match possible, the plus fraction was de-lumped into several pseudo-components to allow for a higher degree of freedom for the regression parameters. The new composition after de-lumping can be found in Table 2. In our de-lump, we have added two real components (C_6 and C_7), two pseudo-components (C_8-C_{12} and $C_{13}-C_{19}$), and a new plus fraction ($C_{20}-C_{30+}$). The mole fraction of the new components and the new plus fraction were obtained from the previous plus fraction using PVTsim

5.3.2 Regression

When the oil composition doesn't deliver a satisfactory match of the laboratory data, regression is used to adjust the parameters of the pseudo-components in order to minimise the deviation between measured and simulation data so that the oil exhibits a laboratory like behaviour. Parameters that are most useful to add to the regression include Ω_A and Ω_B , the acentric factor ω , volume shift parameters, binary interaction coefficients, and the critical temperature and pressure of heavy components. To achieve a better match, the viscosity should always be regressed last and separately (Schlumberger, 2008). WinProp was used to regress and simulate the PVT-data of the reservoir oil. The following results have been achieved regressing the provided PVT data and using the Peng-Robinson equation of state [EOS] (Figure 5-3 through Figure 5-8):

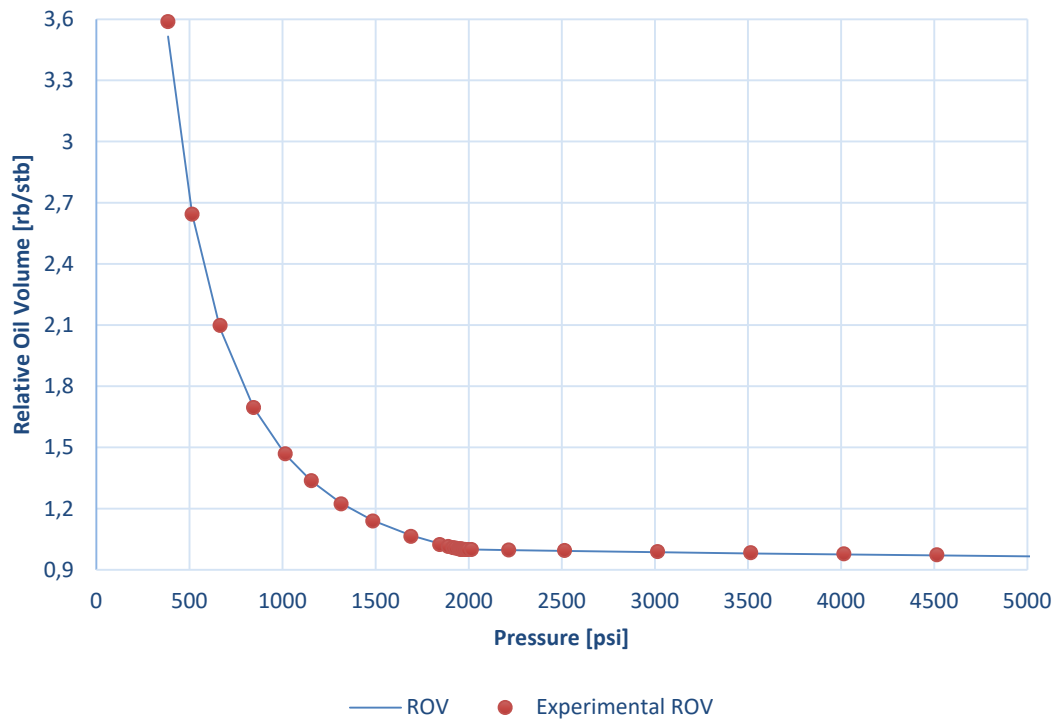


Figure 5-3: Relative Oil Volume (CCE) vs. Pressure

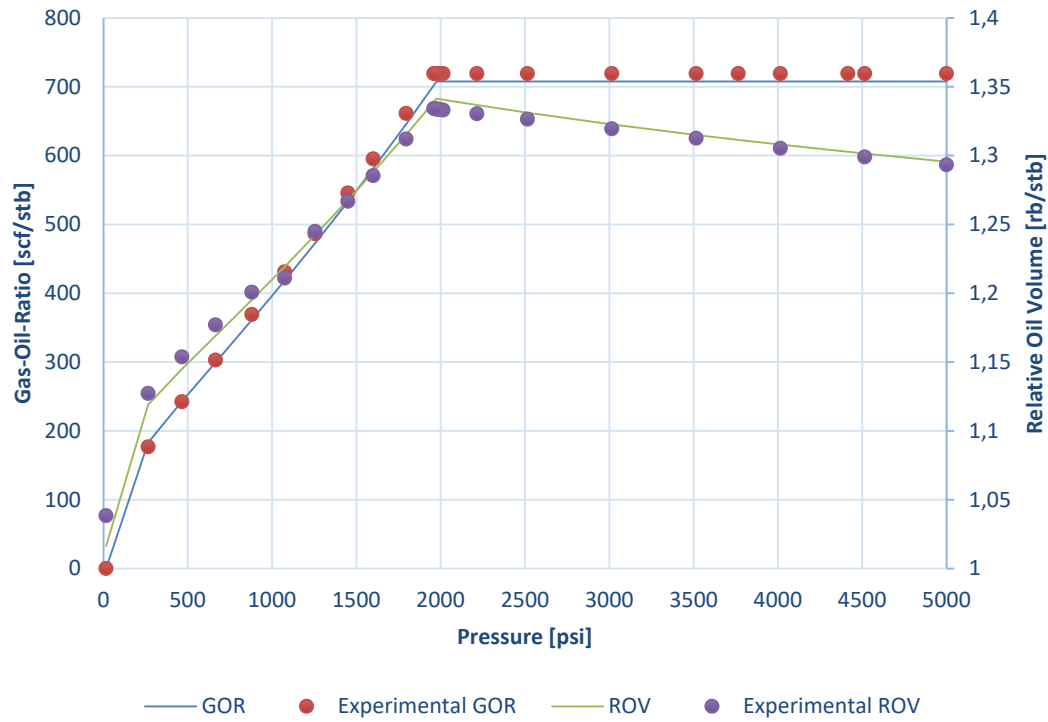


Figure 5-4: Gas-Oil Ratio and Relative Oil Volume (DL) vs. Pressure

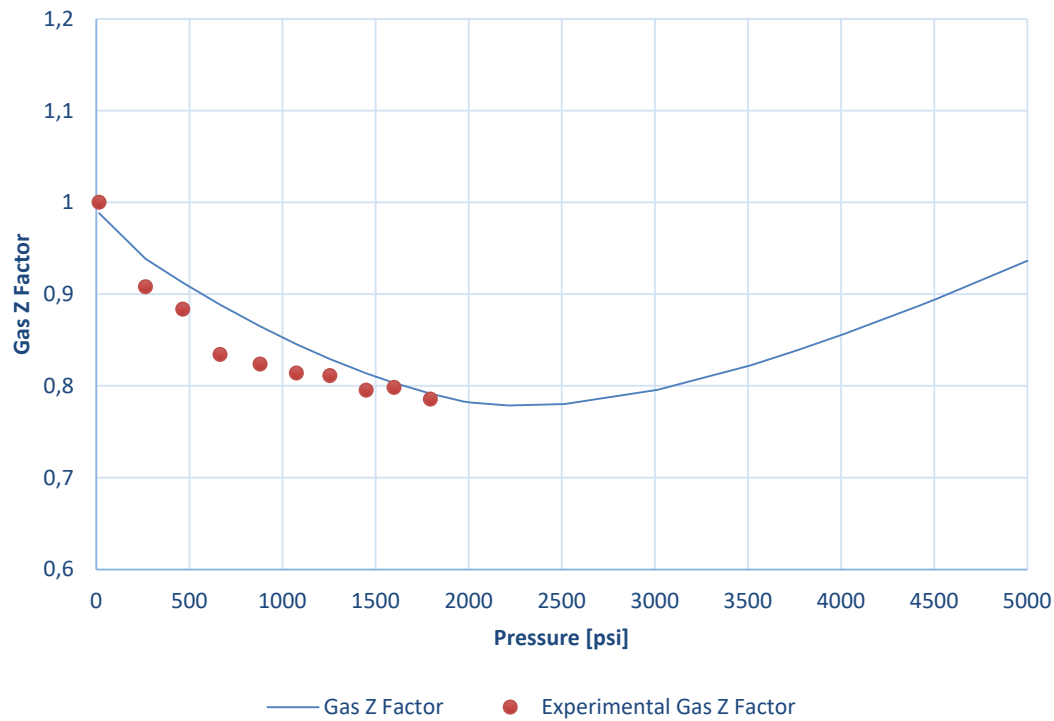


Figure 5-5: Gas Z Factor (DL) vs. Pressure

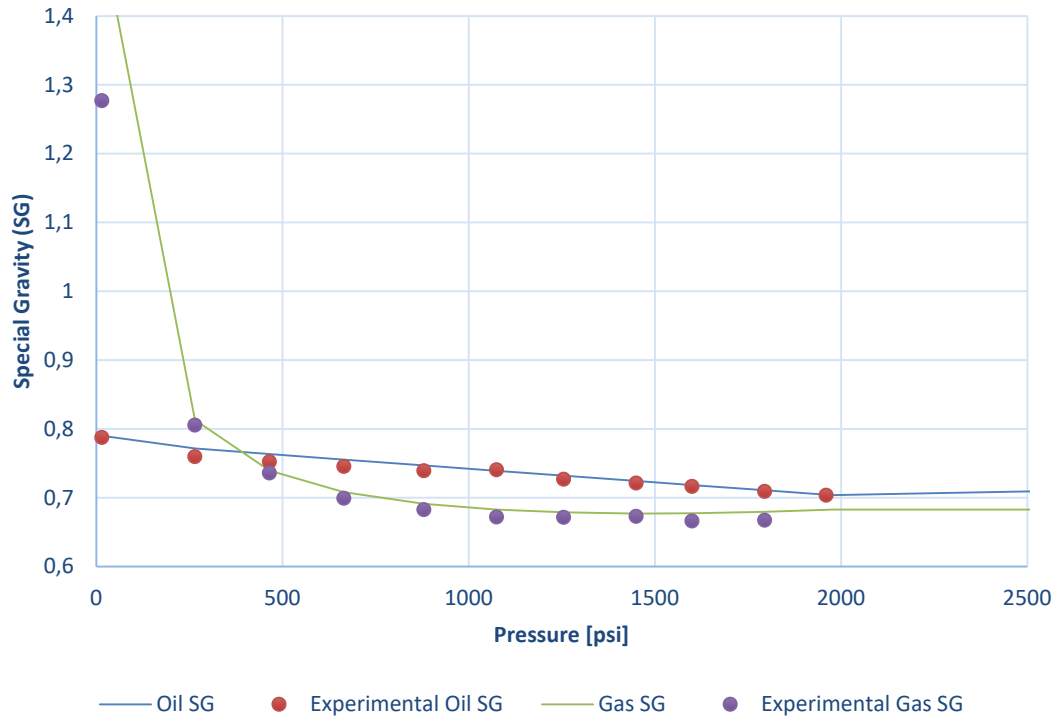


Figure 5-6: Oil SG and Gas SG (DL) vs. Pressure

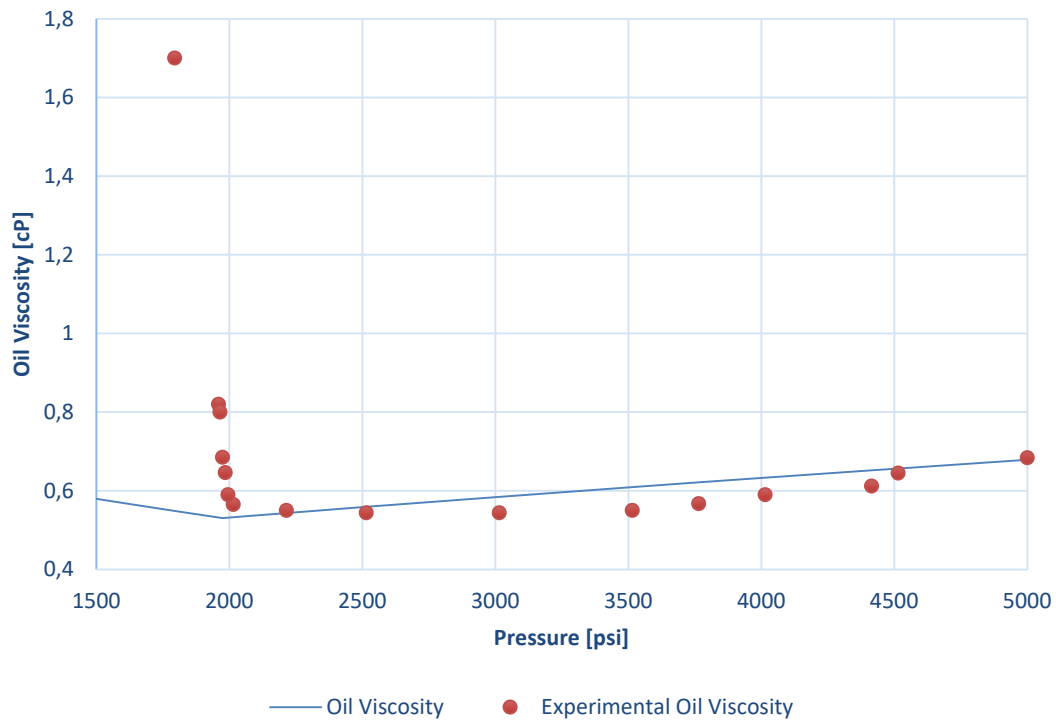


Figure 5-7: Oil Viscosity (DL) vs. Pressure

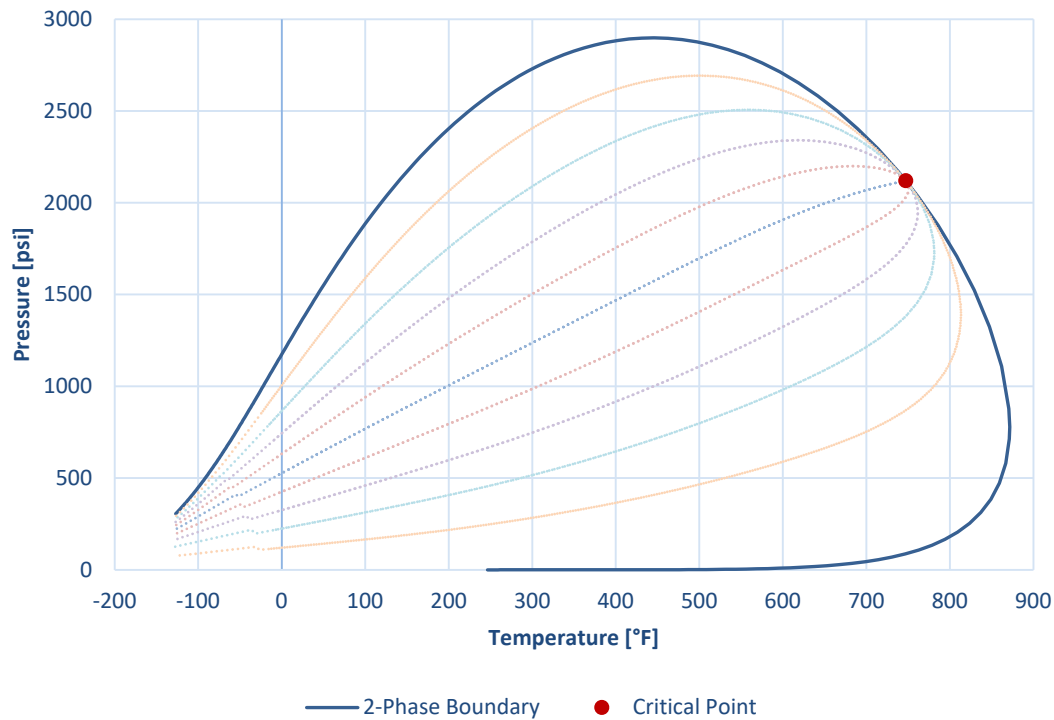


Figure 5-8 Phase Envelope of the matched Reservoir Oil

The phase envelope matches the experimental saturation pressure of 1960 psi at 115°F, while maintaining a solid match with other experimental data such as the Gas-Oil-Ratio or the Relative Oil Volume. This phase behaviour will now be used in the upcoming simulations.

5.3.3 Minimum Miscibility Pressure (MMP)

The minimum miscibility pressure of CO₂ has a tremendous impact on the oil recovery in the upcoming simulations. So, to achieve a three-phase flow, this value was set to approximately 2500psi. This ensures that the carbon dioxide remains in the same phase throughout most simulations even if the reservoir pressure increased substantially.

5.4 Core Flooding Model Setup

Several 1-D core models were constructed in CMG, and its compositional simulator called GEM to respectively represent the core flooding data provided by Gandomkar & Kharrat (2012), Gandomkar, et al. (2012), Nematzadeh et al. (2012) and Motealleh et al. (2012). The grid model was put together from 100x1x1 (x,y,z) cartesian grid blocks to account for numerical dispersion that emerges when working with coarser grid models (Figure 5-9). The dimensions of these blocks are, therefore, a hundredth of the length in the x-direction and 3.3765 cm in y- and z-direction to account for the cylindrical shape of the cores and their 1.5 in diameter. Then the PVT data was imported into the model, and the characteristics of the homogeneous cores were defined. For the sake of simplicity and to reduce computing time, CO₂ solubility in water and the low-salinity effects of the brine were disregarded, as well as capillary pressure with regards to relative permeability, as there were no data on it.

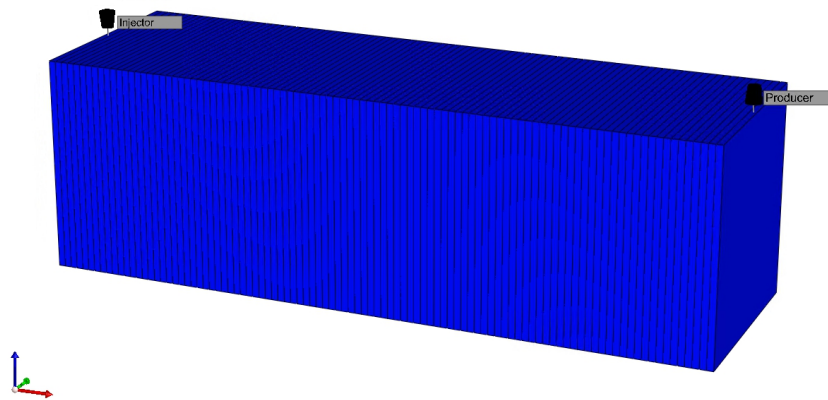


Figure 5-9: Core Simulation Model

5.4.1 CO₂ Core Flooding

The CO₂ flooding is performed to determine the relative permeability curves of the gas and liquid in the model by adjusting the curves according to the production history. The core has a length of 10.79 cm, a porosity of 11.8%, a permeability of 0.6 mD, and a connate water saturation of 27.8%. Exactly two pore volumes were injected into the core. The simulation experiment was conducted at 115°F and 2300 psi. For the relative permeability curves, the following parameters were tuned:

- Residual oil saturation to gas (SORG)
- Irreducible oil saturation to gas (SOIRG)
- Critical gas saturation (SGCRIT)

- K_{rg} at connate liquid saturation (KRGCL)
- Corey exponent of the gas (NG)
- Corey exponent of the oil to gas (NOG)

The history matching tool CMOST-AI by CMG was used to perform this near-perfect match (Figure 5-10). The established relative permeability curve was then used in the subsequent simulations (Figure 5-11).

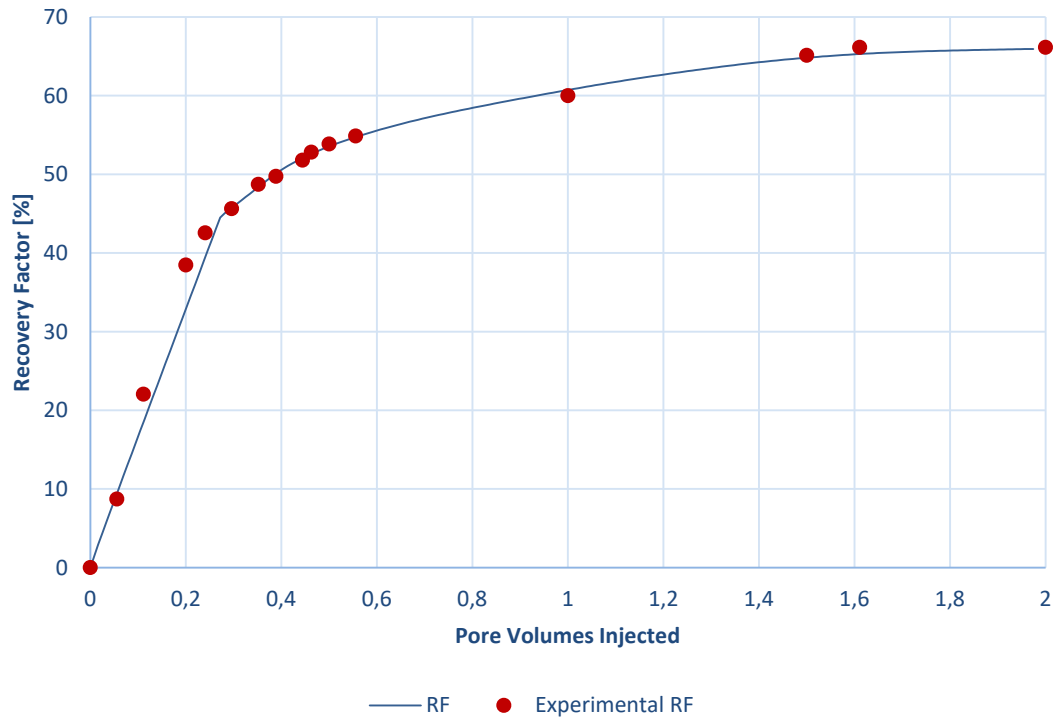


Figure 5-10: CO_2 Recovery Factor – History Match

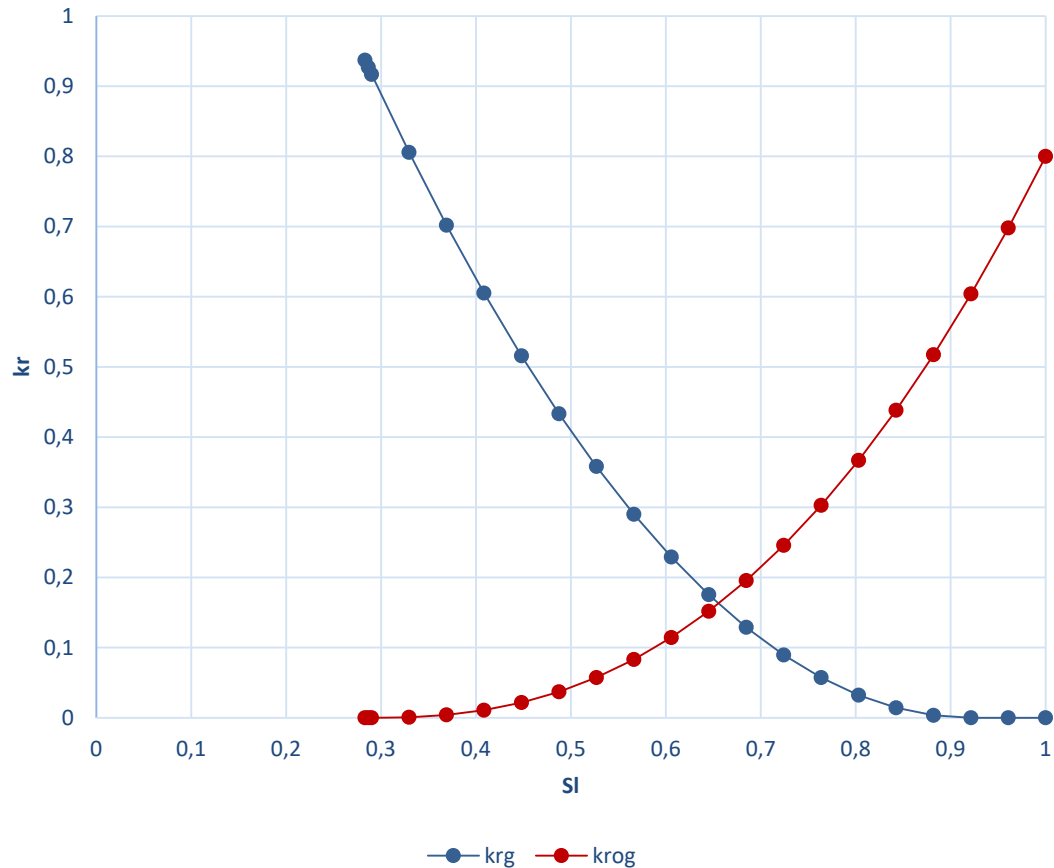


Figure 5-11: Gas relative permeability curve after history match

5.4.2 WAG Core Flooding

Having derived a meaningful relative permeability curve for the gas injection, the next step is to deduce a relevant permeability curve concerning gas and water. The experiment was based on data (Motealleh, et al., 2012). In this experiment, the core was flooded with CO₂ and water at a fixed alternation cycle and ratio. There were twenty cycles in total, and the gas to water ratio was “one to two” and the injection started with gas. This core’s specifications were a length of 15.94 cm, a porosity of 13.7%, a permeability of 0.87, and a connate water saturation of 27.3%. This time, the experiment was conducted at a much lower pressure, i.e., 1600 psi, but at the same temperature of 115°F. Unlike in the other experiments, in this run, three hydrocarbon pore volumes [HCPV] were injected into the core. To account for hysteresis effects, these parameters were included in the history match:

- Residual oil saturation to water (SORW)
- Irreducible oil saturation to water (SOIRW)
- Critical water saturation (SWCRIT)
- K_{ro} at connate water saturation (KROCW)
- K_{rw} at irreducible oil saturation (KRWIRO)

- Corey exponent of the water (NW)
- Corey exponent of the oil to water (NOW)
- Reduction exponent for drainage (increasing gas saturation) relative permeability (ALPHA_{KRG})
- Parameter A used in the STONE1 relative permeability model (AR)
- Maximum residual gas saturation (HYSKRG)

The results can show that the matched and experimental oil recovery are very similar (Figure 5-12 through Figure 5-14). The obtained relative permeability curve shows an intermediate-wet system (with tendencies leaning towards oil-wet) that is often associated with carbonate-dolomite rocks.

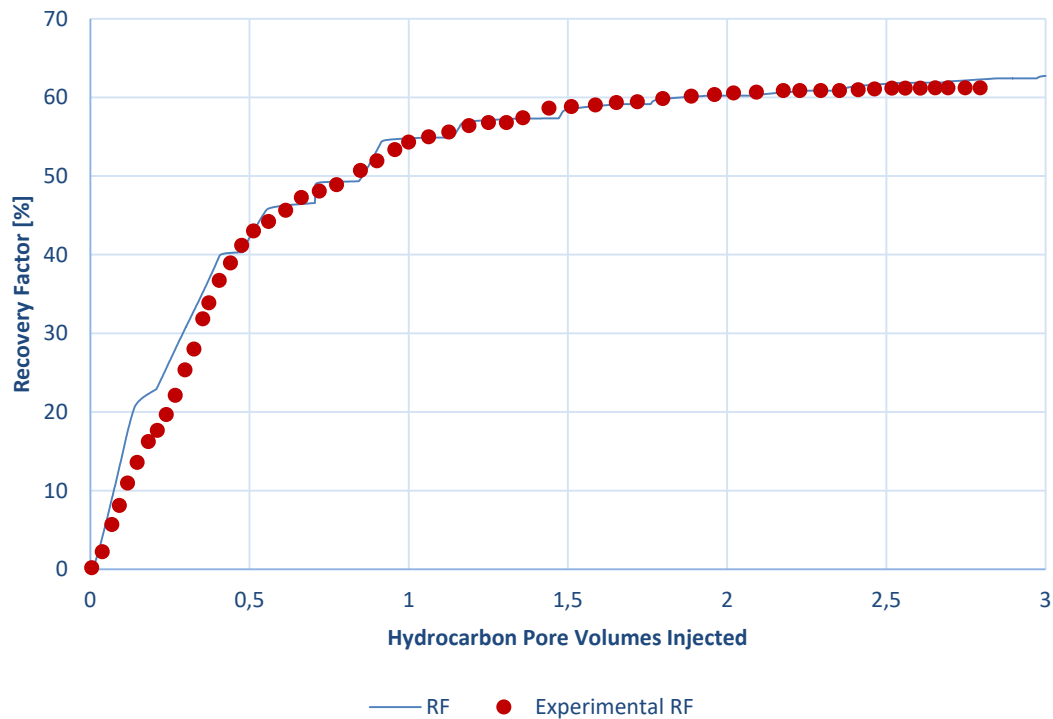


Figure 5-12: WAG Recovery Factor – History Match

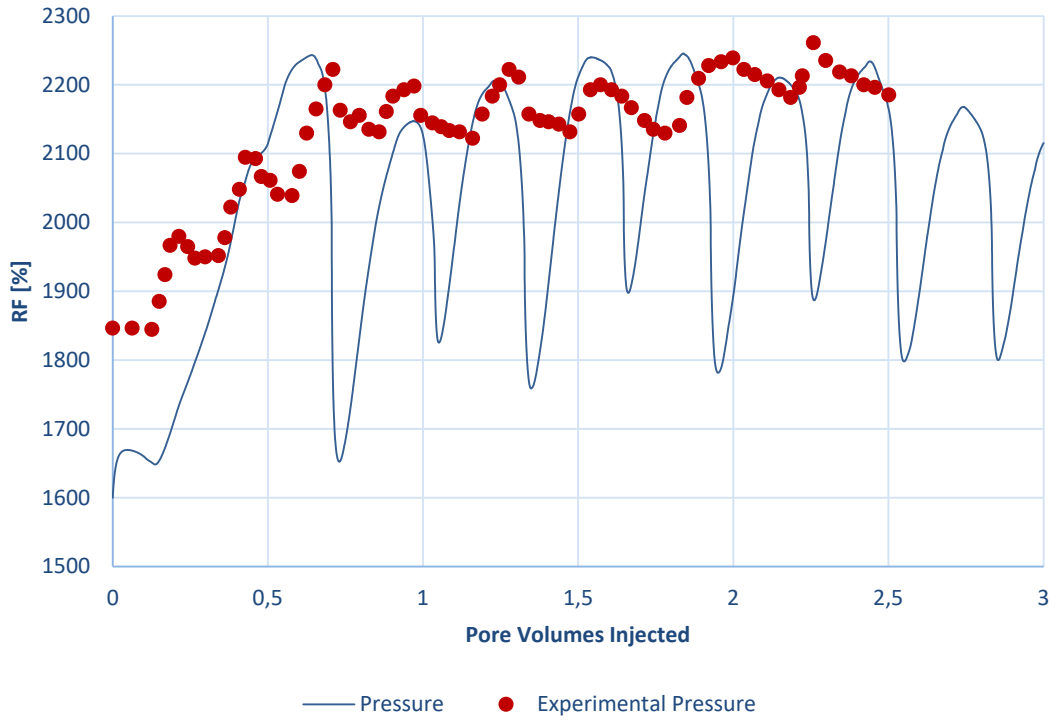


Figure 5-13: WAG Pressure – History Match

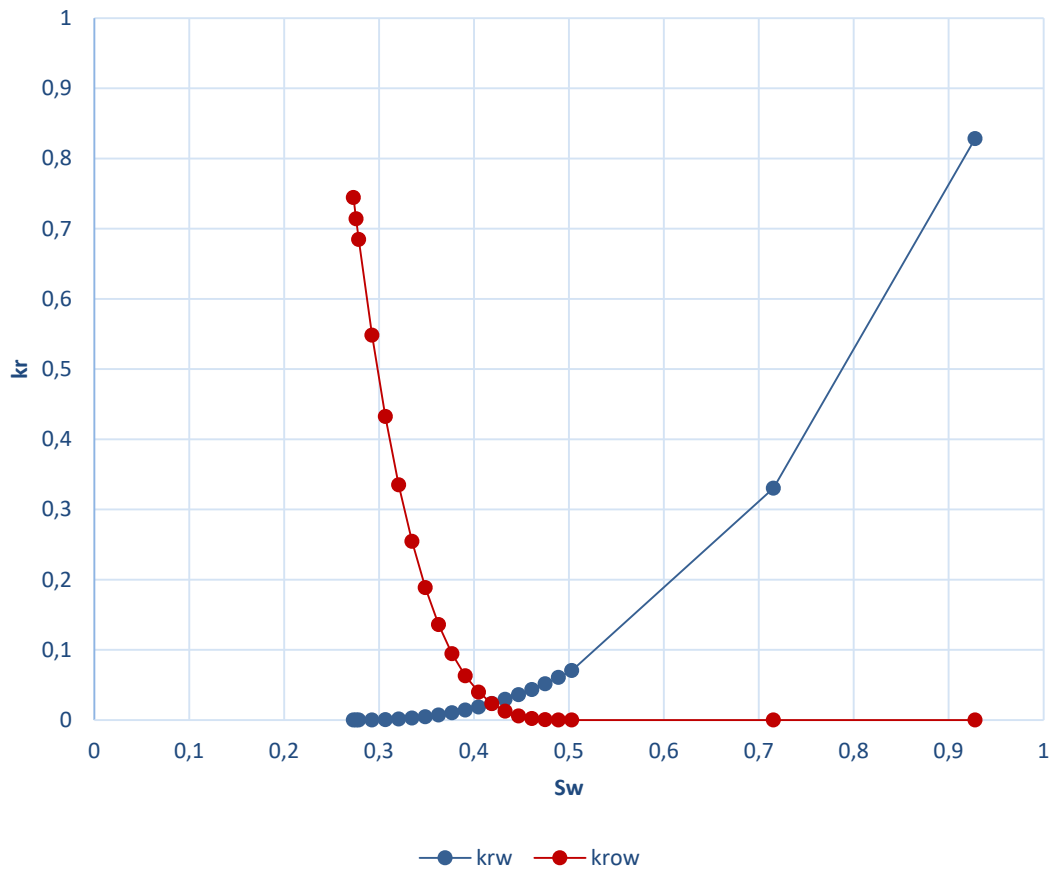


Figure 5-14: Water relative permeability curve after the history match.

5.4.3 FAWAG Core Flooding

The final step to simulating foam flooding correctly is to introduce the established relative permeability curves to the FAWAG simulation model. The data used for this match can be found in (Gandomkar, et al., 2012). The FAWAG core is 15.88 cm long, has a porosity and permeability of 14.22% and 0.86 mD, respectively, and the flood is conducted at 1700 psi and 115°F. There were 10 cycles (5 cycles for water and gas each) at a ratio of “one to one”. Roughly 1.43 pore volumes were injected into the core. Important to note is the inclusion of surfactant adsorption at different concentrations, as shown in Figure 5-15. These data were obtained from the foam flooding experiments in a circulatory system. Because our model will solely be flooded at a concentration of 2,000 ppm, this value is the most influential one as increases in recovery cease to appear with higher concentrations (Gandomkar, et al., 2012).

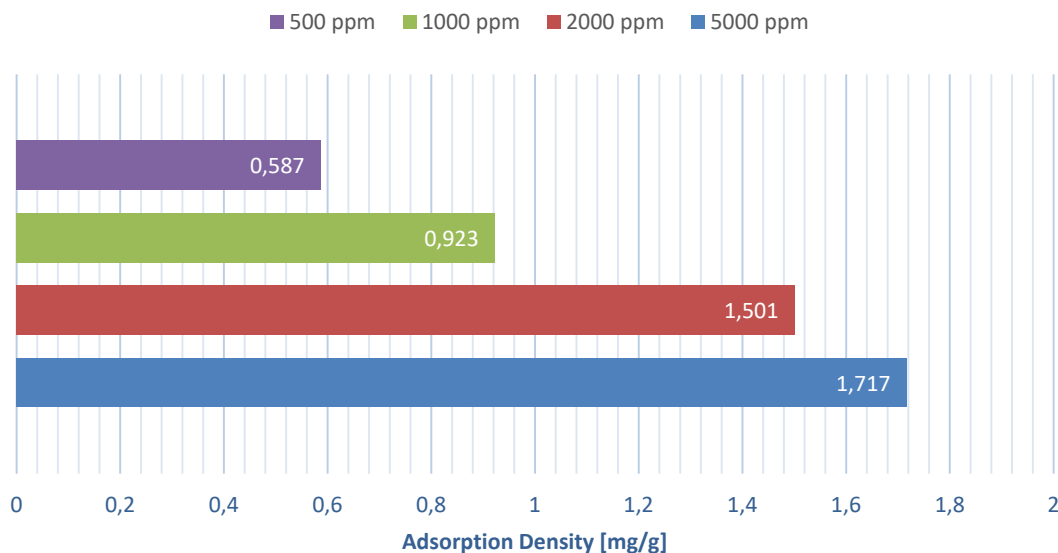


Figure 5-15: Adsorption density vs. surfactant concentration

In this history match, only the FMMOB parameter was varied along with the hysteresis parameters as foam injection is known for altering hysteresis effects. Other foam altering qualities like surfactant concentration, oil saturation dependency, and foam dry-out were left out to reduce computing time and improve results. The resulting match contains some impurities. The reasons for that may be different oil properties of the recombined oil used in the experiment, miscibility effects of the CO₂, or the averaging of results for visual purposes (Figure 5-16 to Figure 5-18). Due to uncertainties in the data preparation of the experiments, about 5% RF have been added to some historical data points, but the residual oil saturation was left untouched. The history match determined the FMMOB value of **14.962357** to be the best fitting. The results suggest that the FAWAG is indeed reducing gas mobility. This is indicated

by the stepwise production of the gas in Figure 5-18. The breakthrough can be seen to be happening at around 0.85 PVI.

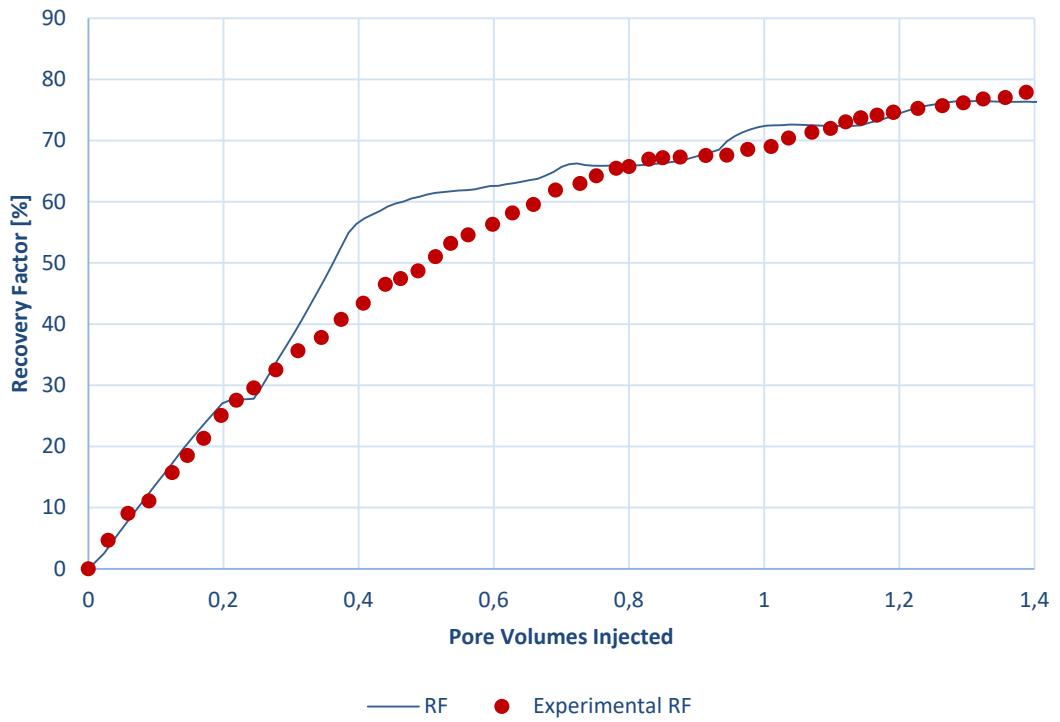


Figure 5-16: FAWAG Recovery Factor – History Match

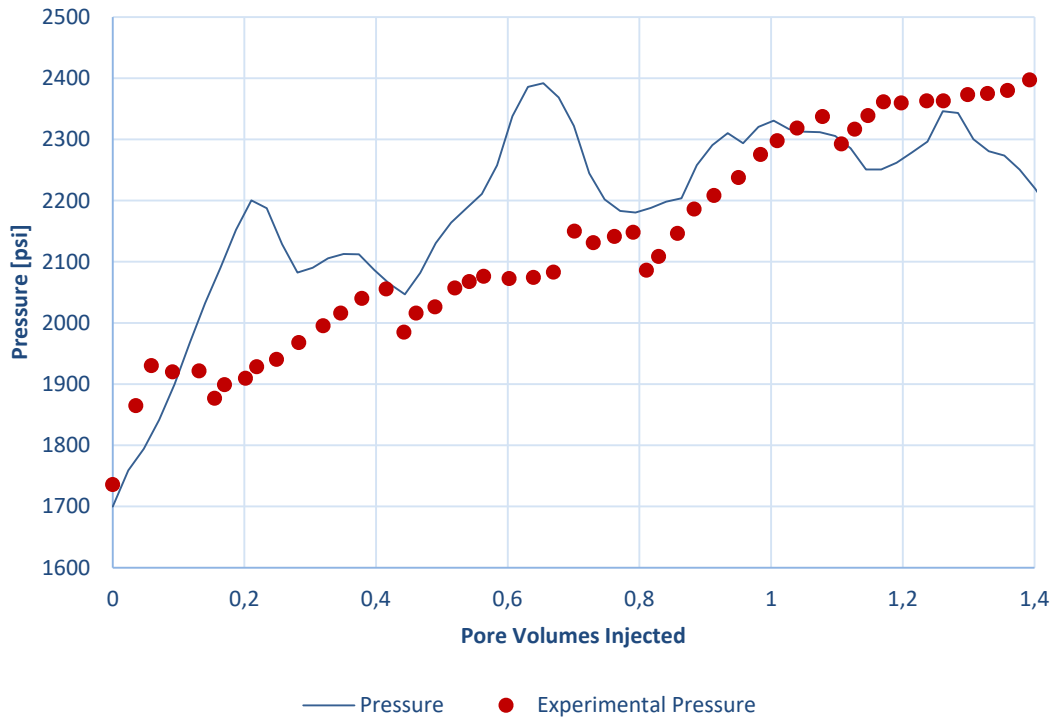


Figure 5-17: FAWAG Pressure – History Match

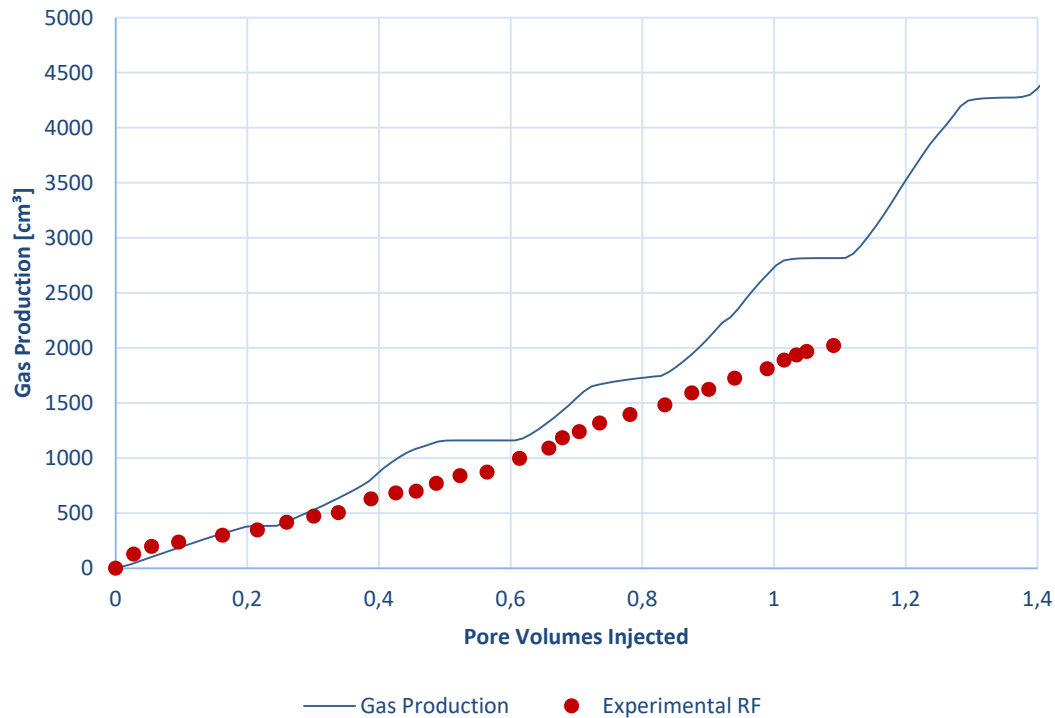


Figure 5-18: FAWAG Gas Production – History Match

5.4.4 Optimum Water to Oil Ratio in FAWAG Processes

To see which water to gas ratio is best for enhancing the oil recovery efficiency of our FAWAG process, the same experimental simulation with 115°F and 1700 psi was reused and altered to inject in fashions of (water to gas):

1 to 3	3 to 2
2 to 3	3 to 1

The trend has shown that a higher gas ratio will always lead to better recovery efficiency (Figure 5-19 and Figure 5-20). Due to the core being intermediate-wet (with a proclivity towards oil-wet), it was expected that a lower water to gas ratio would increase the production and indeed, that was the case. By far, the worst result was produced by a water to gas ratio of 3 to 1. It should be avoided because the oil recovery efficiency is substantially lower in the first two pore volumes than in the other cases. More gas leads to a better foam generation and, therefore, a better sweep efficiency. This, in turn, allows the gas to contact more oil in the process and therefore mobilises the oil more effectively.

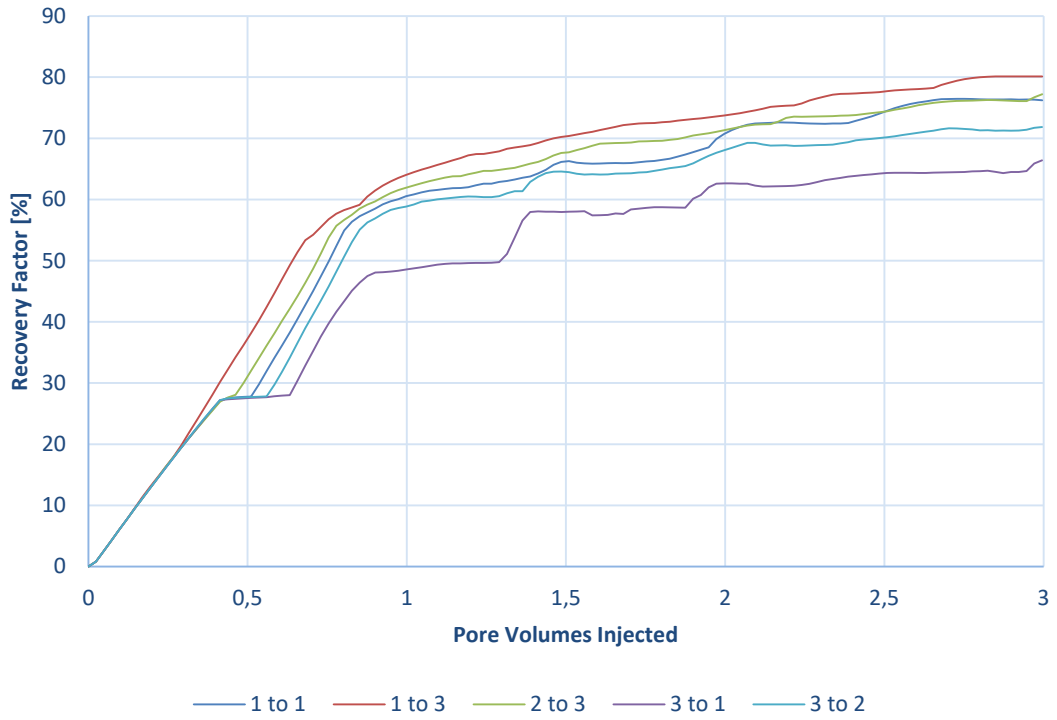


Figure 5-19: Comparison of the recovery factor of different water-gas-ratios for FAWAG injection

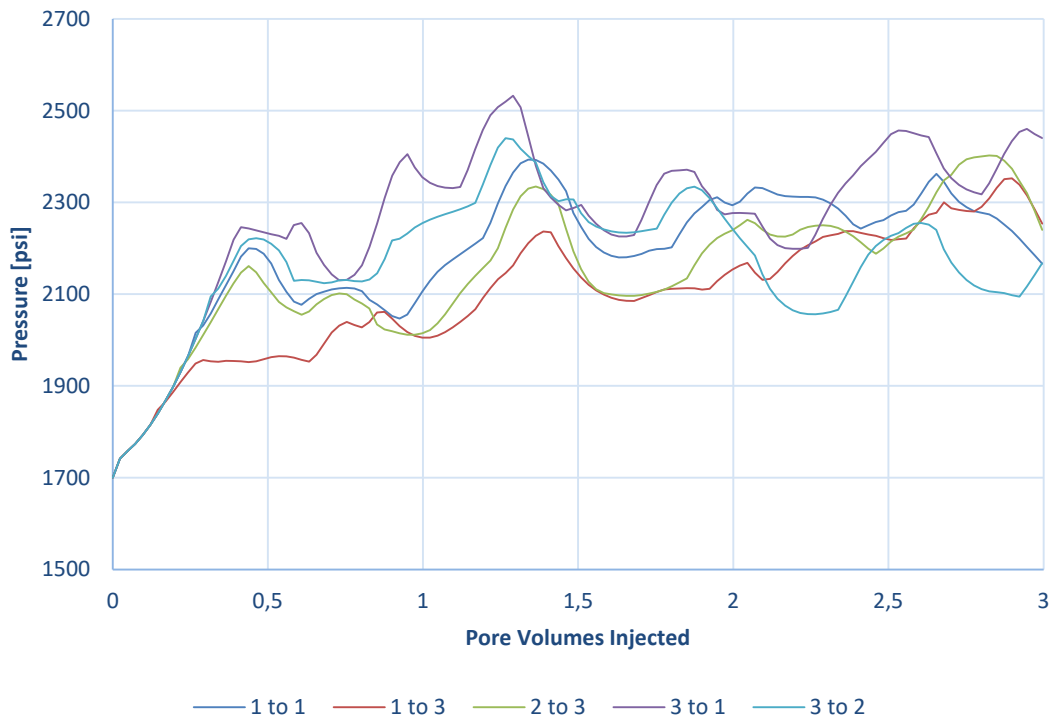


Figure 5-20: Comparison of the core pressure for different water-gas ratios for FAWAG injections.

5.5 Gas Invaded Core [Tertiary Recovery]

After inferring the relative permeability curves from the experiments above, a core was simulated to be flooded with CH_4 to emulate an artificial gas invaded zone in the core of 40% gas saturation, according to Gandomkar's and Kharrat's (2012) work. Two RESTART cases were then created in which the core was then flooded with both WAG and FAWAG processes to compare the efficiency of both in such an environment. Again, the reservoir conditions were 1700 psi and 115°F. The FAWAG process comes on top, showing that it may increase the ultimate recovery by more than 7% compared to pure WAG injection (Figure 5-21 and Figure 5-22). Foam injection has a more stable pressure development as a result. This is due to the gas's low mobility in the core. It travels at a slower pace than in the WAG process, contacting more oil on its path through the core.

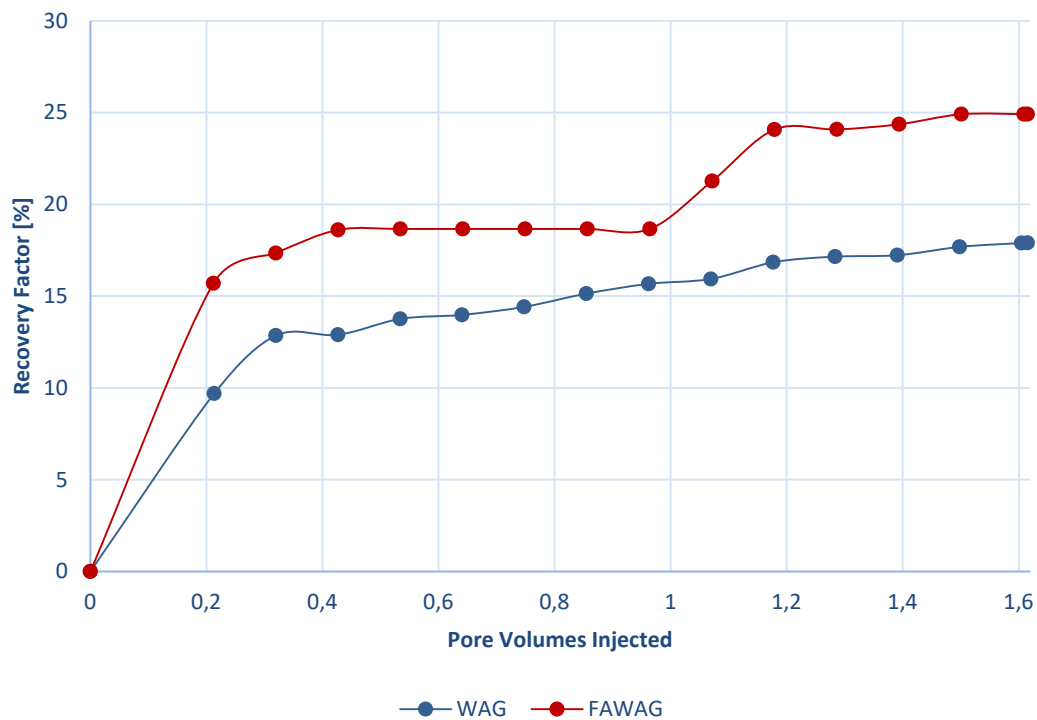


Figure 5-21: Comparison of the recovery factor for WAG and FAWAG as a tertiary recovery process.

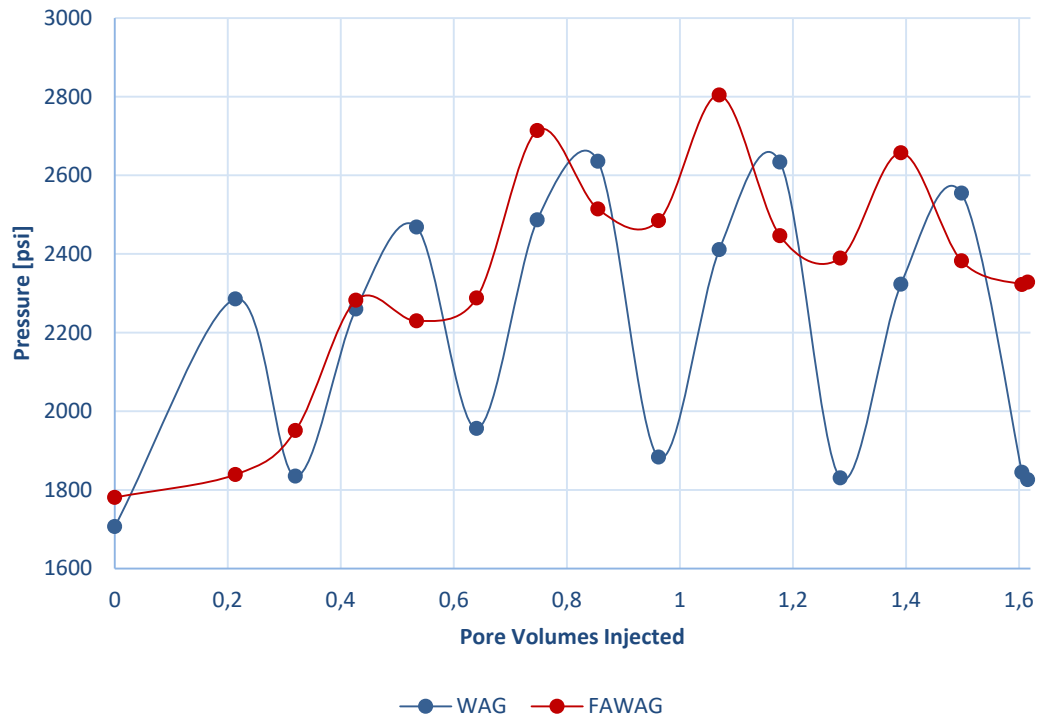


Figure 5-22: Comparison of the core pressure for WAG and FAWAG as a tertiary recovery process.

5.6 Pilot Model Setup

The final step was to create a pilot model that will be used to simulate real-life conditions. This pilot model imitates a quarter of a five-spot pattern (Figure 5-23). The reason behind that was the lack of access to appropriate devices with enough computational power due to the pandemic and to reduce run-time overall. The grid in use was 15x15x8 in x, y, and z, with an overall length of 150m x 150m x 6m. The porosity was distributed normally on a range from 0.05% to 32%. The correlation for the permeability characterisation of carbonate rocks used was:

$$k = 1014 * FZI^2 * \frac{\phi^3}{(1 - \phi)^2} \tag{5.1}$$

Where FZI is the flow zone indicator, which is used in regression models and ϕ the porosity, for FZI, the value of 0.861 was used as it is the most suitable for our type of carbonate rock (Chekani & Kharrat, 2009). The number 1014 was derived from FZI’s conversion number. The pilot model was flooded with 0.8 PVI of CO₂, WAG (0.4 PVI each), and FAWAG (0.4 PVI each) at a cycle of 0.2 PVI. Injection of more did not yield more oil recovery on any method and only increased computing time for such a demanding model.

The reservoir conditions were chosen to be 115°F and 1960 psi. This pilot model was set up to be a dual porosity model, meaning that fractures were implemented. The fracture porosity was set to be 5%, and the fracture permeability 1000 mD. The fracture spacing was assigned to be

0.4, 0.4, and 0.2 in x, y, and z, respectively. Lastly, the relative permeability curves were set to be straight lines.

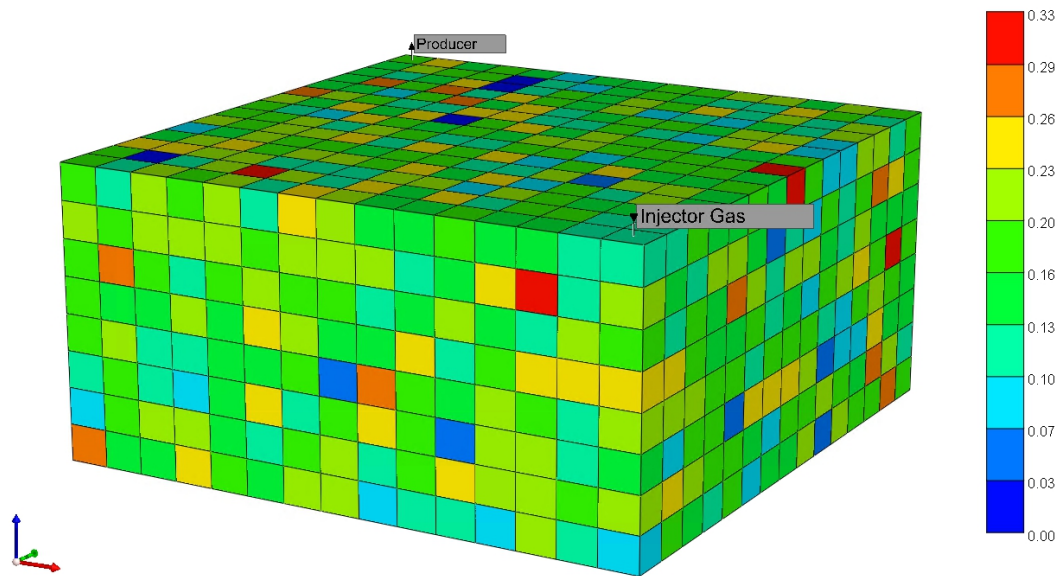


Figure 5-23: Quarter five-spot pilot simulation model (porosity profile)

5.7 Sector Model [Gas Invaded Zone]

The sector model was provided, and simplified replication of a real reservoir model based on actual data. This sector model has a very low permeability ranging between 0.01 mD and 10.1 mD and an average permeability of about 14%, which is representative of the cores that we used in the history match (Figure 5-24). In order to create an artificial gas invaded zone, fictional horizontal injection and production wells were placed on the upper most layer and lower most layer, respectively, to create a suitable gas invaded zone in the sector model (Figure 5-25). Methane was injected and when we reached an approximate 40% of gas saturation in the upper most layers, as it can be seen in Figure 5-26, A dual-five-spot well pattern was installed to test the recovery efficiency of pure water flooding, CO₂ injection, WAG and FAWAG displacement. WAG and FAWAG were injected at alternating 0.2 PVI until injection of 1 pore volume was reached, e.g., three cycles of water and two cycles of gas. In a further experiment, the slugs were reduced to 0.1 PVI, increasing the cycles to five for both fluids, and the injection of CO₂ and the gas associated with the reservoir oil were compared as the preferred gas for FAWAG injection (Figure 5-27, Figure 5-28, and Figure 5-29).

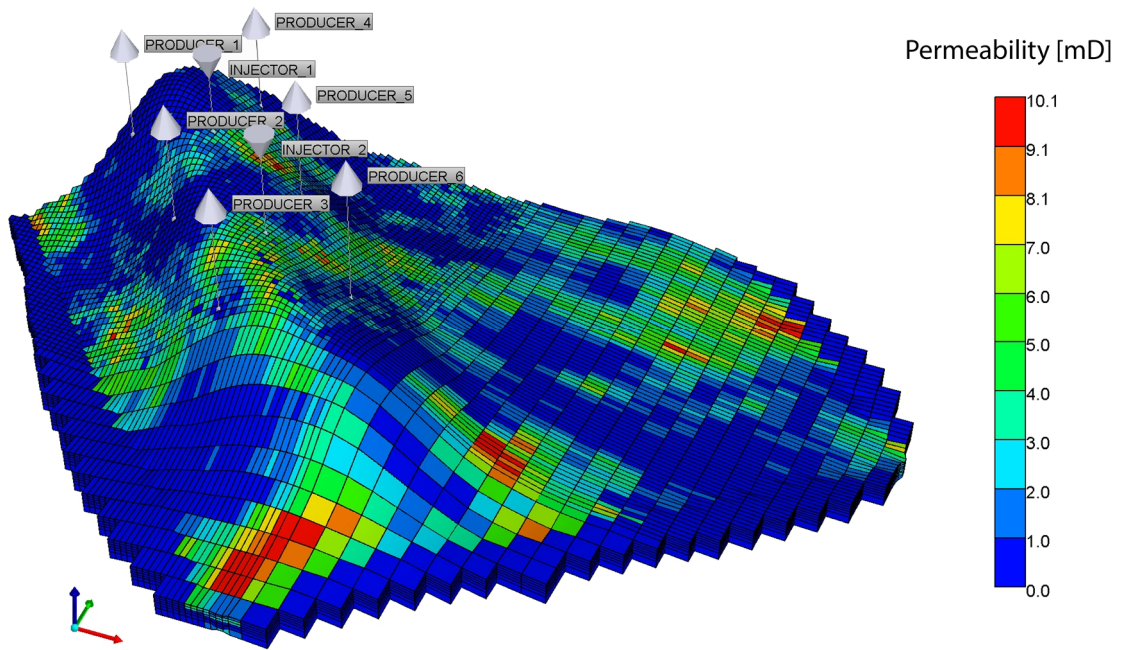


Figure 5-24: The sector model and its dual-five-spot well-placement.

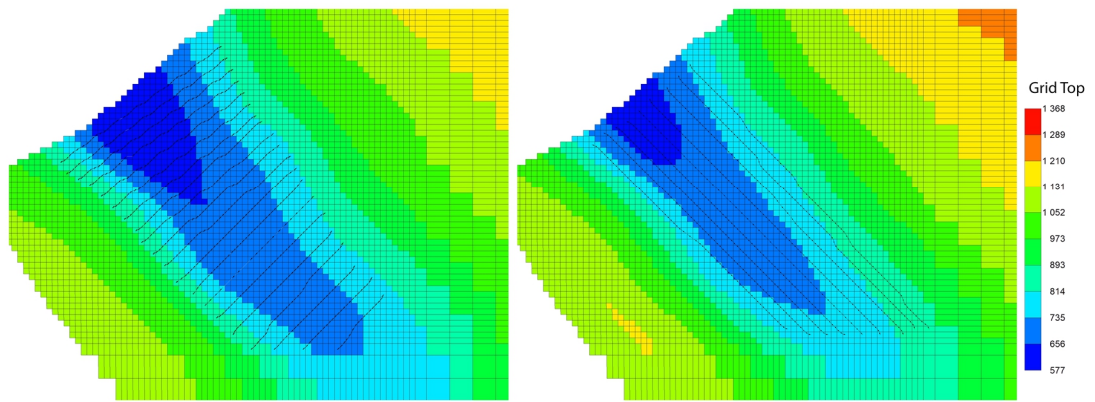


Figure 5-25: Well-placement for the creation of the gas invaded zone; left: injectors (layer 1), right: producers (layer 7). [Grid Top in metres]

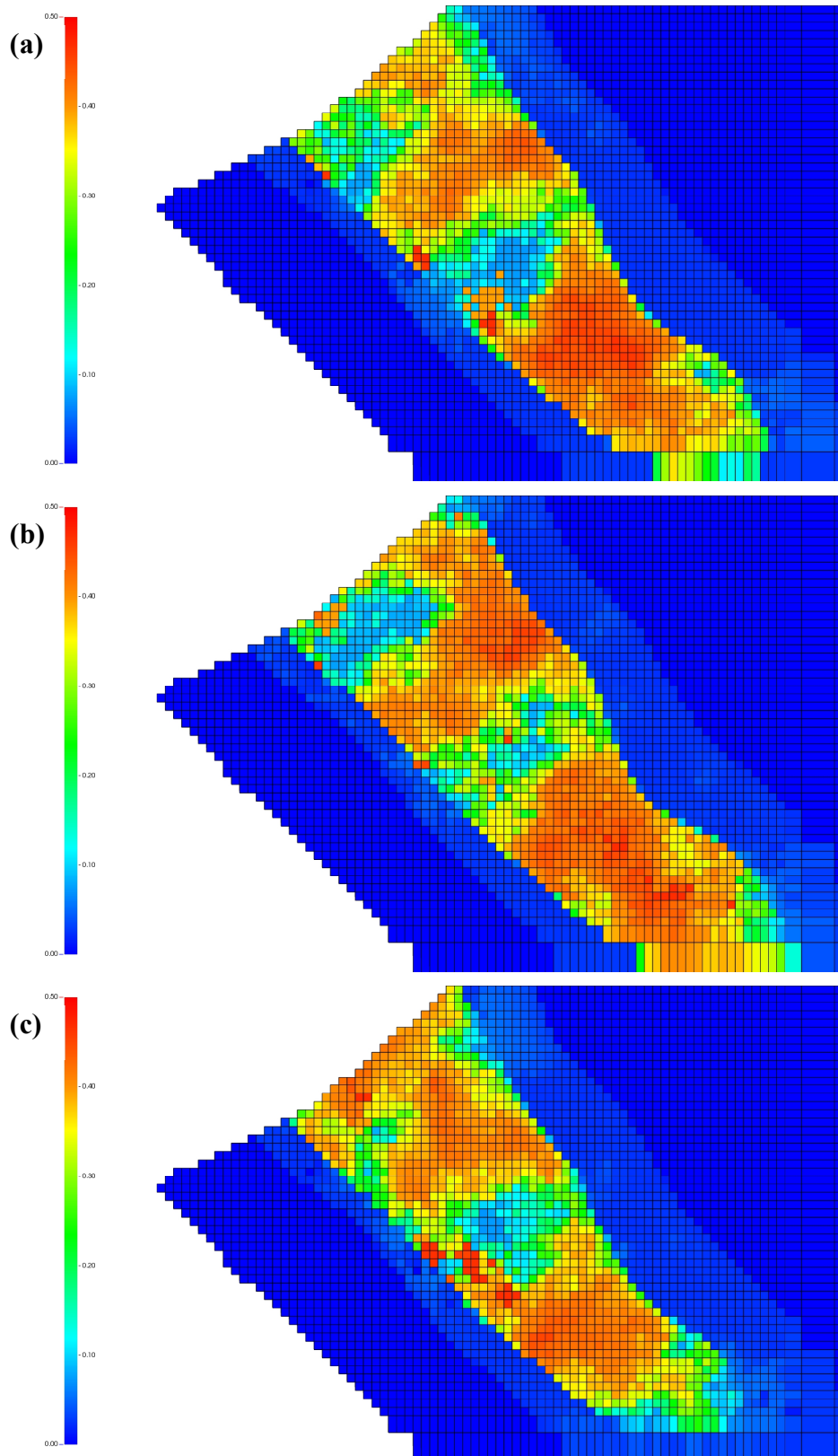


Figure 5-26: Gas saturation after the creation of a gas invaded zone in layer 1 (a), 2 (b) and 3 (c).

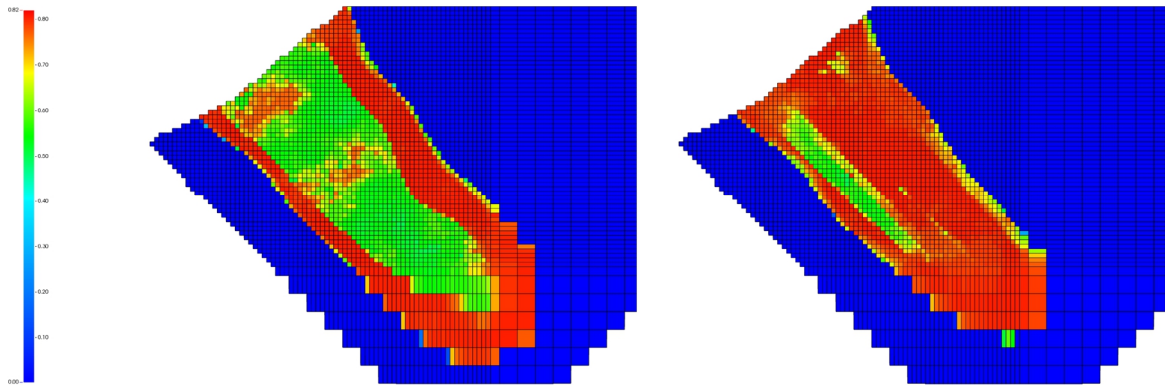


Figure 5-27: Oil saturation after the creation of the gas invaded zone in layer 1 (left) and layer 7 (right).

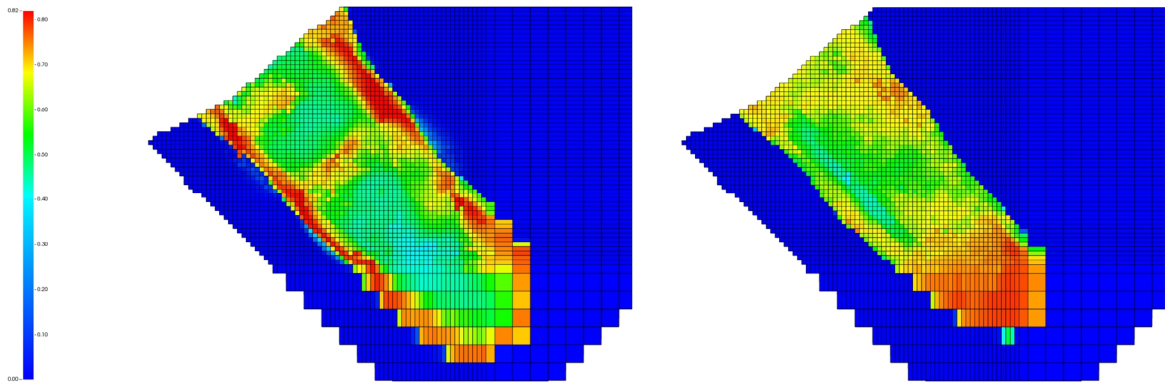


Figure 5-28: Oil saturation after 1 PV of WAG displacement in layer 1 (left) and layer 7 (right).

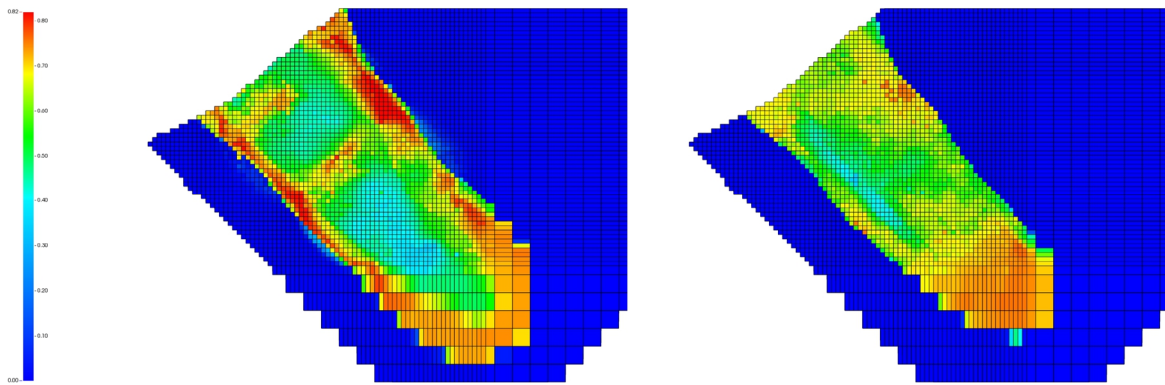


Figure 5-29: Oil saturation after 1 PV of FAWAG displacement in layer 1 (left) and layer 7 (right).

Chapter 6

Results

6.1 Pilot Model [Secondary Recovery]

The results show an undeniable advantage of using foam as the EOR method of choice. The ultimate recovery of the foam injection adds 25% to the recovery efficiency of pure WAG displacement (Figure 6-1). This result can be attributed higher pressure (Figure 6-2) and to the lowering of the gas mobility due to the presence of foam and, therefore, enhanced sweep efficiency. This is undermined by the fact that gas breakthrough is postponed to almost 0.7 PVI injected, which equates to the second gas cycle (0.3 PVI) and can be seen in Figure 6-3.

The reason for the higher recovery can be accredited to the gas's proclivity to high-permeability paths and a foam's tendency to possess a higher apparent viscosity in high-permeability layers. This characteristic also helps to divert the injected fluids into the lower-permeability zones (Hirasaki, 1989).

Gas breakthrough in the WAG process, on the other hand, occurs as early as 0.2 PVI. That means that the breakthrough is happening as soon as the gas injection starts. Furthermore, this fact is supported by the constant pressure build-up, which is an inherent effect of foam injection. CO₂ injection only becomes more effective than WAG displacement after 0.8 PVI, rendering it the most cost-ineffective recovery method. WAG injection enjoys a more favourable mobility ratio, making it a better option than CO₂.

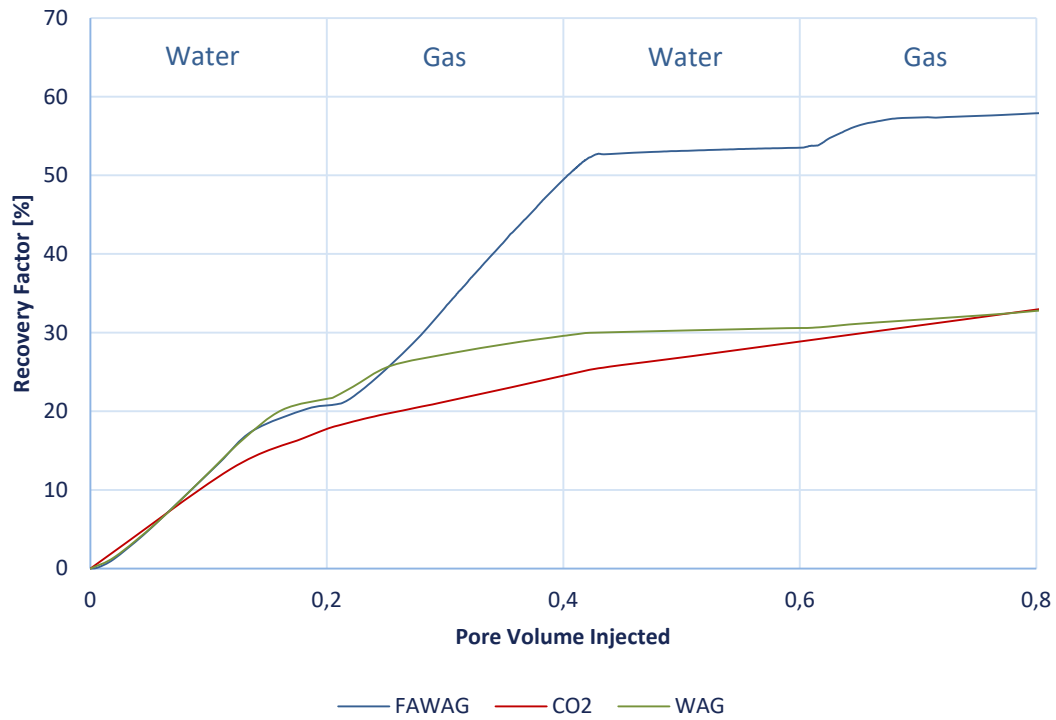


Figure 6-1: Comparison of the recovery factor of WAG, FAWAG and CO₂ injection in the pilot model.

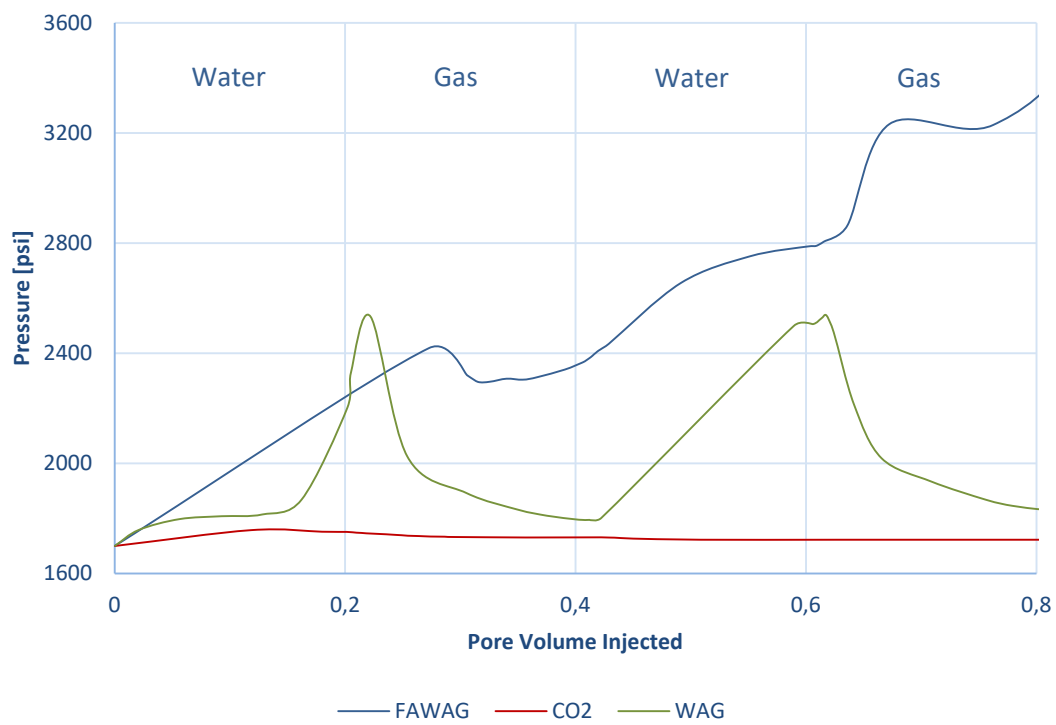


Figure 6-2: Comparison of the reservoir pressure for WAG, FAWAG and CO₂ injection in the pilot model.

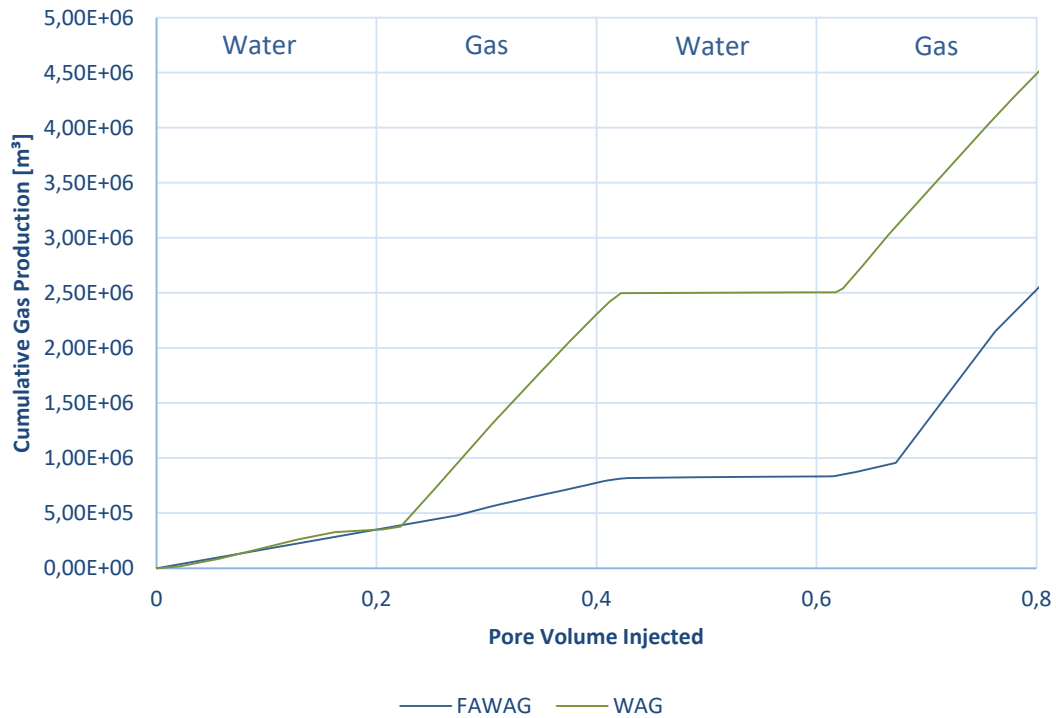


Figure 6-3: Comparison of the cumulative gas production in WAG and FAWAG processes in the pilot model.

6.2 Pilot Model [Tertiary Recovery]

In this model, the quarter five-spot model was firstly flooded with gas until a gas saturation of 40% was reached, and then CO₂, WAG, and FAWAG were introduced to the injection strategy. The recovery factor, reservoir pressure, and cumulative gas production are shown in Figures 6-4 to 6-6, respectively. FAWAG enhances the oil recovery by a remarkable 20% on top of a simple WAG strategy. Injecting CO₂, again, becomes better than WAG after 1 PVI taking it out of consideration. The high gas saturation in the model increases the gas mobility and thus enhances effects like gravity override and fingering, leading to an early breakthrough. FAWAG recovery increases stepwise. This can be explained by the low mobility of the gas that is allowing it to contact more of the reservoir. Practically, the low gas mobility hinders the gas invaded fractures to act as a “highway” for the injected gas.

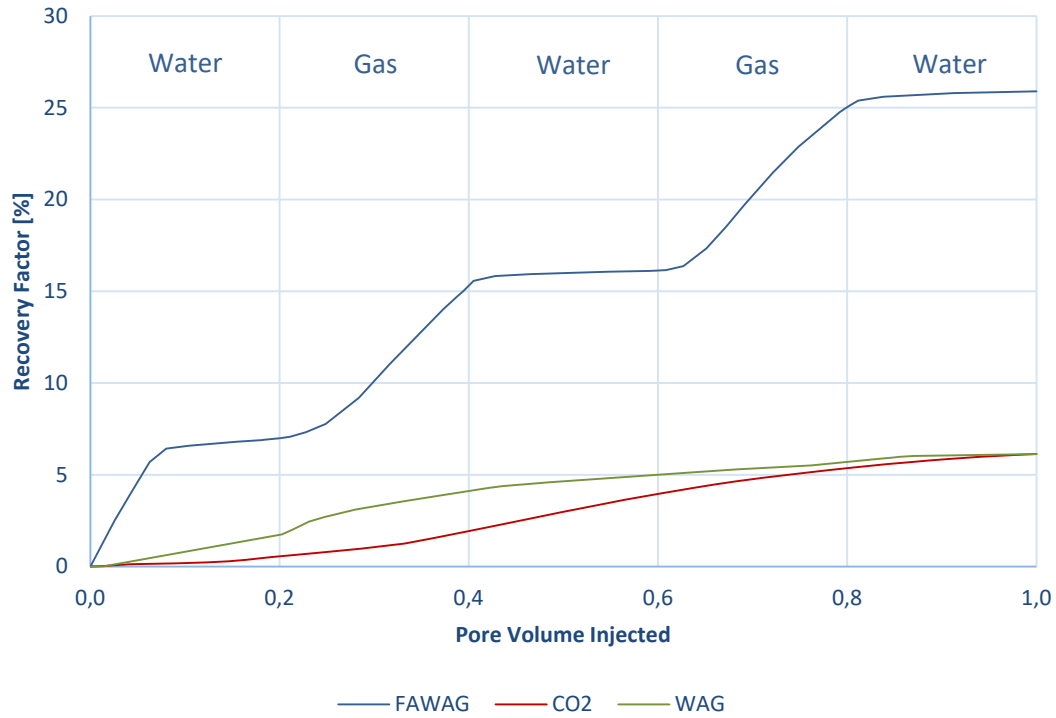


Figure 6-4: Comparison of the recovery factor of WAG, FAWAG, and CO₂ injection in the pilot model with a gas invaded zone of 40%.

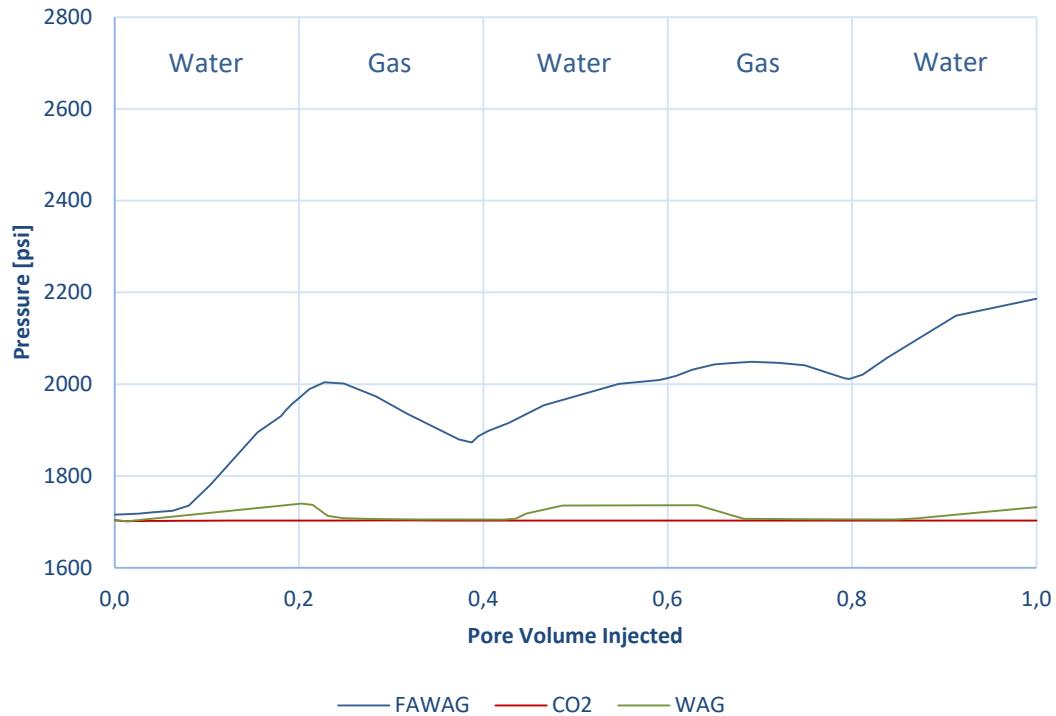


Figure 6-5: Comparison of the reservoir pressure for WAG, FAWAG, and CO₂ injection in the pilot model with a gas invaded zone of 40%.

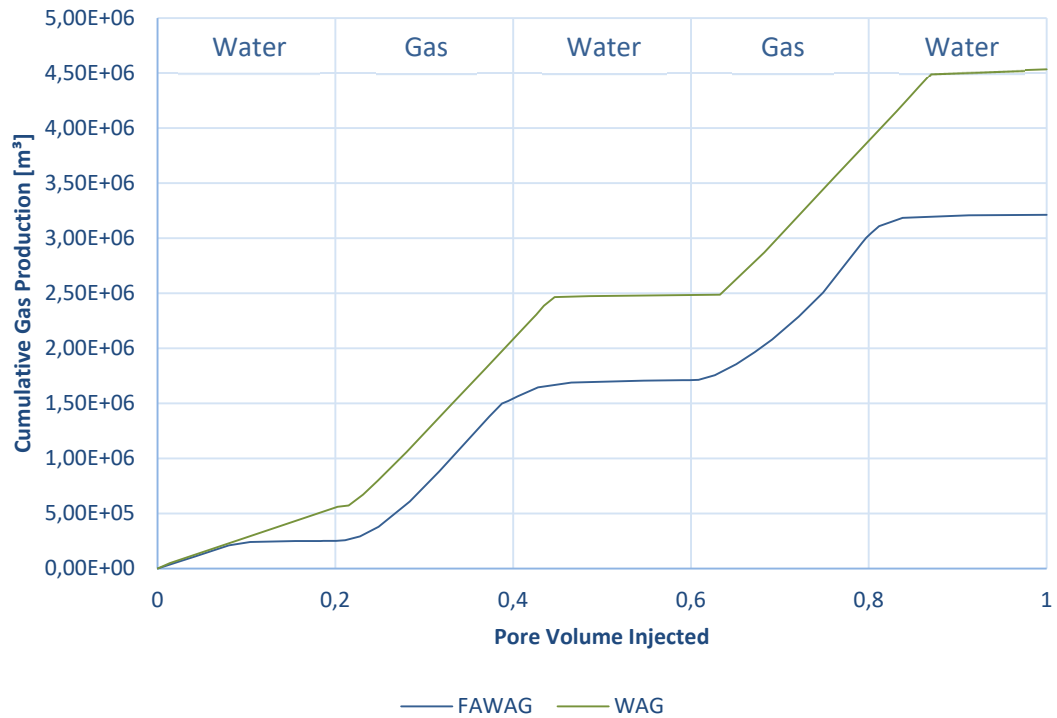


Figure 6-6: Comparison of the cumulative gas production in WAG and FAWAG processes in the pilot model with a gas invaded zone of 40%.

6.3 Homogeneous Cross-Section

To illustrate foam-dependent gas mobility reduction and gas movement in a reservoir and their effect on oil recovery, a fine cross-section-like model was set up (and then injected with both a WAG and a FAWAG displacement process. It consists of 5000 grid blocks (100x1x50) to enhance the visualisation of the fluid movement (Figure 6-7).

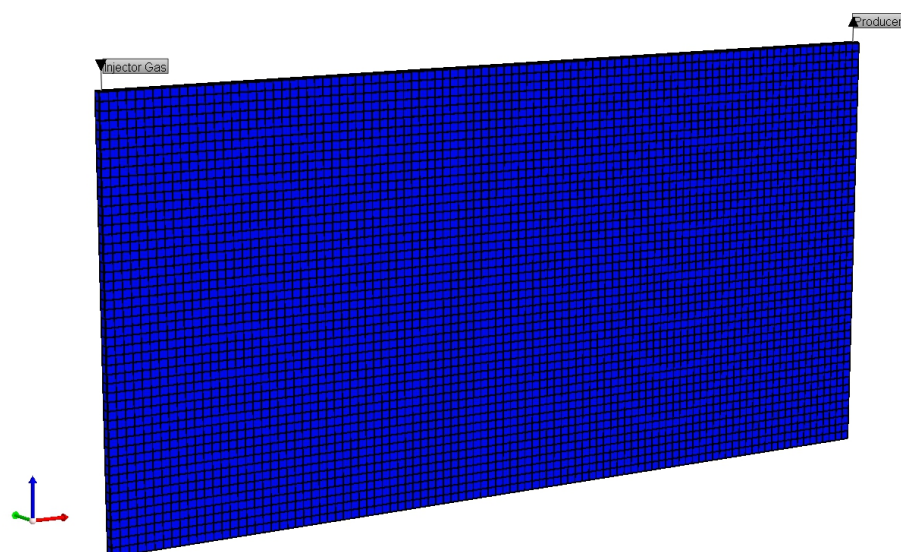


Figure 6-7: Homogeneous Cross-Section Model

The fractional flow model was chosen to be a dual-porosity – dual-permeability model to account for flow between fractures and the matrix and vice versa. The properties of this homogeneous model are:

- k_{Matrix} : 8.169
- k_{Fracture} : 100 mD
- Φ_{Matrix} : 23.8%
- Φ_{Fracture} : 5%
- Fracture Spacing: 0.4 m; 0.4 m; 0.2 m (x; y; z)
- x-length: 1 m
- y-length: 1 m
- z-length: 0.5 m

This model was firstly flooded with 0.2 PVI of water for each case and then with another 0.2 PVI of CO₂. Figure 6-8 below shows the gas saturation in the fractures of the model at precisely the injection of 0.05 PV of CO₂. The gas mobility reduction effect of the foam is noticeable. The gas front is much sharper in the FAWAG process, and gravity override of the gas much less of a concern. The sweep efficiency is, thus, greatly enhanced, leading to much higher oil recovery. The high mobility of a gas forces it to move along the fractures.

Movement along the matrix is rare. Foam has the proclivity to occupy space in the fractures. This means that it also flows through the fractures, but at a much slower pace, allowing for a better sweep efficiency.

The same was realised for a cross-section model that contains a 40% gas invaded zone. Here we injected 0.02 PV of CO₂, and through the CO₂ movement along the fractures it is again visible that the foam allows for a greater volumetric sweep efficiency, displacing fluids from the bottom that the WAG process cannot (Figure 6-9). The Breakthrough is delayed significantly.

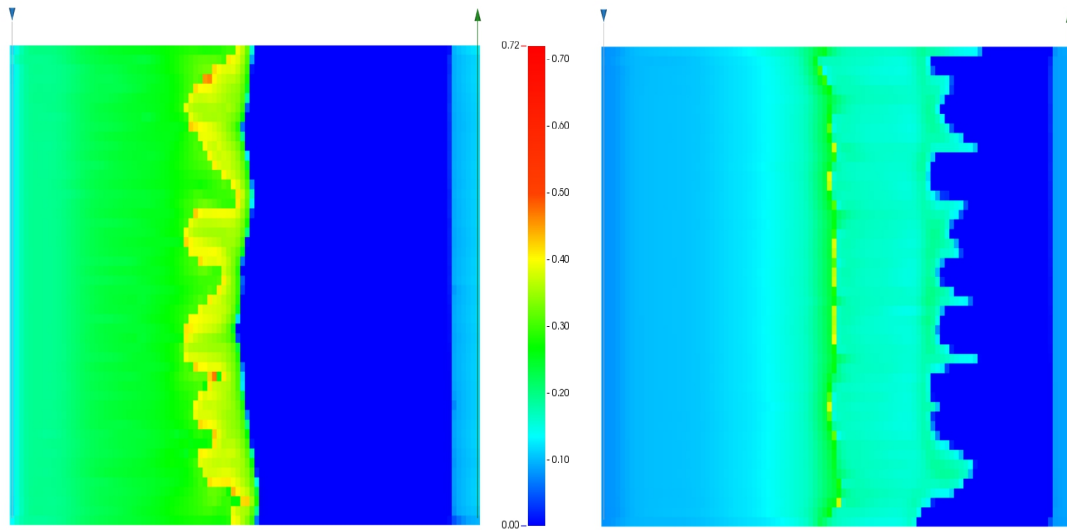


Figure 6-8: Comparison of gas-phase movement for FAWAG (left) and WAG (right) displacement processes after injection of 0.05 PV of CO_2 (gas saturation).

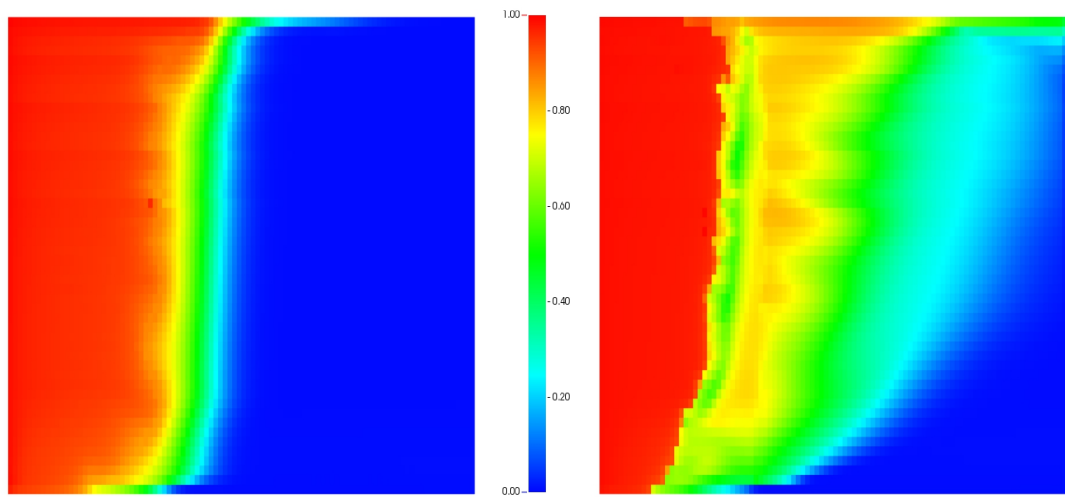


Figure 6-9: Comparison of gas-phase movement for FAWAG (left) and WAG (right) displacement processes after the injection of 0.02 PV of CO_2 in a model with a 40% gas invaded zone (CO_2 mole fraction).

6.4 Sensitivity Analysis

To further investigate the variables that the production from a fractured reservoir depends on, a sensitivity analysis was set-up on the cross-sectional model that we used before but with an initiated gas cap of 40%. Three main variables were investigated on their effect on the oil recovery after injection of 0.2 PV of water and 0.2 PV of gas, and the results are illustrated in Figure 6-10 to 6-12. These are the block height, the fracture permeability, and the fracture spacing. The base case in this study assumes a fracture permeability of 1000 mD. The block height has a big impact on vertical sweep efficiency and was, therefore, varied between half the size of the base model (x0.5), doubling the blocks in the z-direction from 50 to 100, and five times the size (x5), reducing the z-block count from 50 to 10. The next variable was the fracture permeability, which was varied between 100 mD (x0.1), 1000 mD (base case), and 2000 mD (x2). The last variable was fracture spacing. This is a particularly interesting value, as it is used to calculate the fracture size. The basic transmissibility formula used in CMG allows for the fracture spacing to be given values bigger than the actual block size, and still be valid. Only weak matrix-fracture coupling can be a concern. Large fracture spacing implies that all blocks contained in the fractured element will be fractured (Computer Modelling Group LTD., 2019). In the sensitivity analysis, the fracture spacing was varied between a tenth of the original 0.4m / 0.4m / 0.2m in x/y/z-direction (x0.1), i.e. 0.04m / 0.04m / 0.02m, and ten times the original value (x10), i.e. 4m / 4m / 2m. The sensitivity analysis results are shown in Figure 6-13.

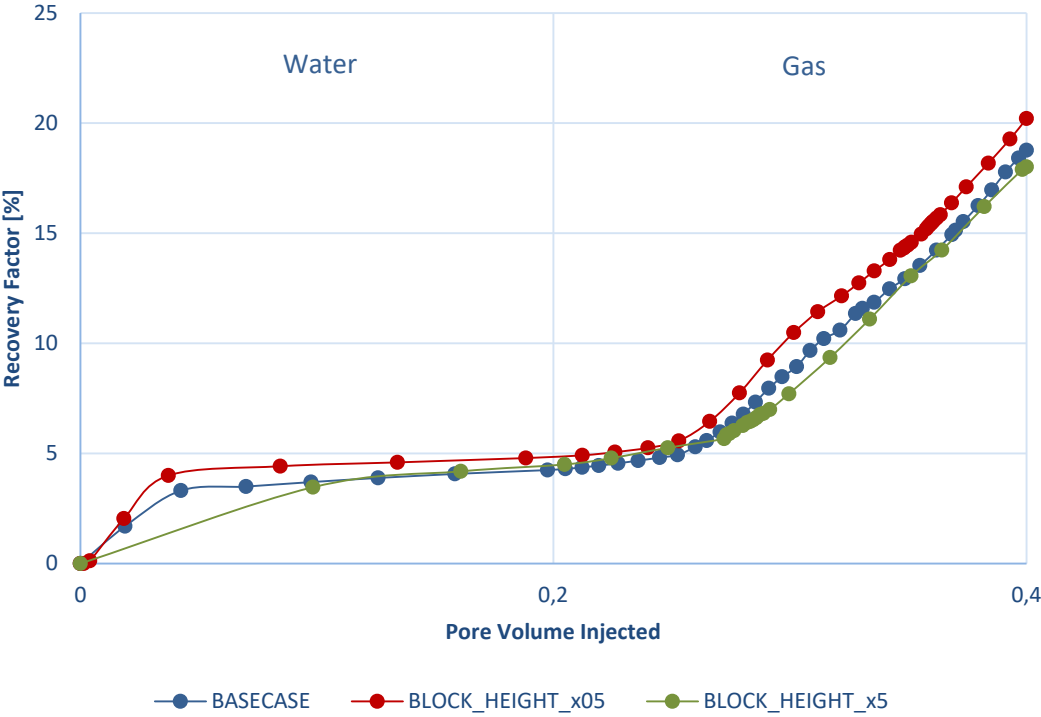


Figure 6-10: Sensitivity Analysis - Block Height

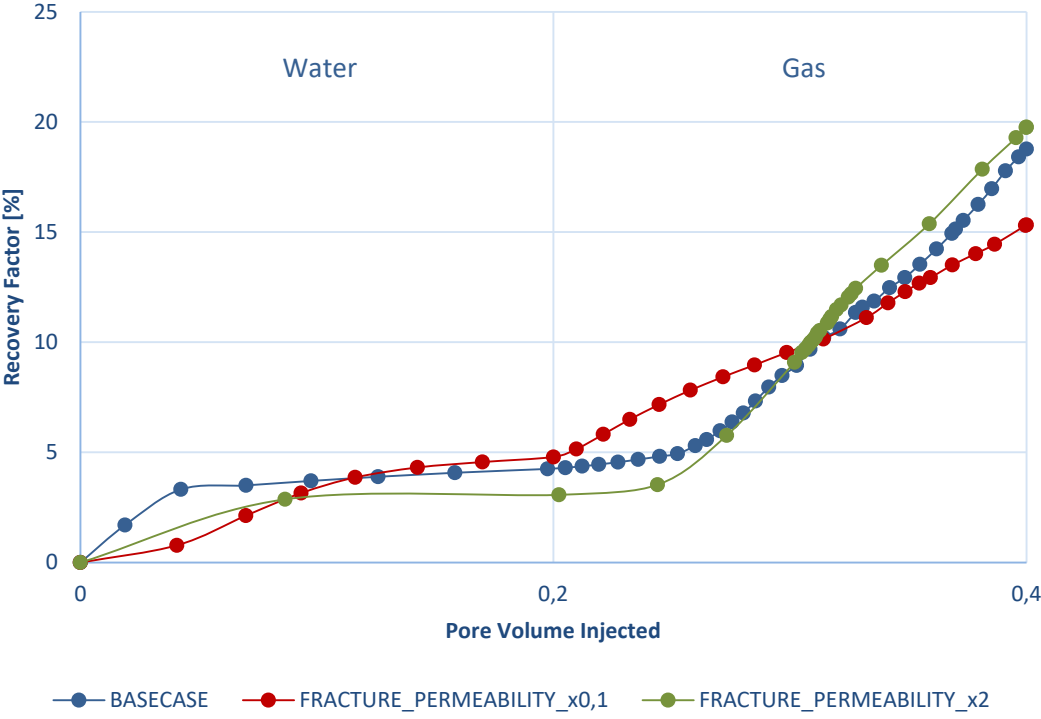


Figure 6-11: Sensitivity Analysis - Fracture Permeability

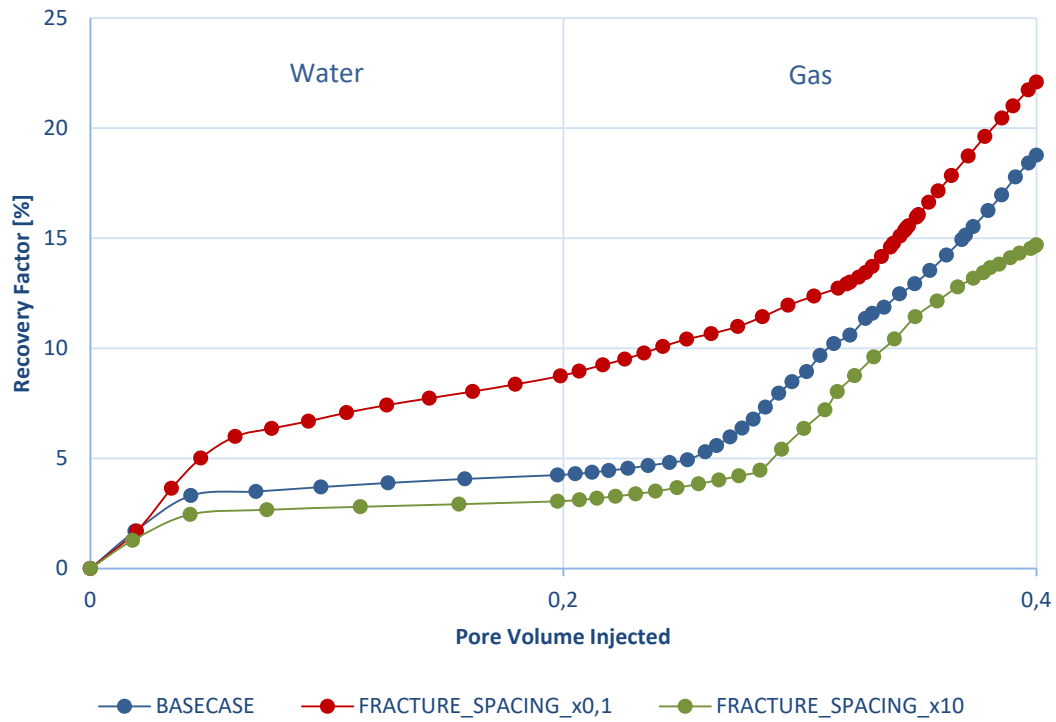


Figure 6-12: Sensitivity Analysis - Fracture Spacing

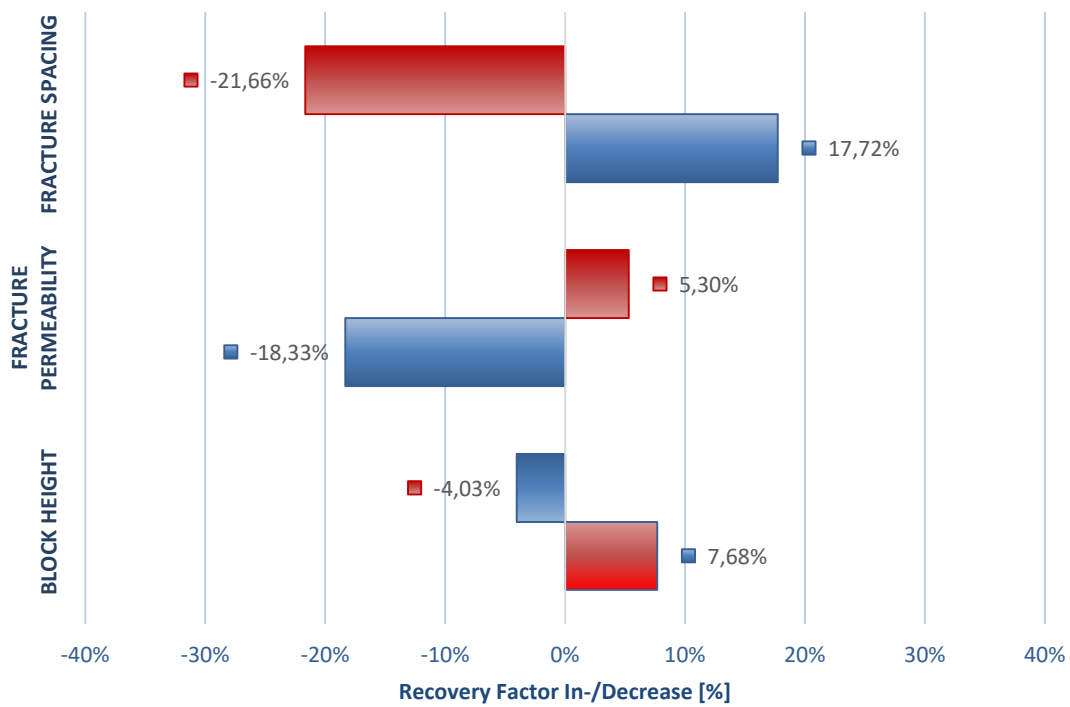


Figure 6-13: Sensitivity Analysis – Recovery factor comparison after 0.4 PVI (red: decrease / blue: increase)

6.5 Sector Model [Tertiary Recovery]

The implementation of FAWAG in the sector model leads to interesting results (Figure 6-14 to Figure 6-20). This simulation run shows that FAWAG was able to outperform WAG by more than 2%. This low number can be justified by the fact that the dual-five spot well placement contacts only roughly two-thirds of the sector oil. Interestingly enough, the GOR and the water cut both increase immediately after the injection of each fluid starts. This is an indication of the presence of highly permeable streaks in the sector. Nevertheless, the GOR in the FAWAG process stays at lower values (Figure 6-18) ultimately leading to a lower gas production (Figure 6-15). The water cut stays the nearly the same for both processes, which was to be expected (Figure 6-19). The average reservoir pressure does not fall as rapidly due to the generation of foam (Figure 6-16). With regards to the WAG-ratio, a lower ratio of 0.1 PV per cycle is preferred (Figure 6-20). The foam generated by the injected gas is a mighty tool to lower the gas mobility. This goes to show that more foam will lead to a higher recovery. Furthermore, there was no significant difference between using CO₂ or associated gas. CO₂ had the higher recovery, but when considering economic reasoning, the use of associated gas for cost reduction is a very valid option (Figure 6-20).

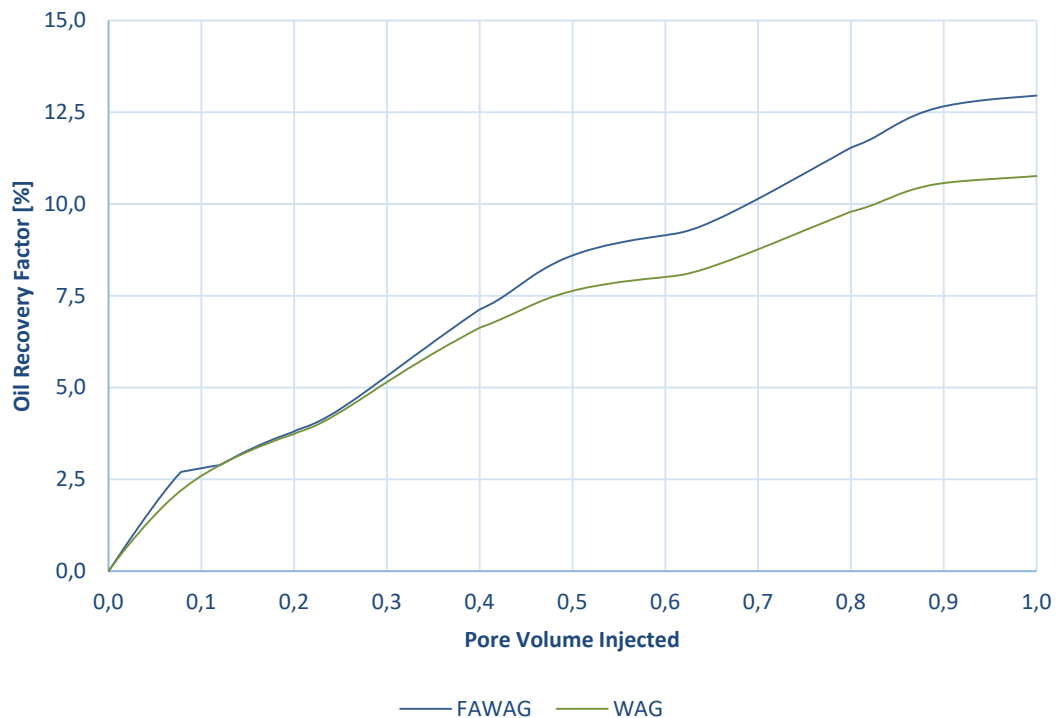


Figure 6-14: Recovery Factor - Sector Model

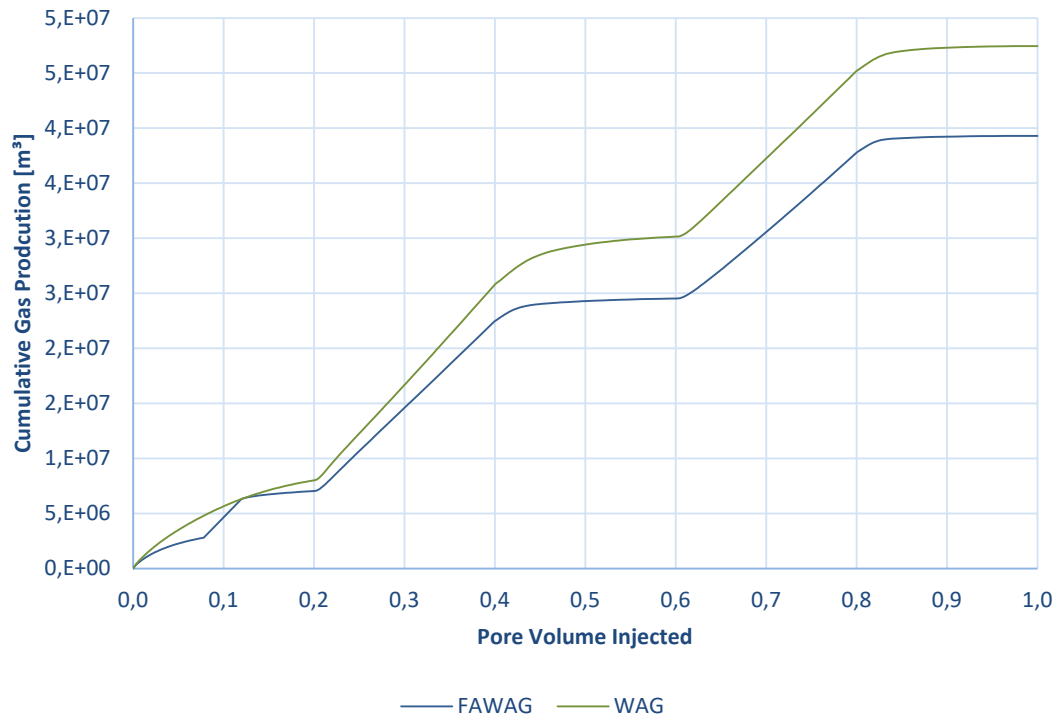


Figure 6-15: Cumulative Gas Production - Sector Model

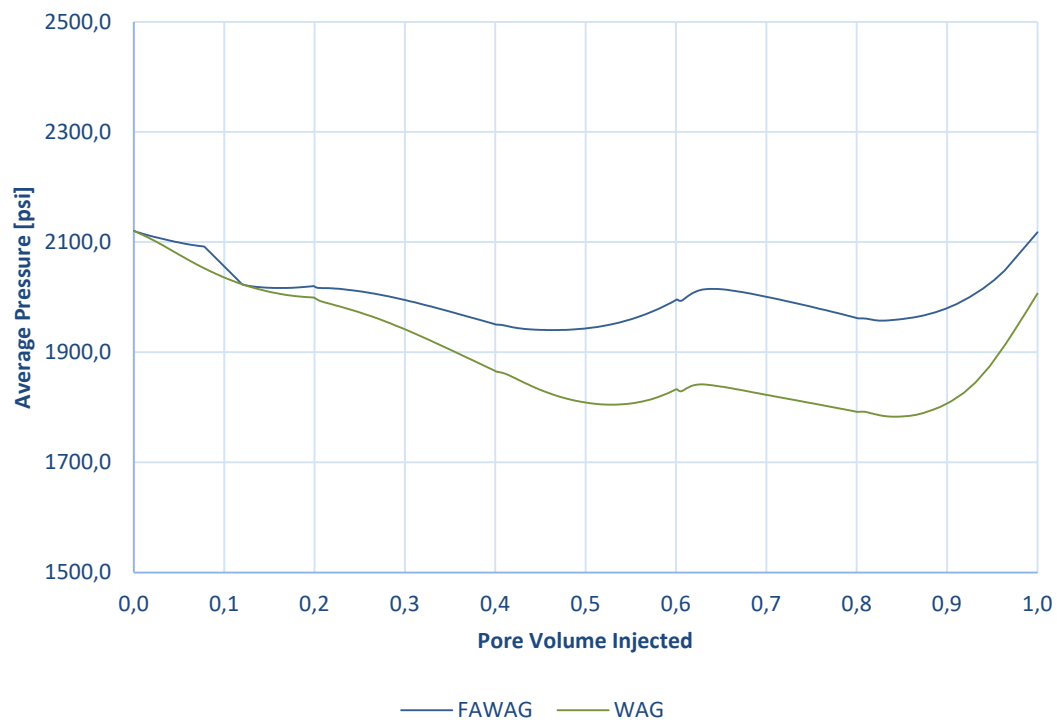


Figure 6-16: Average Pressure - Sector Model

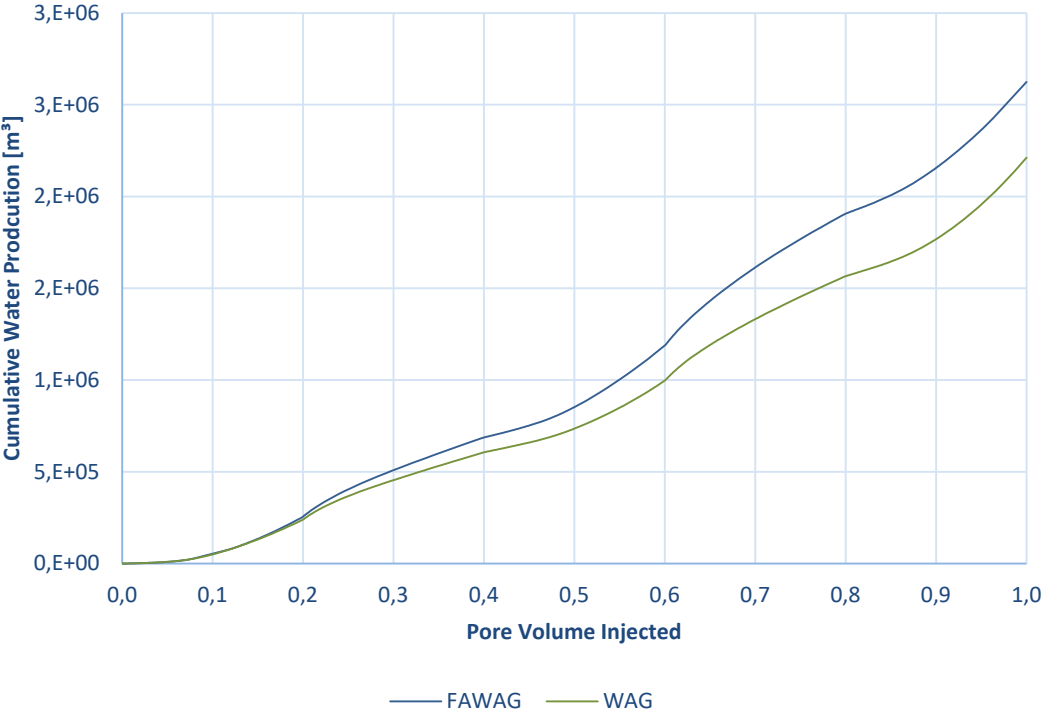


Figure 6-17: Cumulative Water Production - Sector Model

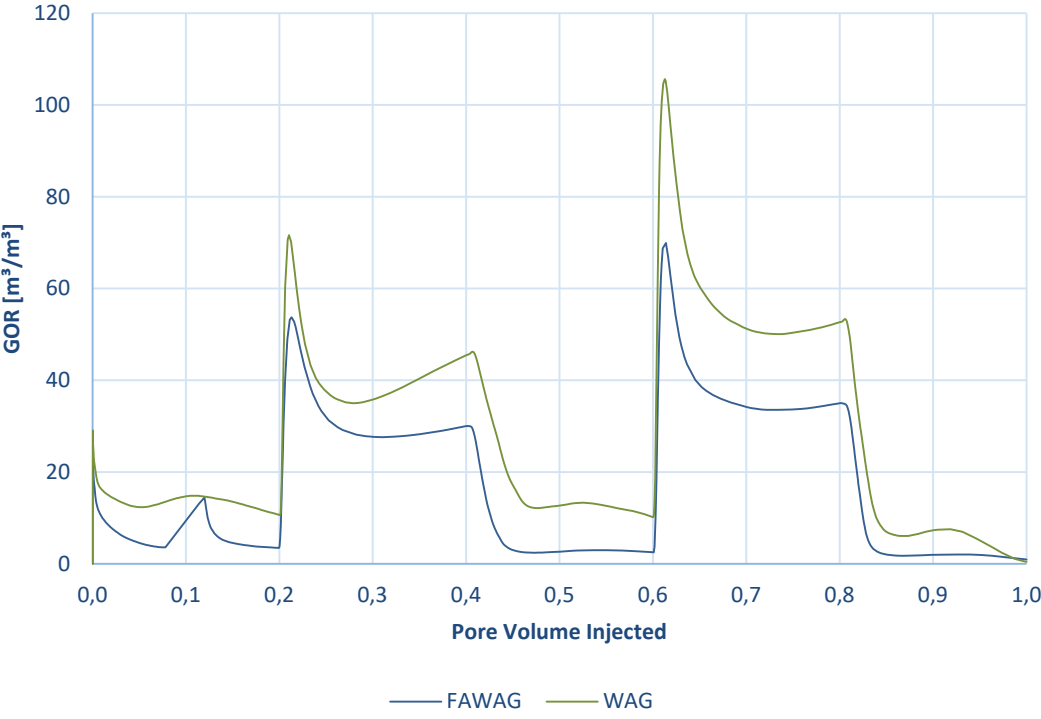


Figure 6-18: Gas-Oil-Ratio - Sector Model

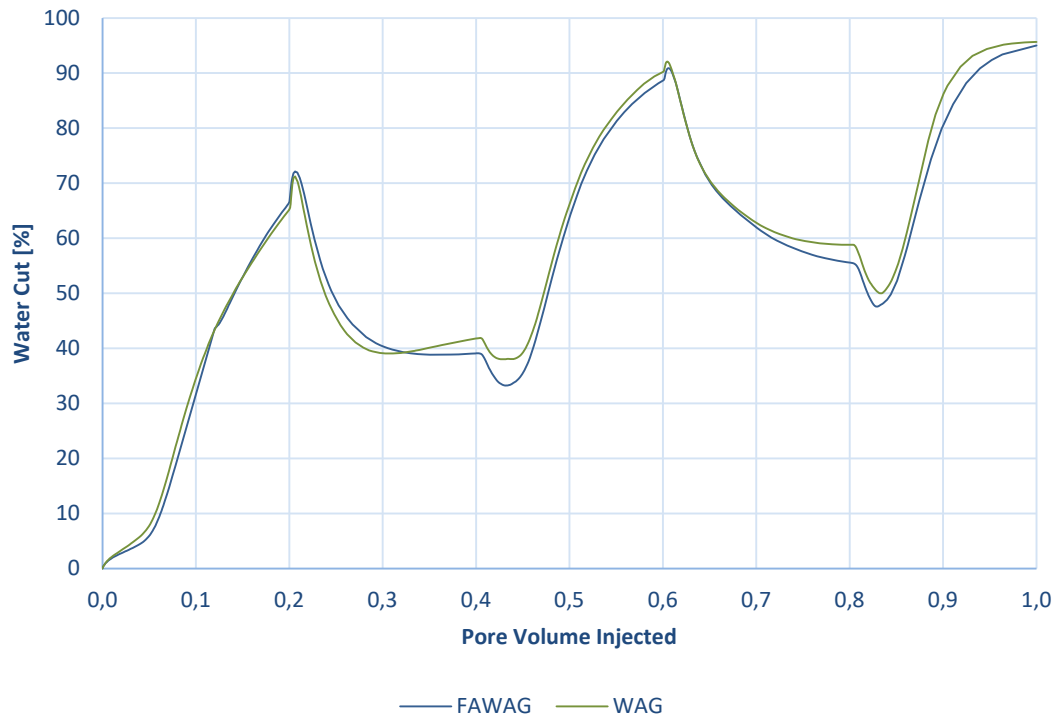


Figure 6-19: Water Cut - Sector Model

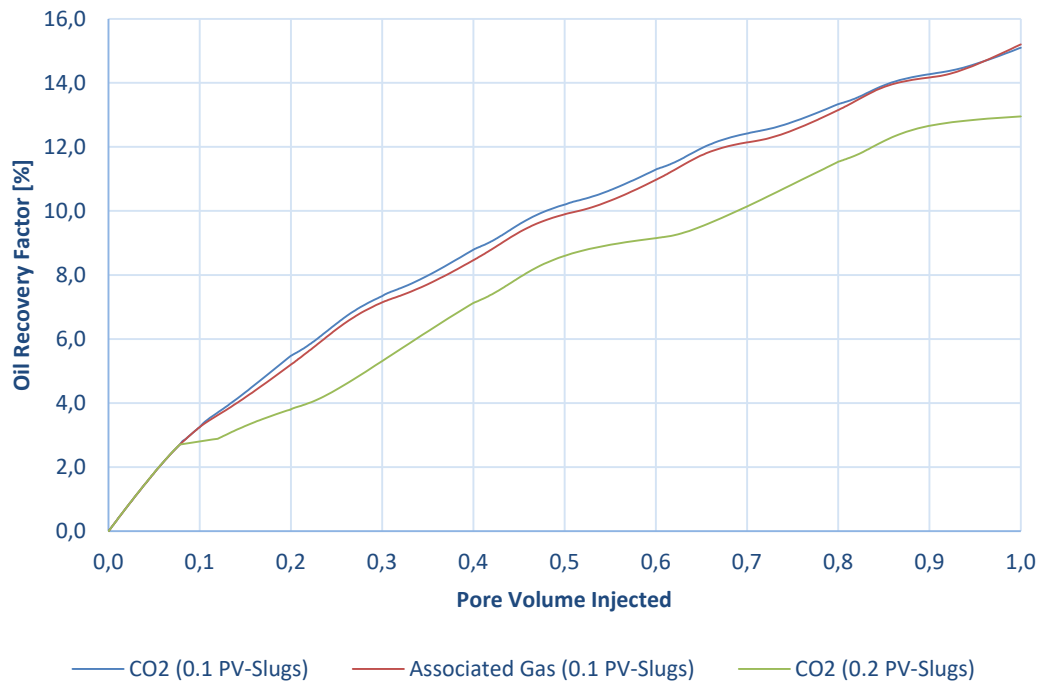


Figure 6-20: Comparison RF of FAWAG - CO₂ with 0.1 PV and 0.2 PV slugs, and associated gas with 0.1 PV slugs.

Chapter 7

Discussion

7.1 Discussion of the Gas Mobility Reduction Mechanisms

7.1.1 Core Model

The generation of foam is affecting the injected gas in such a way that its mobility is being reduced. This reduction enhances the sweep efficiency by avoiding the formation of gaseous viscous fingers and the fast passing of the oil. The oil recovery enhancing efficiency can be seen in Figure 7-1. Here we can see the comparison of the oil recovery between the WAG and FAWAG core model simulation run. In this graph, the injected hydrocarbon pore volumes of the WAG case were converted into PVI to allow for a truthful comparison. When comparing the core floods and the oil recovery enhancing methods, it is noticeable that a clear breakthrough is happening nearly 0.1 pore volumes later for the FAWAG case. This means that the gas mobility reducing effect is working, leading to a higher recovery of about 16% on top of what WAG injection offers. The formed oil bank is much denser in oil compared that of the WAG injection. The reason for the lower recovery of the FAWAG recovery process between PVI 0.2 and 0.3 is most probably the different cycling of the injected water and gas. Whereas the WAG experiment starts with gas and follows it up with water, the FAWAG experiment started with water, which generally yields a lower recovery and reaches the residual oil plateau much earlier. The mobility reduction effect can be further underlined by the higher pressure build-up as it can be seen in Figure 5-17 in the result section when comparing it to that of the WAG injection process (Figure 5-13).

Similar results can be seen for the core with the artificial gas invaded zone consisting of methane (Figure 5-21). The foam stabilises the gas movement and allows to contact more oil in the displacement process. WAG injection reaches a plateau very soon, whereas FAWAG can achieve an 8% percent higher oil recovery. The higher pressure build-up is again a natural consequence of foam formation and gas mobility reduction.

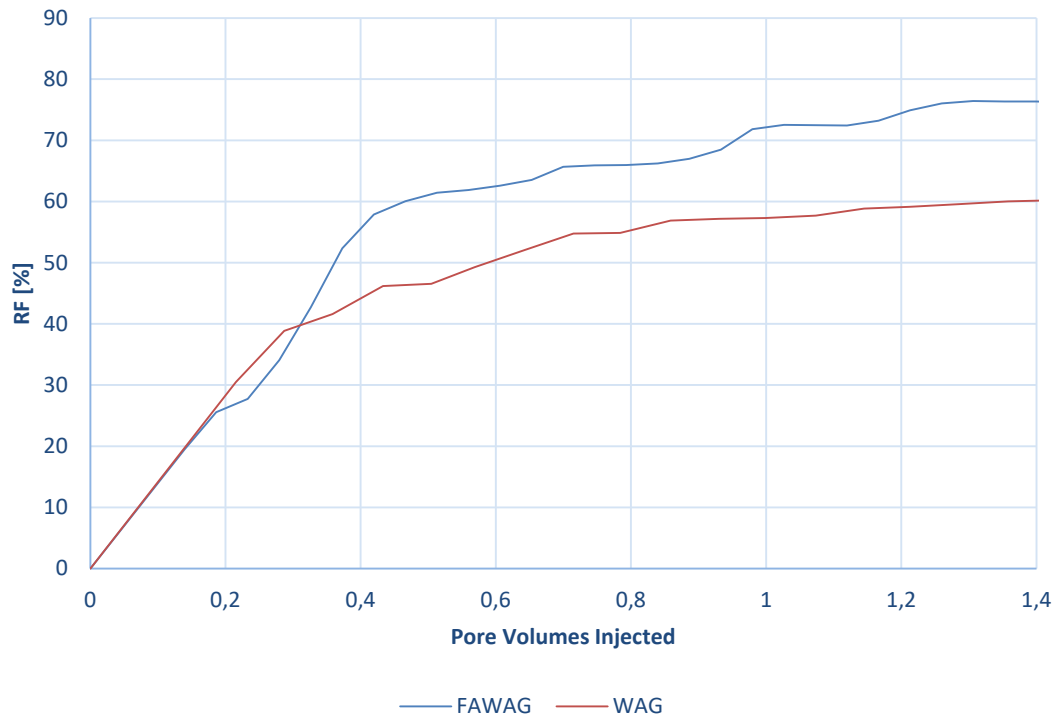


Figure 7-1: Core Model - Oil Recovery Factor Comparison WAG vs. FAWAG.

Testing different water-gas ratios for the FAWAG recovery method leads to the conclusion that a lower water to gas ratio will increase oil recovery substantially (Figure 5-19). This suggests that the forces acting in the cores are predominantly gravity forces. Viscous forces and capillary forces are weak, and therefore a high water to gas ratio is not recommended. The optimum WAG ratio in secondary floods is, therefore, a function of the total CO₂ slug size. This holds true to the works of Jackson (1985), where similar results were obtained.

7.1.2 Pilot Model

After matching the recovery profiles for the CO₂, WAG, and FAWAG core experiments, the derived relative permeability curves, and the foam parameters were then used in a pilot model to simulate a quarter of a five-spot well pattern. The gas breakthrough in the secondary recovery phase occurred at 0.4 PV later than in the water-alternating-gas case (Figure 6-3). This late gas breakthrough shows the lowered mobility of the gas by the foam and leads to an oil recovery factor 25% percent higher than in the case without foam (Figure 6-1).

As expected, similar results were obtained for the pilot model with a gas invaded zone of 40%. Gas breakthrough occurs at about 0.03 more PVI later than in the WAG case (Figure 6-6), leading to an increase of 20% in the oil recovery (Figure 6-4). The much steeper initial oil recovery curve for the FAWAG case can be explained by the oil recovery enhancing effects of the surfactant that has been added to the water.

By lowering the interfacial energy between the oil and aqueous phase, the capillary forces in the matrix and fractures are reduced and trapped oil is mobilised. Although, significant in the total amount recovered, this effect loses its ability to displace more oil very quickly after only 0.8 PVI. As soon as gas injection starts, foam effects are more predominant.

7.1.3 Cross-Sectional Model

To further understand the foams ability to reduce the gas mobility, the cross-sectional model gives a great presentation of how the gas front moves along the fractures. The gas front has a much sharper edge in the FAWAG displacement compared to the WAG (Figure 6-8) and moves at a slower pace. At the same time, the foam gas front has moved about half along the cross-section, whereas the foam-less gas front passed more than two thirds the way to the producer. This allows for a much higher saturated oil bank to form. The gas movement in the WAG process is clearly characterised by viscous fingering and a visible higher gas concentration on the top of the cross-section, suggesting a gravity override. The lower levels of the cross-section are poorly swept by the WAG gas front. The FAWAG process is a more reliable method for reaching the lowest parts of the reservoir by gas, as can be seen in Figure 6-8. This means that the FAWAG enhances the vertical sweep efficiency by a substantial amount. Especially for the case with the gas invaded zone, the foam is able to postpone the gas breakthrough and to contact the lower parts of the cross section as it can be seen in (Figure 6-9)

7.1.4 Sensitivity Analysis

Comparing different fracture variables and their magnitude's effect on oil recovery in a gas invaded reservoir lead to interesting results. Increasing the block height, and reducing the total block count by doing so, showed a worse vertical sweep efficiency in the cross-section model, whereas a block count increase lead to a better recovery. This could be because of high initial production of high block count models and that the injection time was limited to 0.4 PVI only (Shariat, et al., 2006). A higher fracture permeability leads to a decrease in recovery. This is due to the bypassing of the matrix blocks. Increased fracture spacing has the effect that more oil can be transported. Why this is affecting the recovery in such a way is a matter of further investigation.

7.1.5 Sector Model

Lastly, implementing the foam in the sector model showed expected results indicating that a FAWAG displacement is preferred over a conventional WAG injection. Figure 6-14 shows that we can increase the recovery by 2% in the tertiary stage after the injection of 1 PV. This value is even increased if we tune the WAG-ratio (Figure 6-20). In a tertiary recovery stage, these are significant improvements worth considering for future development of fractured reservoirs that have evolved a gas invaded zone. This shows that the foam model is working correctly and that implementation of foam-assisted WAG injection on a field scale is possible.

Chapter 8

Conclusion

8.1 Summary

This research has shown that foam-assisted water-alternating-gas injection is a viable enhanced oil recovery method for naturally fractured carbonate reservoirs. In an idealised pilot model, the additional recovery of oil increased by 25%, and in the case of having a gas invaded zone by an incredible 20%. In both cases, an effective delay of the gas breakthrough is noticeable. The cross-sectional model helps tremendously in understanding the mechanisms behind the greater oil recovery achieved by FAWAG in the secondary and tertiary recovery stages of a reservoir. These visualisations show that viscous fingering is suppressed by the low gas mobility and that the lower portions of the reservoir are better swept. A much sharper and higher saturated gas front is moving along the cross-section. Applying all this knowledge onto a sector model that in fractured reservoirs that have developed a gas invaded zone over the lifetime of their production. The oil recovery of a sector model based on actual reservoir data could be improved by two percent over pure WAG after injecting one pore volume of FAWAG. Tuning the WAG-ratio can improve this number by over seven percent, leaving room for additional recovery when tweaked appropriately. As this type of zonation is developing in many reservoirs worldwide, mainly in the Middle East, the inclusion of foam as a tertiary recovery step might be inevitable.

8.2 Evaluation

There are only a few numerical studies that were conducted on foam in naturally fractured carbonate reservoirs, let alone on studies purposely conducted on a field scale in the late tertiary stage of recovery. This work tries to pave the way for future studies on foam, especially in fractured carbonate reservoirs. Obviously, this work is just scratching the surface on what could be done on properly investigating the ability to use foam-assisted recovery methods to enhance oil recovery in fractured reservoirs, as there are still many other zones present in a developed fractured carbonate reservoir, such as the water invaded zone, gassing zone and die undersaturated zone. This thesis laid a good foundation for further studies, but there is still much left to be investigated.

8.3 Future Work

Re-evaluation of the FAWAG core flooding should be done. There are many parameters still left untouched that could potentially enhance the history match, which the used parameters alone were not able to achieve. Due to simulation runtime constraints, the effect of low salinity water used in the experimental core floods had to be left out, potentially enhancing the history matching on both the WAG and the FAWAG core flooding simulations. Furthermore, due to the pandemic, access to the software and facilities and devices with proper computer power was limited, imposing a strong time constraint on my work. This leads to unresolved problems with hysteresis parameters that might have been resolved otherwise. Furthermore, matching the PVT data of the reservoir oil lead to the inclusion of many components, which increased runtime substantially. It is recommended to address this problem by lumping and matching the PVT data to reduce computing time.

References

- Abdallah, W. et al., 2007. Fundamentals of Wettability. *Oilfield Review*, Issue 19.
- Ahmed, T. H., 2010. *Reservoir Engineering Handbook*. 4th ed. ed. 30 Corporate Drive, Suite 400, Burlington, MA 01803, USA: Elsevier Inc.
- Ahmed, T. H., 2016. *Equations of State and PVT Analysis: Applications for Improved Reservoir Modeling*. 2nd ed. 50 Hampshire Street, 5th Floor, Cambridge, MA 02139, USA: Elsevier Inc.
- AlMaqbali, A. et al., 2015. *Modelling Foam Displacement in Fractured Carbonate Reservoirs*. Abu Dhabi International Petroleum Exhibition and Conference, 9-12 November, Abu Dhabi, UAE: Society of Petroleum Engineers.
- Alvarado, V. & Manrique, V., 2010. *Enhanced Oil Recovery: Field Planning and Development Strategies*. 1st ed. 30 Corporate Drive, Suite 400, Burlington, MA 01803, USA: Elsevier Inc.
- Beydoun, Z., R., 1998. Arabian plate oil and gas: Why so rich and so prolific?. *Episodes*, 1 June, 21(2), pp. 74-81.
- Chambers, K. & Radke, C., 1991. Capillary Phenomena in Foam Flow through Porous Media. In: *Interfacial Phenomena in Petroleum Recovery*. New York: Marcel Dekker, Inc., pp. 191-255.
- Chekani, M. & Kharrat, R., 2009. *Reservoir Rock Typing in a Carbonate Reservoir-Cooperation of Core and Log Data: Case Study*. SPE/EAGE Reservoir Characterization and Simulation Conference, 19-21 October, Abu Dhabi, UAE, Society of Petroleum Engineers.
- Clemens, T. & Wit, K., 2001. *The Effect of Fracture Spacing on Gas/Oil Gravity Drainage in Naturally Fractured Reservoirs*. 30 September-3 October, New Orleans, Louisiana, Society of Petroleum Engineers.
- Computer Modelling Group LTD., 2019. *GEM 2019.10 Manual*. 3710 33 Street NW, Calgary, Canada: s.n.

Corey, A. T., 1954. The Interrelation between Gas and Oil Relative Permeabilities. *Prod. Monthly*, Nov., 19(1).

David, A. & Marsden, S. S., 1969. *The Rheology of Foam*. Presented at the 44th Annual Fall Technical Conference and Exhibition of the Society of Petroleum Engineers, Denver, Colorado, 1969, Society of Petroleum Engineers.

Enick, R. M., Olsen, D. K., Ammer, J. R. & Shuller, W., 2012. *Mobility and Conformance Control for CO₂ EOR via Thickeners, Foams, and Gels -- A Literature Review of 40 Years of Research and Pilot Test*. SPE Improved Oil Recovery Symposium, 14-18 April, Tulsa, Oklahoma, USA, Society of Petroleum Engineers.

Gandomkar, A. & Kharrat, R., 2012. The Tertiary FAWAG Process on Gas and Water Invaded Zones: An Experimental Study. *Energy Sources, Part A: Recovery, Utilization, and Environmental Effects*, 20 August, 34(2012), pp. 1913-1922.

Gandomkar, A. et al., 2012. An Experimental Investigation of Foam for Gas Mobility Control in a Low-Temperature Fractured Carbonate Reservoir. *Petroleum Science and Technology*, 13 April, 30(10), pp. 976-985.

Green, D. W. & Willhite, G. P., 2018. *Enhanced Oil Recovery*. Second Edition Hrsg. Richardson(Texas): Society of Petroleum Engineers.

Grogan, A. T. & Pinszewski, W. V., 1984. *The Role of Molecular Diffusion Processes in Tertiary Carbon Dioxide Flooding*. Tulsa, OK, USA, 16 Apr 1983, Society of Petroleum Engineers.

Heinemann, Z. E. & Mittermeir, G., 2014. Natural Fractured Reservoir Engineering. *Textbook Series - Professor Heinemanns Doktorandengruppe*, February. Volume 5.

Hirasaki, G. J., 1989. The Steam-Foam Process. *Journal of Petroleum Technology*, pp. 449-456.

Jackson, D., Andrews, G. & Claridge, E., 1985. *Optimum WAG Ratio vs. Rock Wettability in CO₂ Flooding*. September 22-25, Las Vegas, Society of Petroleum Engineers.

Jarrell, P. M., Fox, C., Stein, M. & Webb, S., 2002. *Practical Aspects of CO₂ Flooding (SPE Monograph Series, Vol. 22)*. s.l.:Society of Petroleum Engineers.

Kovscek, A. & Radke, C., 1994. Fundamentals of Foam Transport in Porous Media. In: *Foams: Fundamentals and Applications in the Petroleum Industry*. Washington, DC: American Chemical Society, pp. 115-163.

- Lake, L. W., 1987. Chemical Flooding. In: *Petroleum Engineering Handbook*. Richardson, Texas: Society of Petroleum Engineers, p. Chapter 47..
- Lake, L. W., 1989. *Enhanced Oil Recovery*. Englewood Cliffs, New Jersey 07632: Prentice-Hall.
- Lemonnier, P. & Bourbiaux, B., 2010. Simulation of Naturally Fractured Reservoirs. State of the Art: Part 1 - Physical Mechanisms and Simulation Formulation. *Oil & Gas Science and Technology - Revue de l'Institut Français du Pétrole*, March, Issue 65, pp. 239-262.
- McGuire, W. J. & Sikora, V. J., 1960. The Effect of Vertical Fractures on Well Productivity. *Journal of Petroleum Technology*, 01 October, Volume 12, pp. 72-74.
- Motealleh, M. et al., 2012. An Experimental Study on the Applicability of Water-alternating-CO₂ Injection in the Secondary and Tertiary Recovery in One Iranian Reservoir. *Petroleum Science and Technology*, 15 October, 30(24), pp. 2571-2581.
- Nelson, R. A., 1987. Fractured Reservoirs: Turning Knowledge into Practice. *Journal of Petroleum Technology*, 1 April, 39(04), pp. 407-414.
- Nematzadeh, M. et al., 2012. An Experimental Study of Secondary WAG Injection in a Low-Temperature Carbonate Reservoir in Different Miscibility Conditions. *Petroleum Science and Technology*, 14 May, Issue 30, pp. 1359-1368.
- Nikolov, A. D., Wasan, D. T., Huang, D. W. & Edwards, D. A., 1986. *The Effect of Oil on Foam Stability: Mechanisms and Implications for Oil Displacement by Foam in Porous Media*. New Orleans, Louisiana, Society of Petroleum Engineers.
- Patton, J. T., Holbrook, S., Kuntamukkula, M. & Long, R. L., 1985. *Enhanced Oil Recovery by CO₂ Foam Flooding, Final Report*, United States: U.S. Department of Energy Office of Scientific and Technical Information.
- Pedersen, K. S., Christensen, P. L. & Shaikh, J. A., 2015. *Phase Behaviour of Petroleum Fluids*. 2nd ed. 6000 Broken Sound Parkway NW, Suite 300: Taylor & Francis Group.
- Pirson, S. J., 1958. *Oil Reservoir Engineering*. 2nd ed. New York: McGraw-Hill.
- Ransohoff, T. & Radke, C., 1988. Mechanisms of Foam Generation in Glass-Bead Packs. *SPE Reservoir Engineering*, May, 3(02), p. 13.
- Raza, S. H., 1970. Foam in Porous Media: Characteristics and Potential Applications. *Society of Petroleum Engineers Journal*, December, 10(04), p. 9.

Satter, A. & Iqbal, G. M., 2016. *Reservoir Engineering: The Fundamentals, Simulation, and Management of Conventional and Unconventional Recoveries*. 225 Wyman Street, Waltham, MA 02451, USA: Elsevier Inc.

Schlumberger, 2008. *PVTi Reference Manual*, s.l.: s.n.

Schlumberger, 2018. *Eclipse Technical Description*, s.l.: s.n.

Selley, R. C., 2005. Limestones. In: R. C. Selley, L. R. M. Cocks & I. R. Plimer, eds. *Encyclopedia of Geology*. Imperial College London, London, UK: Elsevier Ltd., pp. 107-113.

Shariat, A., Behbahania, A. R. & Beigy, M., 2006. *Block to Block Interaction Effect in Naturally Fractured Reservoirs*. International Oil Conference and Exhibition in Mexico, 31 August-2 September, Cancun, Mexico, Society of Petroleum Engineers.

Sheng, J. J., 2011. *Modern Chemical Enhanced Oil Recovery*. 30 Corporate Drive, Suite 400, Burlington, MA 01803, USA: Elsevier.

Sheng, J. J., 2013. *Enhanced Oil Recovery Field Case Studies*. 1. Hrsg. 225 Wyman Street, Waltham, MA 02451, USA: Gulf Professional Publishing.

Skjæveland, S. M. & Kleppe, J. eds., 1992. *SPOR Monograph - Recent Advances in Improved Oil Recovery Methods for North Sea Sandstone Reservoirs*. Stavanger: Norwegian Petroleum Directorate.

Stearns, D. W. & Friedman, M., 1972. Reservoirs in Fractured Rock: Geologic Exploration Methods. In: H. R. Gould, ed. *Stratigraphic Oil and Gas Fields--Classification, Exploration Methods, and Case Histories*. s.l.: American Association of Petroleum Geologists, pp. 82-106.

Syahputra, A. E., Tsau, J. S. & Grigg, R. B., 2000. *Laboratory Evaluation of Using Lignosulfonate and Surfactant Mixture in CO₂ Flooding*. 3-5 April, Tulsa, Oklahoma, Society of Petroleum Engineers.

Tiab, D. & Donaldson, E. C., 2016. *Petrophysics - Theory and Practice of Measuring Reservoir Rock and Fluid Transport Properties*. Fourth edition ed. 225 Wyman Street, Waltham, MA 02451, USA: Elsevier.

Tzimas, E., Georgakaki, A., Garcia-Cortes, C. & Peteves, E., 2005. Enhanced Oil Recovery Using Carbon Dioxide in the European Energy System. December.

Van Golf-Racht, T., 1982. *Developments in Petroleum Science 12 - Fundamentals of Fractured Reservoir Engineering*. Molenwerf 1, P.O. Box 211, 1000 AE Amsterdam, The Netherlands: Elsevier Scientific Publishing Company.

Witowski, A., Majkut, M. & Rulik, S., 2014. Analysis of pipeline transportation systems for carbon dioxide sequestration. *Archives of Thermodynamics*, 35(1), pp. 117-140.